S100A10 FACILITATES THE TUMOR PROMOTING ASSOCIATION OF MACROPHAGES WITH TUMOR CELLS

by

Kyle D. Phipps

Submitted in partial fulfilment of the requirements
for the degree of Doctor of Philosophy

at

Dalhousie University
Halifax, Nova Scotia
August 2011

DALHOUSIE UNIVERSITY

DEPARTMENT OF BIOCHEMISTRY AND MOLECULAR BIOLOGY

The undersigned hereby certify that they have read and recommend to the Faculty of Graduate Studies for acceptance a thesis entitled "S100A10 FACILITATES THE TUMOR PROMOTING ASSOCIATION OF MACROPHAGES WITH TUMOR CELLS" by Kyle D. Phipps in partial fulfilment of the requirements for the degree of Doctor of Philosophy.

Dated: August 17th 2011

External Examiner: _____

Research Supervisor: _____

Examining Committee: _____

_____

_____

Departmental Representative: _____

DALHOUSIE UNIVERSITY

DATE: August 17, 2011

AUTHOR: Kyle D. Phipps

TITLE: S100A10 FACILITATES THE TUMOR PROMOTING ASSOCIATION OF MACROPHAGES WITH TUMOR CELLS

DEPARTMENT OR SCHOOL: Department of Biochemistry and Molecular Biology

DEGREE: PhD CONVOCATION: October YEAR: 2011

_____

Signature of Author

TABLE OF CONTENTS

LIST OF TABLES

LIST OF FIGURES

ABSTRACT

Hematopoietic cells are recruited to and co-opted by the growing tumor making expansive tumor growth possible. Although several cell types become associated with the growing tumor, macrophages play a fundamental role. The movement of macrophages across the basement membrane and through the extracellular matrix to the tumor site requires the activation of proteases, such as plasmin, at their cell surface. The proteolytic aspect of macrophage recruitment may represent an exploitable aspect of tumor growth in terms of therapeutic strategies. Here I show that the S100A10 protein facilitates the infiltration of macrophages into the site of tumor growth by stimulating the generation of the protease plasmin at their surface. Using a mouse model in which wild-type (WT) and S100A10-null mice are inoculated with tumor cells, a decrease in tumor-associated macrophages (TAMs) and greatly diminished tumor growth in tumors grown in S100A10-null mice was observed. Although tumor growth in S100A10-null mice could be restored by intraperitoneal injection of WT macrophages, S100A10-null macrophages only restored tumor growth when directly injected into the tumor. Lastly, selective depletion of macrophages from a WT mouse by liposome encapsulated clodronate treatment resulted in similar tumor growth deficits as in the S100A10-null mouse. These results highlight a new role for the S100A10 protein in the recruitment of TAMs to the tumor site and demonstrate a potential therapeutic strategy in which the tumor associated cells may be targeted.

LIST OF ABBREVIATIONS AND SYMBOLS USED

A2T – annexin A2 heterotetramer

bFGF – basic fibroblast growth factor

BSA – bovine serum album

CCL5 – chemokine ligand 5

CSF-1 – colony stimulating factor 1

CMV – cytomegalovirus

DAPI – 4',6-diamidino-2-phenylindole

DC-1 – type 1 dendritic cells

EGF – epidermal growth factor

FACS – fluorescence assisted cell sorting

GM-CSF – granulocyte macrophage colony-stimulating factor

H2B – histone 2b

HBSS – Hank's balanced salt solution

HIF-1– hypoxia inducible factor-1

Hr – hour

IFN-γ – interferon-γ

IL – interleukin

IL-1ra – IL-1 receptor antagonist

iNOS – inducible nitric oxide synthase

K – kringle

LBP –LPS binding protein

LLC – Lewis lung carcinoma

LPS – lipopolysaccharides

MCP-1 – monocyte chemotactic protein-1

M-CSF – macrophage colony-stimulating factor

Min – minute

MMP – matrix metalloprotease

MR – mucin receptor

MTT – 3-(4,5-Dimethylthiazol-2-yl)-2,5-diphenyltetrazolium bromide

NO – nitric oxide

PA – plasminogen activator

PAI – plasminogen activator inhibitor

PAN – plasminogen apple nematode

PBS – phosphate buffered saline

PCNA – proliferative cell nuclear antigen

PD-ECGF – platelet-derived endothelial cell growth factor

PECAM – platelet endothelial cell adhesion molecule-1

PTX3 – pentraxin-related protein

Pg – plasminogen

PGE2 – prostaglandin E2

PgR – plasminogen receptor

Pm – plasmin

PN-1– protease nexin 1

PyMT – polyoma middle T

RNI – reactive nitrogen intermediate

ROI – reactive oxygen intermediates

RT – room temperature

sctPA – single-chain tissue-type plasminogen activator

scuPA – single chain urokinase type plasminogen activator

serpin – serine protease inhibitor

TAM – tumor associated macrophage

TCR – T-cell receptor

tctPA – two-chain tissue-type plasminogen activator

tcuPA – two chain urokinase type plasminogen activator

TGF-β – transforming growth factor-β

Th-1 – type 1 helper T-cell

TLR – toll-like receptor

TNF-α – τumor necrosis factor-α

TNF-β – Tumor necrosis factor-β

tPA – tissue-type plasminogen activator

TRAIL – TNF-related apoptosis inducing ligand

uPA – urokinase-type plasminogen activator

uPAR – urokinase-type plasminogen activator receptor

VEGF – vascular endothelial growth factor

ACKOWLEDGEMENTS

It is a pleasure to acknowledge those who have made this work possible. First and foremost I would like to express my sincere gratitude for the supervision Dr. David Waisman has given over these past five years. Dr. Waisman's infectious enthusiasm for research has been an easy source of motivation and his openness to new ideas has allowed me the flexibility to seek out my own initiatives. I would like to thank the members of the Waisman lab for providing an enjoyable work environment. I would also like to thank my thesis committee, Dr. Rob Liwski, Dr. Jonathan Blay and Dr. Hyo-Sung Ro for their advice and guidance. It was greatly appreciated.

CHAPTER 1

INTRODUCTION

1.1 Mononuclear phagocyte system

Leukocytes, or white blood cells, are considered to be the primary cells of the immune system. The mononuclear phagocytes are a subgroup of leukocytes whose lineage originates in the bone marrow as hematopoietic stem cells (HSCs). HSCs differentiate into committed myeloid progenitor cells, which give rise to monoblasts which become monocytes and enter circulation (Figure 1). Under steady state conditions approximately half of the monocytes exit circulation each day to differentiate into macrophages[1,2]. The majority of cell proliferation in the mononuclear phagocyte system occurs at the monoblast level with proliferating mature macrophages making a small contribution to maintaining tissue macrophage levels[3].

Relatively recently it has been established that there are functionally different subsets of monocytes. Monocytes expressing low levels of the fractalkine receptor (CX3CR1) become recruited to inflammatory sites, whereas monocytes expressing high levels become resident tissue macrophages[4]. Additionally, Ly6C (GR-1) granulocyte surface antigen has also been reported as a monocyte subtype marker. Ly6C expression status has been used to identify monocytes along a differentiation continuum, the Ly6C (high) cells being less mature[5].

There are numerous subtypes of mononuclear phagocytes along the continuum from stem cell to terminally differentiated macrophage, representing the extreme versatility of this system[6]. Like the monocyte, the macrophage becomes further specialized into subtypes, being the M1 or M2 polarized phenotype differing on their means of activation. M1 and M2 polarized macrophages generally differ in their high

expression of either IL-12 or IL-10 respectively, however other differences include receptor expression, cytokine production and effector molecule type and function[7,8]. It should be noted that the M1/M2 concept is a functionally simplified framework to facilitate macrophage discussion. In the *in vivo* setting, macrophages exist in a continuum of functional states as they are subjected to a plethora of opposing signals. The M1/M2 phenotypes describe the extreme poles of the continuum[6]. With this caveat, the accepted role of the M1 macrophage, considered to be the classical activated form, is that of an effector cell which kills microorganisms and tumor cells and stimulates inflammation through the production of pro-inflammatory cytokines. The M2 designation refers to a macrophage activated by any means other than the classical M1 schema and are generally associated with tissue repair, inflammation suppression and phagocytosis.

Macrophage polarization to the M1 phenotype can occur in response to selected cytokines from activated helper T-cells (Figure 2). Type 1 dendritic cells (DC-1), following the engulfment and breakdown of a microorganism, present a corresponding antigen to the T-cell receptor (TCR) on a pre-helper T-cell[9]. Along with the secretion of interleukin-12 (IL-12), this association allows the DC-1 cell to activate the pre-helper T-cell to the mature type 1 helper T-cell (Th-1). Mature Th-1 cells produce IFN-γ and tumor necrosis factor-β (TNF-β), stimulating the M1-macrophage polarization.

M1 macrophage polarization can also occur through a more direct route via macrophage interaction with microbial signals (Figure 2). A major membrane component of Gram-negative bacteria is lipopolysaccharides (LPS), which becomes released after cell lysis[10]. Free LPS can become bound to the circulating LPS binding protein (LBP), which forms a complex with the CD14 receptor on the macrophage cell surface[11]. The

M1 macrophage kills target cells through two classes of effector molecules; reactive oxygen intermediates (ROI), primarily H_2O_2 and reactive nitrogen intermediates (RNI), primarily nitric oxide (NO). In M1 macrophages, NO is primarily produced from L-arginine by inducible nitric oxide synthase (iNOS)[12]. M1 macrophages also release several pro-inflammatory cytokines such as tumor necrosis factor- α (TNF-α), IL-1, IL-6, and IL-23[13].

Figure 1. Hematopoietic stem cell differentiation. Lineage map of hematopoietic stem cell differentiation highlighting the formation of the leukocyte lineage[14].

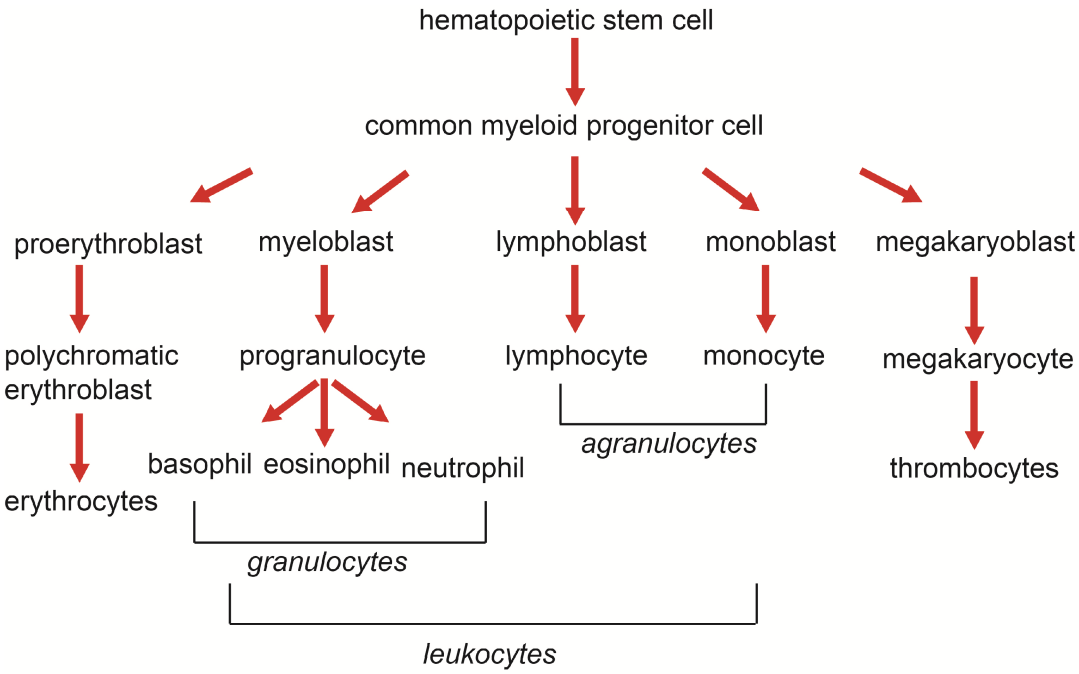
hematopoietic stem cell
common myeloid progenitor cell
proerythroblast
myeloblast
lymphoblast
monoblast
megakaryoblast
polychromatic erythroblast
progranulocyte
lymphocyte
monocyte
megakaryocyte
basophil
eosinophil
neutrophil
agranulocytes
erythrocytes
thrombocytes
granulocytes
leukocytes

Figure 2. Classical M1 macrophage activation. Activation to the M1 macrophage phenotype is initiated by type 1 dendritic cells (DC-1) presenting an antigen to the pre-helper T-cell (pre-Th) and the release of co-stimulatory cytokines to create a mature T-cell (Th-1). The activated mature Th-1 cell is now able to stimulate the M1-macrophage polarization. Alternatively, M1 polarization can occur through LPS, a major membrane component of Gram-negative bacteria. M1 macrophages kill target cells through reactive oxygen intermediates (ROI) and reactive nitrogen intermediate (RNI) and release several pro-inflammatory cytokines.

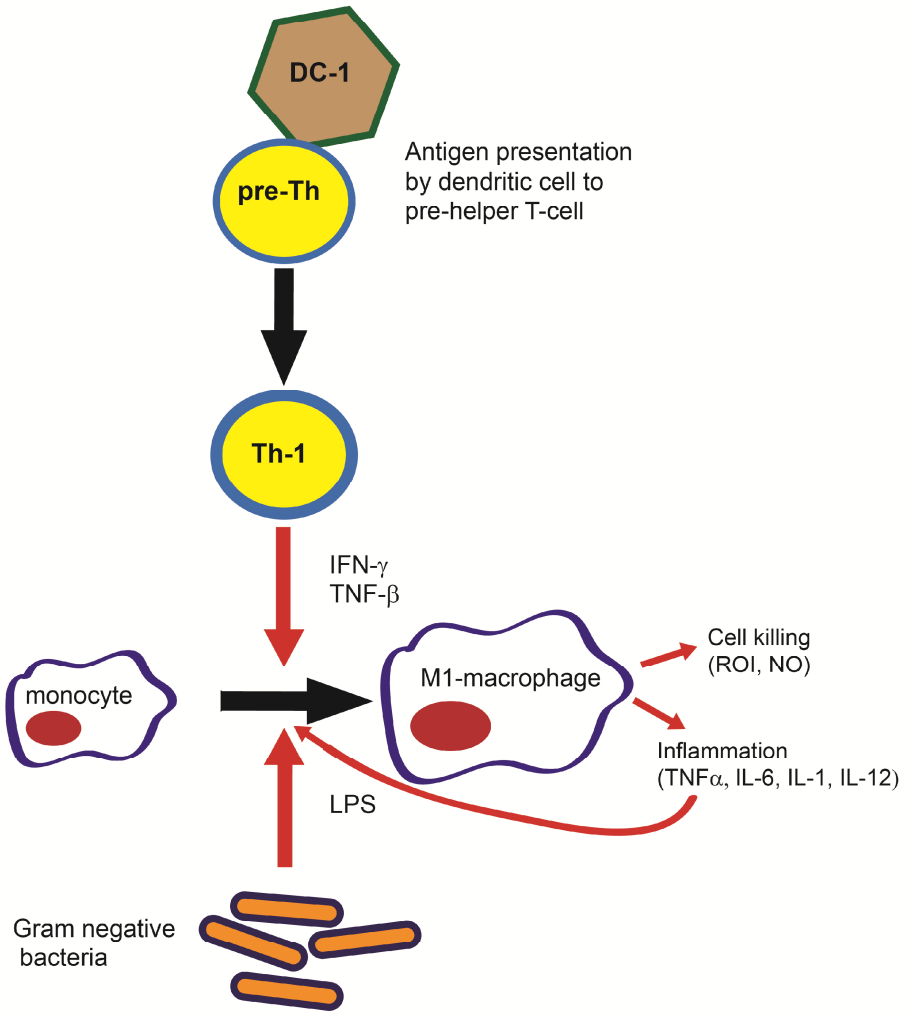
DC-1
pre-Th
Antigen presentation
by dendritic cell to
pre-helper T-cell
Th-1
IFN-γ
TNF-β
monocyte
M1-macrophage
Cell killing
(ROI, NO)
Inflammation
(TNFα, IL-6, IL-1, IL-12)
LPS
Gram negative
bacteria

1.1.2 Alternatively activated macrophages

The M2, or 'alternate', macrophage phenotype is a generic designation for macrophages which are not activated to the classical M1 phenotype. Several means of activation exist, thus there exists a large heterogeneity in M2 macrophages (Figure 3). Traditionally, the M2 phenotype has been subdivided into three distinct subtypes; M2a, M2b and M2c, representing distinct activation pathways and functions. M2a macrophage differentiation is induced by IL-4 and IL-13, M2b macrophage differentiation is driven by the interaction with a variety of immune complexes, toll-like receptor (TLR) stimulation, or by IL-1 receptor antagonist (IL-1ra). The M2c phenotype is produced by exposure to the immunosuppressive IL-10[15].

The M2 sub-phenotypes display a variety of functional differences relative to the M1 phenotype, broadly they suppress inflammation, enhance phagocytosis and promote tissue repair. Like the M1 macrophage, the M2 cells express iNOS, however the cell killing NO production is modulated by an overexpression of arginase. Arginase, like iNOS, utilizes arginine as a substrate but produces L-ornithine and urea instead of NO and citrulline, thus increased arginase expression decreases availability of substrate for iNOS[16,17]. Additionally, it has been reported that the enhanced L-ornithine production by M2 macrophages promotes tumor cell proliferation *in vitro* as cancer cells have a heightened rate of DNA synthesis and L-ornithine may be used to create adenine[17].

Figure 3. Alternative M2 macrophage activation. All macrophage activation which is not to the classical M1 phenotype is considered to be the M2 phenotype. M2 macrophages may be subdivided into four distinct subtypes M2a-d induced by varying signals, depicted below. Broadly, M2 macrophages suppress inflammation, enhance phagocytosis, stimulate angiogenesis and promote tissue repair.

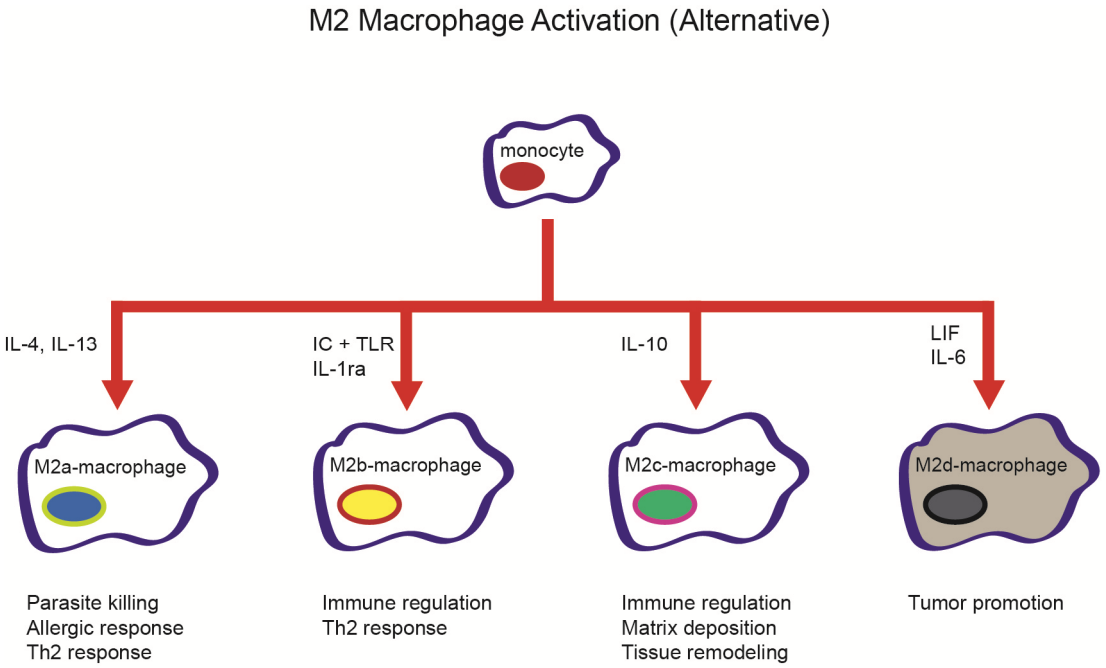
M2 Macrophage Activation (Alternative)
monocyte
IL-4, IL-13
IC + TLR
IL-1ra
IL-10
LIF
IL-6
M2a-macrophage
M2b-macrophage
M2c-macrophage
M2d-macrophage
Parasite killing
Allergic response
Th2 response
Immune regulation
Th2 response
Immune regulation
Matrix deposition
Tissue remodeling
Tumor promotion

1.2 Tumor associated macrophage recruitment

Tumors recruit and co-opt macrophages for their growth and dissemination[7]. Thus, there exists an increasingly large body of evidence correlating tumor associated macrophage (TAM) density with poor prognosis in a varied number of cancers such as breast cancer, hepatocellular carcinoma, cholangiocarcinoma, lung adenocarcinoma, follicular lymphoma, thyroid and endometrial carcinomas[18-23]. Additionally, the metastatic incidence in the spontaneous tumor forming, polyoma middle T (PyMT) mice is reduced upon TAM depletion[24]. The TAM population therefore plays an integral role in tumor progression. The TAM closely resembles an M2 macrophage in terms of function and transcriptome expression[15]. Until recently, TAMs were considered a heterogeneous group of M2a, M2b and M2c macrophages, however in 2007, Duluc *et. al.* reported an M2 TAM which promoted tumor growth and displayed characteristics distinct from M2a-c[25-27]. M2d macrophages contribute to immuno suppression by a constitutive expression of B7-H4, a potent immunosuppressive molecule and express a low level of CD86, a costimulatory molecule for T-cell activation[25]. M2d macrophages produce much lower levels of the antiangiogenic molecule pentraxin-related protein (PTX3) relative to M2a-c phenotypes. M2d macrophages have an increased expression of TNF and transforming growth factor (TGF) both of which promote tumor growth, as well as increased expression of vascular endothelial growth factor (VEGF) and matrix metalloprotease-9 (MMP-9) which promote angiogenesis[25]. These observations indicate that M2d macrophages may be both pro-tumorigenic and immumnosuppressive.

TAM density is directly dependent upon the recruitment of monocytes from circulation in response to chemotactic signals from the tumor[28]. For example, hypoxic

tumor regions cause the release of the chemoattractant lysophosphatidylcholine from apoptotic cancer cells[29]. Cancer cells release chemotactic factors which mimic the wound healing response such as; chemokine ligand-2 (CCL-2) also known as monocyte chemotactic protein-1 (MCP-1), CCL-5 and GM-CSF[30-32]. The macrophage colony stimulating factor (M-CSF or CSF-1) chemokine is also released by cancer cells and is the main growth factor for survival, proliferation, differentiation and chemotaxis of mononuclear phagocytes[7]. Cancer cell released soluble M-CSF blocks tumoricidal action of the immune system by inhibiting dendritic cell maturation, which blocks T-cell antigen presentation and therefore M1 macrophage activation [7](Figure 2). Interestingly, it has been reported that the form that M-CSF takes alters the immune response. Cell surface M-CSF causes macrophages to 'lock on' and kill the cancer cell[7]. In addition to recruitment of macrophages by cancer cells, TAMs also release MCP-1 and CCL-5, further recruiting macrophages to the tumo[8,33].

Taken together, the centralized force driving macrophage recruitment and coercion by the tumor is the inappropriate identification of the tumor as a site requiring tissue repair.

1.3 Tumor associated macrophage function

TAMs promote tumor growth through a variety of mechanisms including the downregulation of the tumoricidal immune response, direct tumor cell growth promotion and the orchestration of tumor angiogenesis.

1.3.1 TAM immunomodulation

The M2 macrophage has an increased ability to inhibit immune function, which is very divergent from the M1 macrophage phenotype. The M1 macrophage has been reported to be proficient in lysing tumor cells, presenting tumor associated antigens to T-cells and producing stimulatory cytokines to promote the anti-tumor functions of T-cells and natural killer cells[34].

TAMs express low levels of MHC II receptors and are therefore poor antigen presenting cells, effectively suppressing T-cell activation[8,35]. TAMs also bind highly glycosylated proteins, called mucins, secreted by cancer cells via the manose receptor (MR)[36]. The MR is typically over-expressed on TAMs, binding of mucin to the MR stimulates the release of the immunosuppressant IL-10 from the macrophage. As mentioned above, IL-10 plays a causative role in the polarization of macrophages from M1 to M2[32]. Transforming growth factor-β (TGF-β) and prostaglandin E2 (PGE2) released by TAMs and by cancer cells also have an immunosuppressant effect thereby impeding anti-tumor immunity[37]. PGE2 mediated immunosuppression functions through the inhibition of IL-12 and TNF-α production, whereas TGF-β immunosuppression functions through blocking IL-2 inflammatory signals[38,39]. Transcription factor activity from NF-κB is essential for several pro-inflammatory genes to be expressed. TAMs have a defective NF-κB response when exposed to M1 polarizing stimuli such as LPS and tumor necrosis factor alpha (TNF-α)[37].

In addition to TAMs functioning to protect cancer cells from being targeted by the immune system, they may also inhibit cancer cell apoptosis directly. A wide variety of tumor cells have been shown to be sensitive to TNF-related apoptosis inducing ligand

(TRAIL), a potent initiator of apoptosis[40]. It has been recently shown that tumor cells and TAMs form a feedback loop which functions through the transcription factor Snail to confer cancer cell resistance to apoptosis[41].

1.3.2 TAM promotion of tumor growth

TAM density has been shown to correlate with increased tumor cell proliferation rates in both endometrial tumors and in renal cell carcinomas[42,43]. Several studies have found that TAMs release factors which increase tumor cell growth and survival rates including epidermal growth factor (EGF), platelet-derived growth factor (PDGF), TGF-β1, hepatocyte growth factor and basic fibroblast growth factor (bFGF)[34,44,45]. However, polyoma-middle T (PyMT) induced tumors in the CSF-1 knock-out mouse (deficient in macrophage recruitment) displayed no difference in primary tumor incidence or growth rates[24]. It is likely that TAM influence on tumor growth rate is tumor type specific. Cancer cells exist as a heterogeneous population of cells and contain a number of different activated pathways. Conceptually, if a certain growth pathway is constitutively activated intracellularly, then external stimuli for that pathway would have no effect. Thus, it serves to assume that the dependency of extracellular growth promotion would vary.

1.3.3 TAM induced angiogenesis

Angiogenesis, the formation of a vascular network, is essential for tumor progression. It has been reported that a tumor lacking angiogenesis remains constrained to 1-2 mm in diameter due to a lack of oxygen and nutrients; first described by Dr. Judah Folkman in 1971. TAM density has long been associated with tumor angiogenesis[46,47].

TAMs have been reported to accumulate in hypoxic regions of the tumor where they initiate a pro-angiogenic cascade. The low oxygen tension in hypoxic tumor environments causes the stabilization and activity of transcription factor hypoxia inducible factor-1 (HIF-1, resulting in the release of vascular endothelial growth factor (VEGF) as well as other angiogenic stimuli such as TNF-α, bFGF and IL-8 from the macrophage[28,35]. Additionally, HIF-1 activity causes decreased expression of angiogenic inhibitors such as platelet factor-4, thrombospondin and angiostatin[28,35]. The shift in the chemical balance towards angiogenic stimulatory factors causes the migration of endothelial cells from neighboring blood vessels[48].

TAMs are also able to stimulate angiogenesis independent of hypoxia via the IL-1β cytokine which is primarily released by monocytes and macrophages and is typically found in the tumor microenvironment[46]. IL-1β has been shown to mimic hypoxia by specifically stabilizing the HIF-1 transcription factor, allowing for the release of VEGF as well as the release of pro-angiogenic TNFα and angiogenin[49].

Although much is known about the macrophage recruitment in terms of tumor originating chemotactic stimuli and the ways in which TAMs promote tumor growth, the mechanism by which TAMs infiltrate into the tumor microenvironment is poorly understood.

1.4 Plasmin and plasminogen

In order for leukocytes to reach the growing tumor they must exit circulation by a process known as exocytosis, this occurs in post capillary venules as the hydrodynamic shear force is lessened. Leukocytes recognize cytokine-induced cell adhesion molecules

(CAMs) expressed by endothelial cells in response to inflammatory signals[50]. A class of CAMs, known as selectins, serves to slow down the monocyte by adhering, with marginal affinity, to carbohydrate ligands on the monocyte[50]. These interactions are made and broken under the shear force of blood flow and serve to form a "rolling adhesion". A secondary, "tight adhesion", is formed by leukocyte integrins and their endothelial counterparts. The integrins bind with higher affinity and serve to anchor the leukocyte against the blood flow. A rearrangement of the leukocyte cytoskeleton allows for the extension of pseudopodia through the gaps between endothelial cells. Transmigration occurs as platelet endothelial cell adhesion molecule-1(PECAM-1) proteins on the endothelial cell and the leukocyte interact and pull the leukocyte through the endothelial cell junction. The leukocyte must then cross the underlying basement membrane, a process known as diapedesis, and transit through the extracellular matrix (ECM) to finally enter the tumor stroma. These migratory events rely heavily upon the ability of proteolytic enzymes to remodel the various environments. The broad spectrum serine protease plasmin (pm) has long been implicated in pericellular proteolysis associated with the invasive cellular phenotype[51]. Pm is a broad spectrum serine protease capable of degrading glycoproteins, proteoglycans and ECM components such as fibrin, fibronectin, laminin, thrombospondin and vitronectin[52-56]. In addition to direct substrate degradation, plasmin is able to activate other proteases such as MMP-1, MMP-3 and MMP-9 which degrade a wide variety of ECM components[57,58]. Pm activity also liberates latent growth factors from within the ECM such as TGF-β, bFGF and VEGF. There are however other hypotheses for TAM accumulation which do not rely upon protease activation. Hashizume *et. al.* has proposed that TAMs may accumulate through a passive process

mediated by leaky tumor vasculature[59]. It is also possible that these hypotheses are not mutually exclusive, that is that both protease mediated and passive accumulation of macrophages may occur, however we will be focusing on the protease mediated mechanism.

The native form of Pm exists in circulation as glu-plasminogen (glu-Pg), a single-chain zymogen containing 791 amino acids at a concentration of 1.5 - 2.0 μM[60]. Glu-Pg contains an N-terminal PAN (plasminogen apple nematode) domain, five kringle repeats and a trypsin like serine protease domain[61] (Figure 4). The substrate binding pocket for the protease domain remains unaccessible, rendering Pg non-functional with respect to protease activity. Single-chain Pg requires proteolytic activation to two-chain Pm through a specific cleavage at Arg^{561}-Val^{562} by specific Pg activators (PA); the urokinase-type and tissue-type PAs (uPA and tPA)[62]. This cleavage forms a two chain molecule, the heavy chain containing the kringle repeats and the light chain containing the protease domain. The kringle repeats are specialized lysine binding pockets that stabilize lysine R-groups through hydrophobic, salt-bridging and charge-charge interactions (Figure 5). The five kringles have differing lysine affinities, the highest being in kringle 1 (K1) and K4, whereas K5 displays moderate binding and K2 has the lowest affinity[63]. Kringle binding allows the protein to associate with PAs and with substrates, such as partially degraded fibrin which contains an exposed C-terminal lysine[61]. Additionally, intramolecular kringle binding to lysine residues maintains the Pg in the closed, inactive conformation (discussed below).

Figure 4. Structure of plasminogen. The structure of plasminogen represented by the 1-letter amino acid code. Kringle domains are identified as K1-5. Disulfide bonds are shown as black connecting lines and the PAN and protease domains are labeled. A single black arrow indicates the cleavage site for activation to Pm. Adapted from Rejante *et al.* (1994)[64].

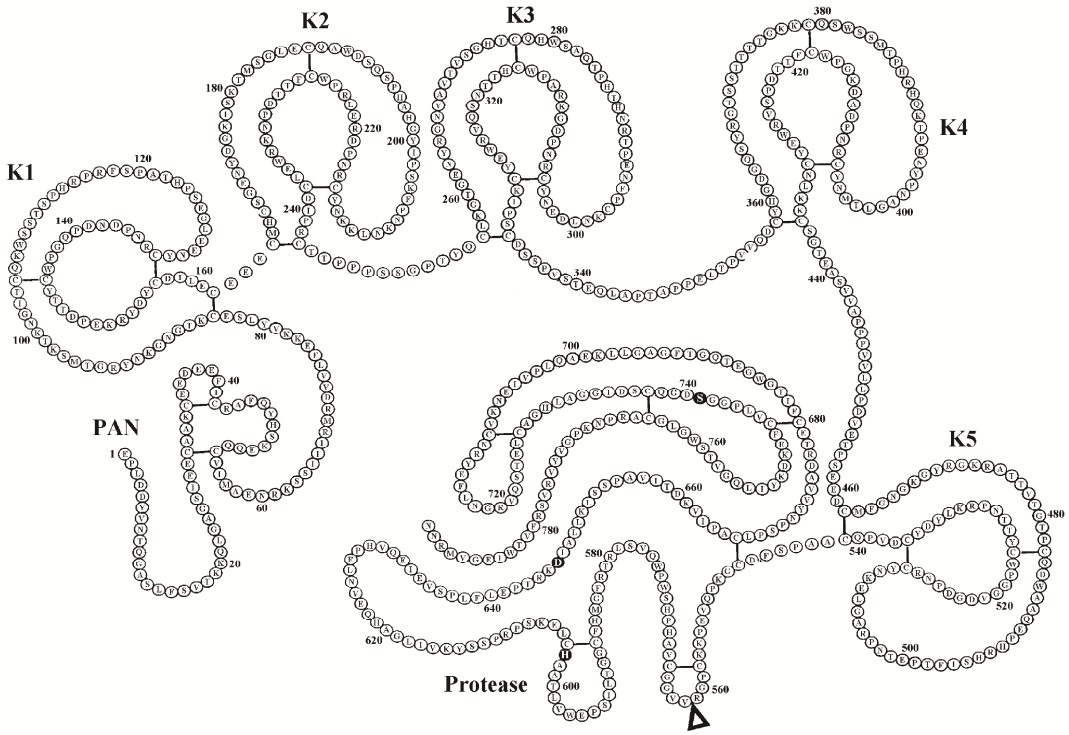
K1
K2
K3
K4
K5
PAN
Protease

Figure 5. Lysine interaction with kringle domain. Multiple interactions of the lysine R-group with the kringle domain facilitate binding such as hydrophobic interactions, the formation of salt bridges and charge-charge interactions.

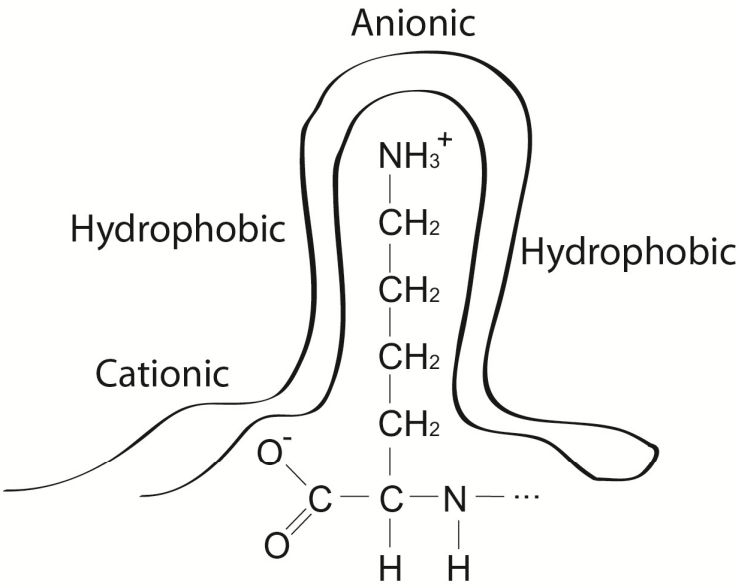
Anionic
Hydrophobic
Hydrophobic
Cationic
NH3+
CH2
CH2
CH2
CH2
O-
C
C
N
O
H
H

1.4.1 Plasminogen activation

Pg is synthesized in the liver and exists in two states: glu-Pg and lys-Pg with respective half-lives of 50 hr and 20 hr. Glu-Pg, the native form, is named for its N-terminal glutamic-acid residue and remains in a closed conformation due to intramolecular interactions between lysine^{50} and or lysine^{62} of the PAN domain with kringle 5 (Figure 6)[61]. As mentioned above, activation of Pg requires a specific cleavage event between arginine^{561}- valine^{562}, which creates a new N-terminal, non-polar valene ^{562} residue which interacts with aspartate^{740}. This cleavage and re-association causes a conformational shift which stabilizes the protease oxyanion hole and substrate binding pocket around the catalytic triad, composed of histidine^{603}, aspartate^{646} and serine^{741} forming fully Pm[65].

The closed conformation of native glu-Pg effectively buries the arginine^{561}-valine^{562} activation site within the molecule, making it relatively unreceptive to activation by PAs (Figure 6). Lys-Pg is formed when a second plasmin protease creates a cleavage between lysine^{76} and lysine^{77}, causing the removal of the PAN domain and a significant opening of the molecule, allowing PAs to gain access to the activation site[66]. Conversely glu-Pg may also bind the lysine residues of either a cell-surface Pg receptor or Pm substrates such as partially degraded fibrin and enter a more relaxed conformation. This relaxation is thought to be due to external lysine residues competing with the PAN domain lysine for binding at K5[61]. This release of the intramolecular lysine binding allows for PAs to access and cleave the activation site, forming glu-Pm. Glu-Pm is able to autocatalytically cleave lysine^{76} and lysine^{77} removing the PAN domain and

spontaneously become lys-Pm. Interestingly, the cleavage between lysine^{76} and lysine^{77} in glu-Pg, forming lys-Pg, may be accomplished by either lys-Pm or glu-Pm.

Figure 6. Plasminogen activation. Lys-Pg is formed from glu-Pg by a Pm dependent cleavage between lysine^{76} and lysine^{77} causing the removal of the PAN domain and a significant opening of the molecule. The open conformation allows Pg activators to cleave Arg^{561}-Val^{562} activating the lys-Pg to lys-Pm. Conversely binding glu-Pg to either fibrin or cell surface receptors allow the molecule to adopt a more relaxed conformation which facilitates cleavage by Pg activators forming glu-Pm. Glu-Pm is able to autocatalytically cleave lysine^{76} and lysine^{77}, removing the PAN domain and becoming lys-Pm.

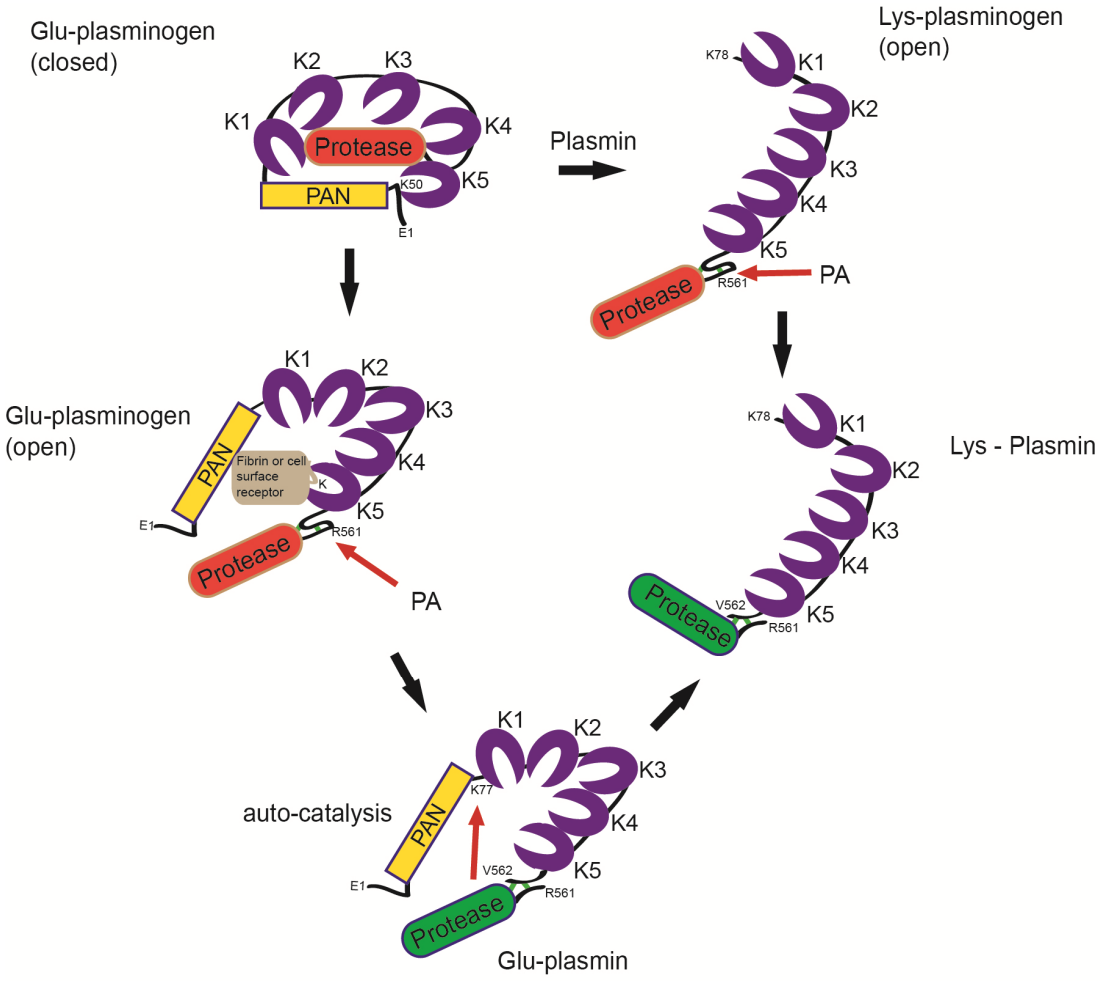
Glu-plasminogen
(closed)
K2
K3
K1
K4
Protease
PAN
K50
K5
E1
Plasmin
Lys-plasminogen
(open)
K78
K1
K2
K3
K4
K5
R561
PA
Protease
Glu-plasminogen
(open)
K1
K2
K3
PAN
Fibrin or cell
surface
receptor
K
K4
K5
E1
R561
Protease
PA
K78
K1
K2
K3
K4
Protease
V562
R561
K5
Lys - Plasmin
auto-catalysis
K1
K2
K3
PAN
K77
K4
V562
K5
E1
R561
Protease
Glu-plasmin

1.4.2 Plasminogen activators

Urokinase-type plasminogen activator (uPA) is secreted by various cell types in a precursor form as a 411 amino acid, single-chain urokinase-type plasminogen activator (scuPA)[67]. The scuPA binds to its cell surface receptor (uPAR) where it is cleaved at lysine[158]- isoleucine[159] by Pm to form the active two chain form (tcuPA). This dual activation event in which Pm activates its own activator, is known as reciprocal zymogen activation and represents a critical step in the self-amplification of active Pm[68]. UPA contains three domains, the growth factor domain used for association with uPAR, a kringle domain and the active protease domain[69].

Tissue-type plasminogen activator (tPA) is structurally related to uPA and like uPA is synthesized as a single chain (sctPA) precursor which becomes cleaved by Pm to form the active two-chain tPA (tctPA)[70]. tPA is released by endothelial cells into circulation in response to a number of stimuli[71]. tPA contains two kringle domains which allow it to preferentially bind fibrin, which increases the proteolytic activity of tPA for Pg by 1,000-fold[72]. Fibrin binding of tPA and plasmin reduces susceptibility to inhibition by plasminogen activator inhibitor-1 (PAI-1) and α2-antiplasmin (discussed below). Interestingly, the function of the uPA kringle domain has yet to be identified, the uPA/uPAR complex is able to co-localize with A2T through the association of both complexes with glycosphingolipid-enriched microdomains or "lipid rafts"[73,74]. Pm activated by tPA is thought to be associated with vascular response to injury in concert with endothelial cell annexin-A2 heterotetramer acting as the binding partner for both tPA and Pg[75]. Alternatively, tPA activated Pm occurs upon fibrin clot dissolution with

fibrin acting as the binding partner for both tPA and [76]. Plasmin activated by uPa is more commonly associated with cellular movement and tissue remodelling[67].

1.4.3 Inhibitors of plasminogen activation

In addition to the closed, unresponsive conformation adopted by glu-Pg, inhibition of Pm activation is tightly controlled at two levels. The Pg activator inhibitors (PAIs) are a subgroup of serine protease inhibitors (serpins), whose members include PAI-1, PAI-2, PAI-3 and protease nexin 1 (PN-1). PAIs inhibit tPA, both sctPA and tctPA, as well as tcuPA. All serpins utilize the same mechanism of inhibition, in which a reactive center loop mimics a specific substrate and allows the formation of an inactive complex with the target protease in a 1:1 stoichiometry[77,78]. Disassociation of the inactive complex occurs at differing rates depending on the protease-serpin pair and results in the release of a cleaved serpin peptide. Serpins have particularly high target protease specificity; however the specificity is not absolute, allowing some serpins to act as backup-inhibitors[79].

Like the PAs, Pm activity is also controlled by serpins. These serpins include α2-antiplasmin, α2-macroglobulin and α1-antichymotrypsin[80]. The presence of a lysine analogue reduces binding of Pm and α2-antiplasmin by 100-fold however the exact α2-antiplasmin residues partaking in Pm binding have not yet been defined[79]. Both lysine^{436} and lysine^{452} have been reported to be the key residues responsible for Pm binding in the C-terminus of α2-antiplasmin; however it was also noted that several internal lysine residues participated in kringle tethering[79]. Therefore, it is likely that several lysine-kringle interactions occur between Pm and α2-antiplasmin.

1.5 Plasminogen receptors

Although glu-Pg may be activated in solution, much more effective activation is achieved upon cell surface localization with PAs, allowing for a 11-60 fold reduction in the Michaelis constant Km[81]. Receptor binding confers many benefits to the proteolytic system. Active Pm remaining associated with the cell surface is available to convert receptor bound glu-Pg to lys-Pg. Additionally cell-surface Pm allows for a localization of proteolysis to the pericellular area. Furthermore, Pm bound to cell surface receptors confers protection from inhibitors[81].

Pg receptors (Pg-Rs) are a heterogeneous group with a nearly ubiquitous distribution *in vivo* and an extremely high density, between $10^5 – 10^7$ receptors per cell[82]. Pg-Rs are present on most cell types including monocytes, macrophages, endothelial cells, fibroblasts, platelets, adrenal medullary cells and carcinoma cells. Thus far, the only cell types identified without Pg receptors are red blood cells and a lineage of monocytic progenitor cells[81]. For the most part, Pg-Rs are moonlighting proteins with various other cellular functions[81]. The vast majority of Pg-Rs (>95%) contain either exposed C-terminal terminal lysine residues or may be proteolysed in such a way that one becomes exposed[83] (Table 1). This common binding feature gives all Pg-Rs a similar affinity for Pg (K_D ~1μM) and renders most Pg-Rs susceptible to inhibition by carboxy-peptidases or by lysine analogues such as ε-aminocaproic acid[84]. Pg-Rs may be split into two groups; tailed Pg-Rs have a transmembrane domain and/or a cytoplasmic tail whereas tail-less Pg-Rs lack a transmembrane domain and tail. Both tailless and tailed Pg-Rs participate in activating Pm however they may do so in different biological settings[58]. The most abundant tailed Pg-Rs on leukocytes are integrin adhesion molecules

such as αVβ3, α5β1 and αMβ2[58]. The αMβ2 Pg-R functions in transmitting "outside-in" signals which culminate in the activation of kinases ERK1/2 and Akt, as well as other signals for adhesion and migration[85]. Additionally, αMβ2 has been reported to enhance Pg binding to uPA/uPAR[58].

Antibody blocking studies have shown the following tailless Pg-Rs; α-enolase, annexin 2, S100A10 and histone 2b (H2B) to be responsible for the majority of plasmin activation in monocytic cells[58]. The C-terminal lysine residue containing α-enolase was first identified on monocytes and is widely expressed on most eukaryotic cells, transformed cells and some prokaryotic cells[86]. H2B, like the other histones, contains a C-terminal lysine residue and has been identified on the cell surface[87,87,88]. Annexin 2, first identified as a Pg-R on endothelial cells and more recently found on monocytic cells has been proposed to bind Pg after a cleavage event exposes a C-terminal lysine residue, however, the protease responsible for this modification has yet to be identified[58,82]. Other studies have suggested that Pg binding to annexin 2 is facilitated through S100A10, which exists at the cell-surface in a heterotetrameric complex with annexin 2 and contains C-terminal[89-91].

Table 1. Plasminogen receptors. List of cell surface plasminogen receptors and C-terminal lysine status.

Receptor	C-terminal Lys status	Reference
Tailess PgRs		
α-enolase	Present	[92]
S100A10	Present	[93]
Annexin 2	Absent	[94]
H2B	Present	[87]
Amphoterin	Present	[95]
Cytokeratin 8	Present	[96]
S100A4	Present	[97]
HPRG	Present	[98]
Tailed PgRs		
Actin	Absent	[99]
αIIβ1	Absent	[100]
αVβ1	Absent	[101]

1.6 S100A10 structure and function

The S100 family describes a group of low-molecular weight, calcium binding proteins, whose family name is derived from the observation that they are 100% soluble in ammonium sulfate at neutral pH. S100 family members share at least 50% sequence identity and possess two EF-hand calcium binding domains separated by a hinge region[102]. The calcium binding domains are arranged with a calcium binding loop flanked by two helices in a helix–loop–helix configuration[103]. Upon calcium binding, a conformational shift functions to expose surface hydrophobic residues which mediate the binding of specific target proteins. The S100 family members typically form homodimers, which occur through non-covalent interactions of the dimerization interface created by helices I and IV and residues of the C-terminal extension[102]. The dimer arrangement and calcium dependent association with target proteins allows the S100 members to bridge homologous or heterologous proteins in response to calcium. S100 proteins are found in the cytoplasm, nucleus and on the plasma membrane, and partake in a wide variety of cellular functions including cell-cell communication, cell growth, cell shape, energy metabolism, cellular contraction and signal transduction[104].

S100A10, also known as p11, is an unusual family member in that its bridging is calcium independent due to two mutations which constitutively lock the protein into the active form[103]. S100A10 is an asymmetric protein composed of four alpha-helices. Antiparallel homo-dimerization occurs through the stacking of helices I and IV and through the interaction of hydrophobic residues within the protein core[105]. The S100A10 protein may be found as a homodimer or a heterotetramer with two annexin II monomers.

1.6.1. Annexin 2 structure and function

Annexin family members contain a core domain containing four or eight homologous segments of 70-amino acid residues and a variable N-terminal domain. The homologous segments function to bind negatively charged phospholipids through a glycosylphosphatidylinositol (GPI) anchor in a calcium dependent manner, while the N-terminal region allows for binding partner association[106,107]. The twelve N-terminal residues of annexin A2 contains an amphipathic helix which interacts with several regions of the S100A10 protein, including helix III, the C-terminal calcium binding loop and in the C-terminal extension[106-108]. The complex formed when a central S100A10 dimer bridges two annexin A2 monomers is known as the annexin A2 heterotetramer (A2T) (Figure 7). The A2T accounts for 90% of total annexin A2 in the cell and is localized to the cell surface, cytoplasm and nucleus[91]. In addition to maintaining S100A10 on the cell surface, several other functions have been ascribed to annexin A2 including endocytosis, exocytosis, vesicular transport, adhesion molecule interaction, translocation and ion channel stabilization, lipid raft organization and interfacing between cytoskeletal elements and certain membranes through F-actin binding[74,109-114].

1.6.2 The annexin-A2 heterotetramer

The A2T is composed of an antiparallel S100A10 dimer bound to two annexin 2 monomers (Figure 7). Previous findings from our laboratory and others have found A2T to be a key Pg receptor and S100A10 to be the functional unit therein[51,82,115]. As discussed in section 1.4.1, a requisite to plasmin activation is free lysine residues. S100A10 contains two C-terminal lysine residues, which have been shown to mediate Pg

and PA binding. When tethered to the cell surface with annexin 2, S100A10 fulfills the C-terminal lysine requirement for Pg binding, allowing for a suitable microenvironment for Pg activation (Figure 8). Our laboratory has shown that the loss of the C-terminal residues of S100A10 abolished Pg activation by tPA and annexin A2[116,117]. We have also utilized surface plasmon resonance to study S100A10 and A2T association with Pg and PAs on a phospholipid layer[93]. We observed that immobilized S100A10 bound tPA (Kd = 0.45 μM), Pg (Kd = 1.81 μM) and Pm (Kd = 75 nM), whereas the removal of the C-terminal S100A10 residues abolished all binding. Additionally, immobilized annexin A2 monomer did not bind either tPA or Pg but did bind Pm (Kd = 0.78 μM). Immobilized A2T bound tPA (Kd = 0.68 μM), Pg (Kd = 0.11 μM) and Pm (Kd = 75 nM) however this binding was abolished upon treatment with carboxypeptidase B, which cleaves C-terminal lysine residues. These studies served to clarify that PA and Pg binding by the A2T is mediated through the C-terminal lysines of the S100A10 dimer. Our laboratory has also reported that RNA mediated knockdown of S100A10 in cancer cells inhibits plasmin generation by 75%-90%, whereas macrophage S100A10 accounts for 45% of plasmin generation[51,118,119]. It has been reported that annexin II depletion reduces plasmin activation, however, this reduction may be due to the loss of cell surface S100A10[82,89,120].

Figure 7. Annexin A2 heterotetramer. (A2T) is composed of an antiparallel S100A10 dimer bound to two annexin 2 monomers. Annexin 2 is able to bind negatively charged phospholipids in a calcium dependent manner and associates with S100A10 through an N-terminal, amphipathic helix which stabilizes multiple polar residues in S100A10 protein. The C-terminal region of S100A10 contains two lysine residues which allow the complex to sequester plasminogen.

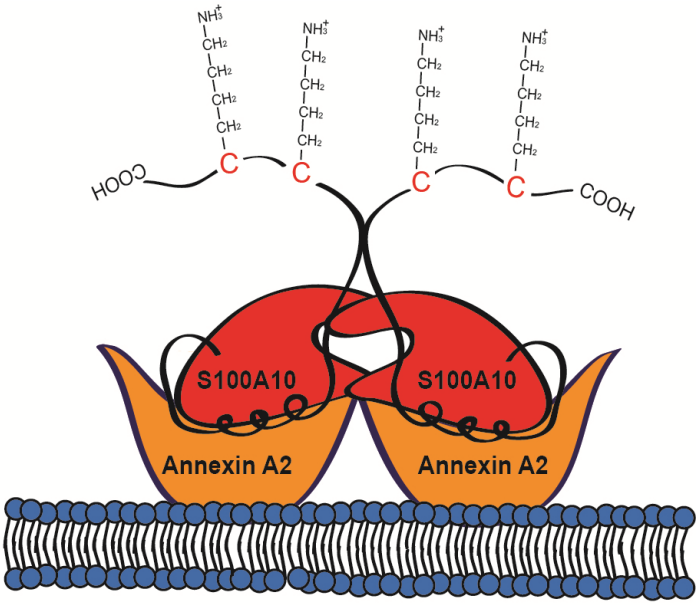
S100A10
S100A10
Annexin A2
Annexin A2

Figure 8. 3D model of plasminogen binding. Pg becomes sequestered to the cell surface through kringle binding to the C-terminal lysine of S100A10. This binding brings the zymogen into close proximity with PAs, facilitating the activating cleavage of Pg at Arg^{561}-Val^{562}. Pm may degrade fibrin, ECM components, basement membrane proteins directly or may promote proteolysis through MMP activation. This model depicts the complex formation leading to Pg activation. For clarity glu and lys-Pg, the PAN domain and PA zymogen activation have been excluded.

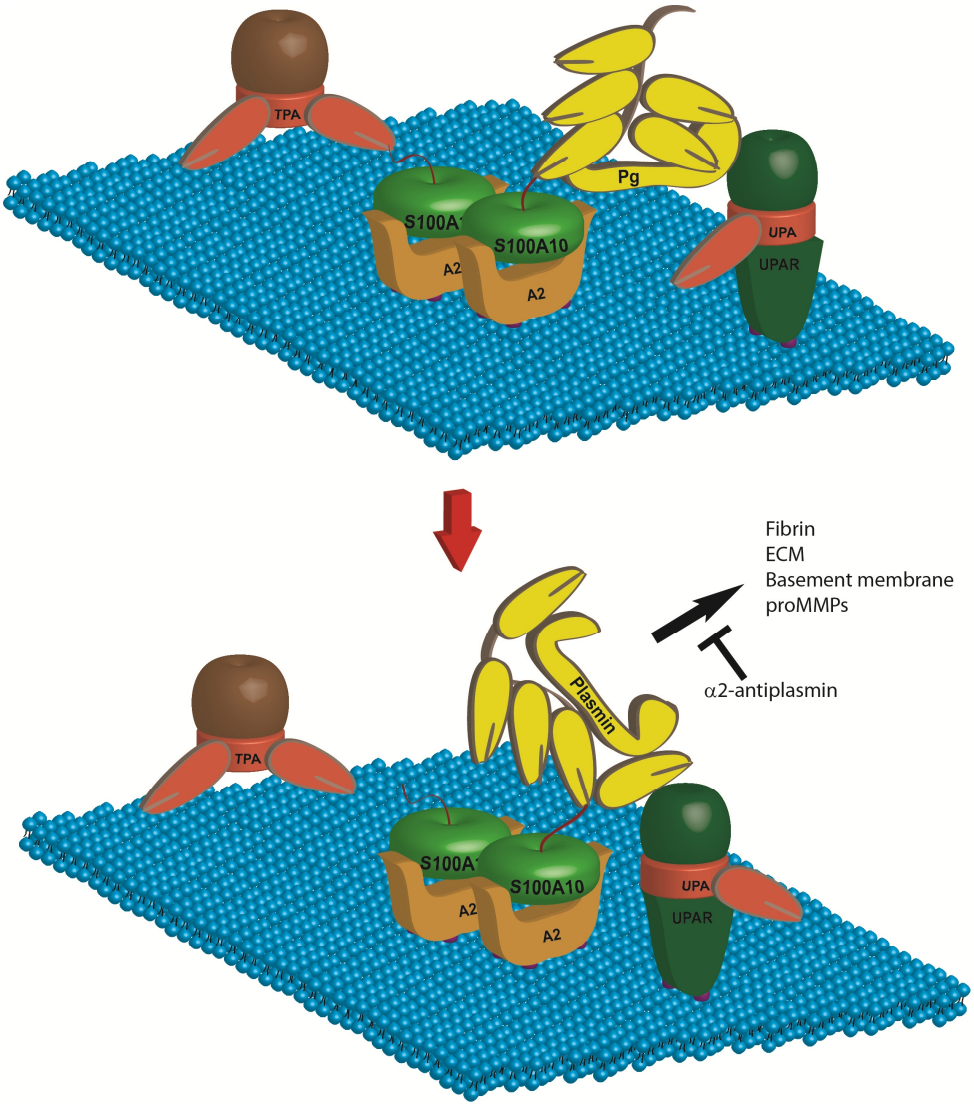
TPA
Pg
S100A
S100A10
A2
A2
UPA
UPAR
Fibrin
ECM
Basement membrane
proMMPs
α2-antiplasmin
Plasmin
TPA
S100A
S100A10
A2
A2
UPA
UPAR

1.7 Conceptual framework

Tumors require TAMs for growth progression. In order for a macrophage to respond to tumor stimuli it must exit the blood vessel through diapedesis which relies heavily on proteolysis. Our laboratory has shown that Pg-R S100A10 is responsible for Pg activation by the A2T complex and that S100A10$^{-/-}$ (S100A10-null) macrophages have a 50% reduction in their plasmin-dependent cellular invasive capability compared to wild type (WT), S100A10 expressing, macrophages[119]. Additionally, S100A10-null macrophages have a 53% inhibition in *in vivo* response to peritoneal inflammation[119].

The inability of these macrophages to respond to this inflammatory stimulus was found to be due to a reduced capability to activate plasmin and downstream proteases, such as the MMPs. We hypothesize that S100A10 expression would be a requisite for macrophage colonization of the tumor site. That is, that S100A10 facilitates the tumor promoting association of macrophages with tumor cells through the activation of plasmin and other downstream proteases (Figure 9).

Figure 9. Macrophage utilization of S100A10 for transition to the tumor site. Macrophages utilize S100A10 to activate circulating Pg to Pm and subsequently activate pro-MMP to active MMP creating a proteolytic hub. This localized proteolysis enables the macrophage to exit from the blood vessel and perform dissolution of the basement membrane, extracellular matrix and tumor stroma to reach the tumor site.

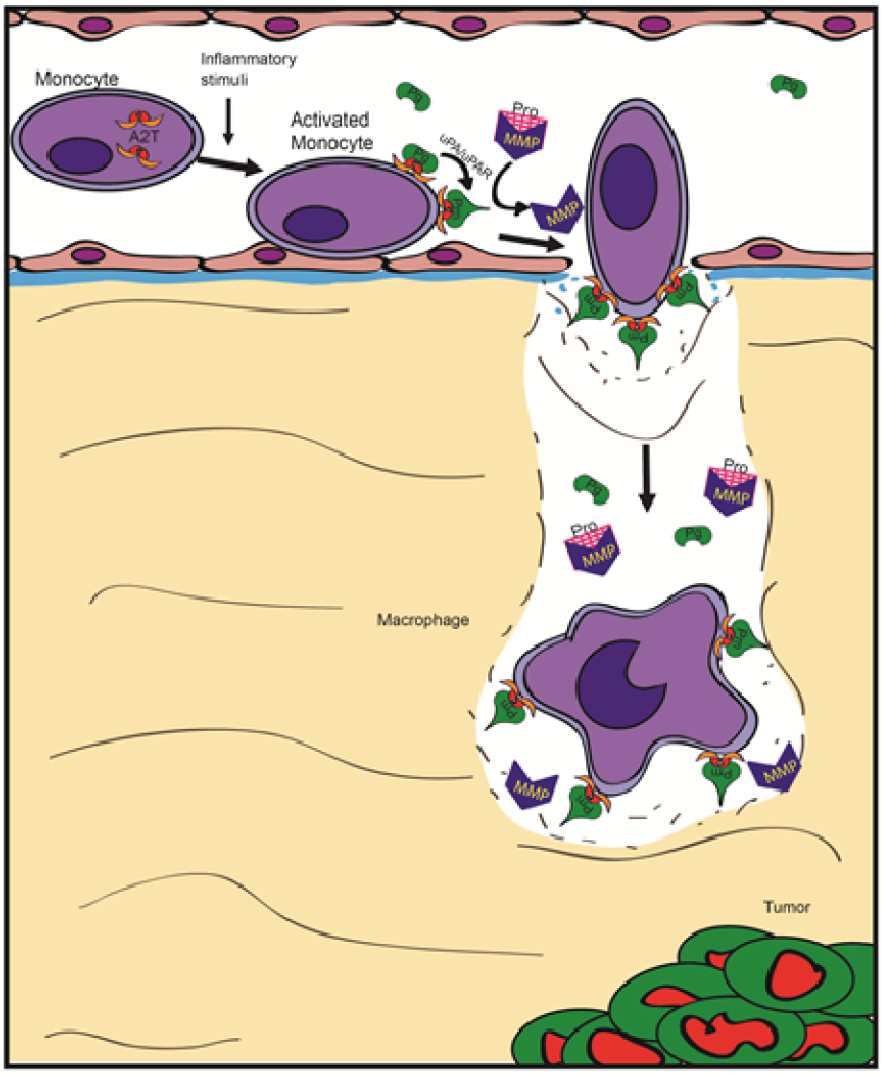
Monocyte
Inflammatory stimuli
A2T
Activated Monocyte
uPA/uPAR
Pro MMP
MMP
Macrophage
Tumor

CHAPTER 2

MATERIALS AND METHODS

2.1 Cell lines and reagents

Human HT1080 fibrosarcoma and murine Lewis lung carcinoma (LLC) cell lines were obtained from ATCC in 2006. The murine T241 fibrosarcoma cell line was obtained from Dr. Y. Cao (Karolinska Instiute). All cell lines were maintained in DMEM (Gibco) supplemented with 10% FCS (Hyclone) and penicillin/streptomycin (Hyclone) at 37^{o}C in 5% CO_2.

2.2 Plasmids

Plasmids for RNA mediated knock down of S100A10 were constructed by cloning a 64-nucleotide double stranded DNA oligomer containing two restriction site overhangs, two 19-nucleotide reverse complementary sequences, homologous to a portion of the S100A10 gene and separated by a hairpin spacer sequence into the BglII and HindIII site of the pSUPERretro-puro plasmid (Oligoengine) (Table 2). The human and murine S100A10 and respective scramble control sequences are listed in Table 2.

Table 2. Target sequences for RNAi knockdown. The 19-nucleotide target sequences analogous to segments of the respective murine and human S100A10 genes are listed below with the associated scramble control sequences. Also depicted is the full double stranded 64-nucleotide oligomer in which the target sequences are inserted within the p.super plasmid.

Plasmid Name	Target	Target Sequence
RNAi1	Human S100A10	5′- CGT GGG CTT CCA GAG CTT CT -3′
RNAiSc 1	Scramble Control	5′- GTG GGA GTT CAG AGC TTC T -3′
RNAiD	Murine S100A10	5′ - GGA TCC TCT GGC TGT GGA C- 3′
RNAiSc D	Scramble Control	5′ - GGA TCC TAG GTC TGT GGA C- 3′

BglII Hairpin HindIII

5′ - GATCCCC target sequence TTCAAGAGA target reverse comp TTTTTA - 3′

3′ - GGG target reverse comp AAGTTCTCT target sequence AAAAATTCGA - 3′

2.3 Transfection and infection

The plasmids described above were transfected into Phoenix cells, HEK293-T cells modified for viral packaging, using Lipofectamine 2000 transfection reagent (Invitrogen) as per the manufacturer's protocol. Following a 48 hr incubation period the Phoenix cell media was collected, cleared of cells by centrifugation and 0.45 μM filtration, and introduced to the LLC and HT1080 target cells. Selection for the LLC and HT1080 cells expressing the puromycin resistance cassette of the plasmid was initiated by the addition of 2 μg/mL puromycin 72 hr after the addition of the Phoenix infection media. The cells were maintained at 2 μg/mL puromycin while in tissue-culture.

2.4 Western blot analysis

Western blot analysis was initiated by the collection of target cells through trypsinization and subsequent cell lysing using a buffer containing 1% NP-40, 20mM Tris-HCl pH 8.0, 150 mM NaCl, 1mM EDTA, 1 mM EGTA and a protease inhibitor cocktail (Sigma-Aldrich). Samples of 20 μg were resolved by electrophoresis on 15% SDS-polyacrylamide gels and transferred via electroblotting onto nitrocellulose membranes. Following transfer, membranes were incubated with respective human and murine antibodies directed against S100A10 (R&D Biosystems, BD Biosciences). Immune complexes were formed by the addition of secondary 800nm near infrared red emitting antibodies (LI-COR Biosciences) and visualized on the Odyssey infrared imaging system (LI-COR Biosciences).

2.5 Plasminogen activation assay

$1x10^5$ cells per well were seeded in 96-well plates and allowed 12 hr to acclimate in FBS free DMEM. Cells were then incubated with or without uPA (50 nM) for 10 min at RT followed by 2 washes in PBS. The chromogenic plasmin substrate S2251 (100 μM) (Chromogenix Diapharma Group) was added to the cells in phenol red free DMEM followed by Pg (0.5 μM) which initiated the reaction. A spectrophotomer was utilized to follow the appearance of S2251 derived para-nitro-analine at 405 nm, taking readings every min for 2 hr.

2.6 Invasion assay

2.6.1 Cancer cells

Cancer cells ($1x10^5$ cells/well) were added to the upper reservoir of Boyden invasion chambers (BD 8 μm pore) with Matrigel (MTG) coated transwell membranes or to chambers with non-coated membranes for migratory control. The invasion assay was carried out in the presence or absence of 0.5 μM Pg (American Diagnostica) in FBS free DMEM. Cells were allowed to invade through the transmembrane insert, towards the lower reservoir containing DMEM supplemented with 10% FBS (Pg depleted) for 48 hr. Cells invading through to the underside of the insert were stained with haematoxylin and eosin (Sigma-Aldrich) and counted.

2.6.2 Macrophages

Thioglycolate-elicited macrophages ($1x10^5$ cells / well) were either added to the upper reservoir of Matrigel (MTG) coated invasion chambers (BD 8 μm pore) or to non-coated migration control chambers in the presence or absence of 0.5 μM Pg (American

Diagnostica), 100mM ε-aminocaproic acid (ACA; Sigma-Aldrich), or 25μM MMP inhibitor GM6001 (Millipore) in DMEM supplemented with 10% FBS. Macrophages were allowed a 48 hr period to invade through the insert, towards the lower reservoir which contained a monolayer of LLC cells ($1x10^5$ cells seeded for 24 hr) in 10% FBS supplemented DMEM. Macrophages on the underside of the insert were stained with haematoxylin and eosin (Sigma-Aldrich) and counted.

2.7 Mice

The S100A10$^{-/-}$ (S100A10-null) mice were generously donated by Dr. P. Swenningson (Karolinska Institute, Stockholm, Sweden). Mice were created by replacing exon 1 of the S100A10 gene, by homologous recombination, with an antibiotic resistance gene cassette introduced via microinjection into S129sv mouse oocytes. The S100A10-null S129sv mice were subsequently crossbred onto a C57BL/6 mouse background. WT control mice were also created through crossing S129sv mice to C57BL/6 mice. Further crossing experiments were performed in which the S100A10-null genotype was crossed with a polyoma middle T (PyMT) expressing C57BL/6 mouse.

Experimental mice were 6-8 week old females and experiments were performed in accordance with protocols approved by the University Committee on Laboratory Animals (UCLA) at Dalhousie University.

2.8 Macrophage collection

Macrophages from S100A10-null and WT mice were collected by peritoneal lavage with 5 mL RPMI (Gibco) 4 days after intraperitoneal injection of 2.5 ml of 4% brewers thioglycolate (Sigma). The lavage fluid was centrifuged and the cell pellet was

resuspended in red blood cell (RBC) lysis buffer containing 150 mM NH_4Cl, 10 mM $KHCO_3$, and 0.1 mM Na_2EDTA at pH 7.4 for 5 min at 4°C before centrifugation at counting on a hemocytometer. Macrophages were further purified by adherence for 4 hrs in 100 mm dishes at 37°C, at which point non-adherent (non-macrophage) cells were eliminated by aspiration. Cells were maintained in RPMI media.

2.9 *In vivo* tumor growth

Tumors were established by subcutaneous injection of $2x10^6$ cells, suspended in 100μL DMEM (Gibco), containing 10% FBS (Hyclone), into the shaved right flank of female 6-8 week old mice under 2% isoflurane anesthetization. All cell lines were found negative for mycoplasma as well as negative for a panel of murine pathogens (Charles River Comprehensive Mouse Panel 1). Tumor volume calculated as (length x $width^2$)/2.

2.10 Immunofluorescence and immunohistochemistry

Tumors, established as in Section 2.9, were harvested after 18 days of growth and cryo-protected by an incubation in 1:1 30% sucrose and optimal cutting temperature compound for 30 min (OCT; TissueTek) prior to liquid nitrogen freezing and cryostat sectioning. Tissue sections (10μm) were incubated with Rodent Block M (Biocare Medical) blocking buffer for 45 min prior to treatment with either an antibody against F4/80 (Abcam; 1:100) for macrophage identification or an antibody against CD31 (Abcam; 1:100) for 2 hr at RT. Positive F4/80 staining cells were visualized by treatment with an alkaline phosphatase secondary system (Biocare Medical) and counterstained with Mayers haematoxylin (Sigma-Aldrich). Positive CD31 staining cells were visualized by fluorescence after treatment with an Alexa-488 secondary antibody (BD Pharmingen)

and counterstained with 4',6-diamidino-2-phenylindole (DAPI; Sigma-Aldrich) on a Zeiss Axioplan 2 microscope with a filter set of BP450-490 (excitation) and BP515-565 (emission).

For anti-fibrin and proliferative cell nuclear antigen (PCNA) immunostaining, harvested 18 day old tumors, established as in Section 2.9, were fixed in 10% formalin and paraffin embedded before sectioning on a microtome to 8 μm. Sections were blocked by incubation with Rodent Block M (Biocare Medical) for 45 min at RT prior to treatment with either an antibody against fibrin (American Diagnostica Inc.; 1:20) or against PCNA (Abcam 1:500) for 2 hr at RT. Fibrin deposits and positively staining PCNA cells were visualized through horse radish peroxidase (HRP) secondary staining. Anti-PCNA treatment was counterstained with Mayers haematoxylin (Sigma-Aldrich) whereas the anti-fibrin reaction was not. Autofluorescent fibrin deposits were visualized on a Zeiss Axioplan 2 microscope with a filter set of BP450-490 (excitation) and BP515-565 (emission).

2.11 Cytokine array

A multiple sandwich ELISA, called Quantibody array, was performed by RayBiotech Inc. (Norcross G.A.) on subcutaneous LLC tumors after 14 days of growth. Briefly, tumor lysates were prepared by applying fresh tumors in lysis buffer containing 1% NP-40, 20mM Tris-HCl pH 8.0, 150 mM NaCl, 1mM EDTA, 1 mM EGTA and a protease inhibitor cocktail (Sigma-Aldrich) to a tissue homogenizer. Tumor lysates were applied to an array of cytokine-specific ‘capture’ antibodies bound to a glass slide. Following the capture of the target cytokine, a second biotin-labeled detection antibody,

which recognizes a different epitope on the target cytokine was added. The cytokine-antibody-biotin complex can then be detected by a laser scanner following the addition of a streptavidin-labeled fluorescent dye. Quantification of the target cytokines was carried out through comparisons to a standard curve created by five standards for each cytokine.

2.12 Terminal deoxynucleotidyl transferase dUTP nick end labeling (TUNEL) assay

TUNEL was performed on snap frozen, cryosectioned tumors as per the manufacturer's instructions with an alkaline phosphatase converter (*In situ* cell death detection Roche). Briefly, treatment of tumor sections with the terminal deoxynucleotidyl transferase enzyme allowed for the addition of fluorescein-dUTP to the free 3'-ends of DNA made available by the single and double stranded breaks occurring during apoptosis. An anti-fluorescein antibody coupled to an alkaline-phosphatase enzyme allowed for the amplification of the signal and subsequent visualization with a haematoxylin counterstain.

2.13 Clodrolip preparation and mouse dosing

Clodronate encapsulate liposomes were created as in Zeisberger *et al*. 2006. Briefly, 10mLs of clodrolip was created from a dry lipid mixture of 1.0 g soy phosphatidylcholine (Avanti Polar Lipids), 0.15 g ovine wool cholesterol (Avanti Polar Lipids) and 5.21µL D,L-a-tocopherol (Sigma-Aldrich), corresponding to 1 : 0.3 : 0.01 mol parts, and solubilised with 2.64 g clodronate (Sigma-Aldrich) in PBS supplemented with 230mM mannitol. The resulting multilamellar liposomes were freeze-thawed in three cycles of liquid nitrogen and 40^{o}C water bath to facilitate clodronate entrapment.

Unilamellar liposomes were created by repetitive (5-10x) filter extrusion through 400 nm membranes. Nonencapsulated clodronate was removed by overnight dialysis (12-1400 mol. Wt. cutoff; Spectrum Laboratories) against PBS-mannitol. Control liposomes (PBS-Lip) were created as above without the addition of clodronate.

An initial dose of 200 μL, corresponding to ~4 mg clodrolip per mouse, of the resultant mixture was injected into the peritoneum of mice, 4-days prior to tumor cell inoculation on day 0. Following the initial dose, mice received an additional 100 μL, corresponding to ~2 mg clodrolip per mouse, every 4 days of the tumor growth period. Injections were carried out on the following days; -4, 0, 4, 8 and 12, the tumors were harvested on day 16. Tumor volume calculated as (length x width^2)/2.

2.14 Tumor dissociation

Harvested tumors were cut into 1mm x 1mm cubes and incubated with a disassociation buffer containing 0.5mg/mL type I collagenase, 0.05mg/mL type IV collagenase, 30 U/ml DNAse and 0.1 mg/mL hyaluronidase (all from Sigma-Aldrich) in Hanks Balances Salt Solution (HBSS; Gibco) at 37^{o}C for 30 min. The resultant tumor slurry was flushed through a 70 μM cell strainer with excess PBS and the cells were collected by centrifugation at 500xg for 3 min. The cellular pellet was then resuspended in RBC lysis buffer containing 150 mM NH_4Cl, 10 mM $KHCO_3$, and 0.1 mM Na_2EDTA for 5 min at 4^{o}C before the cells were once again collected by centrifugation at 500xg for 3 min.

2.15 Flow cytometry

1-2x10^6 cells, prepared from disassociated tumors as described above, were suspended in 100 μL PBS and blocked for 30 min at 4^{o}C with antibodies against CD16/CD32 (Abcam) in order to block the FC receptors. Following blocking, cells were incubated for 30 min at 4^{o}C with antibodies against the F4/80 and CD11B macrophage markers (Abcam). The antibodies were tethered to phycoerythrin (PE) and fluorescein isothiocyanate (FITC) respectively and therefore secondary antibodies were not required. Cells were washed with PBS and resuspended in a running buffer containing 1% bovine serum albumin (BSA), 0.1% Na-Azide and 2 mM EDTA at pH 7.4 before analysis by fluorescence assisted cell sorting (FACS) on a BD FACSCalibur flow cytometer.

2.16 Clodrolip cytotoxicity assay

1x10^5 macrophages and 0.2x10^5LLC cells plated for 24 hr, in 96 well plates, prior to a 4-hr incubation with varying levels of clodrolip. Following a 24 hr recovery period, cells were subjected to an MTT assay (CellTiter 96 Promega) to assess viability, which was measured at 570 nm on a spectrophotometer.

2.17 MTT assay

An MTT (3-(4,5-Dimethylthiazol-2-yl)-2,5-diphenyltetrazolium bromide) assay was performed on macrophages and LLC cells as per the manufacturer's instructions (CellTiter 96 Promega). Briefly, 1x10^5 macrophages and 0.2x10^5 LLC cells treated with clodrolip or a vehicle control, as described in Section 2.16, were incubated with the MTT reagent, a yellow tetrazole, in 120 μL phenol red free DMEM (LLC cells) or phenol red

free RPMI (macrophages) supplemented with 10% FBS. After 1 hr the appearance of the purple farmazan, indicating mitochondrial succinate dehydrogenase activity, was quantified spectrophotometrically at 570 nm.

2.18 Adoptive transfer of splenocytes and macrophages

2.18.1 Splenocyte

A single cell splenocyte population was prepared by applying harvested and diced spleens to a 100 μm cell strainer. Cells were collected by centrifugation and RBC lysis was performed as described in Section 2.14. Splenocyte adoptive transfer was performed by intraperitoneal injection of $9x10^6$ cells, in 0.5 mL RPMI, into mice 1 day prior to subcutaneous LLC cell inoculation as described in Section 2.9.

2.18.2 Macrophage

Macrophages from S100A10-null and WT mice were collected by peritoneal lavage with 5 mL RPMI (Gibco) 4 days after intraperitoneal injection of 2.5 ml of 4% brewers thioglycolate (Sigma). The lavage fluid was centrifuged and the cell pellet was resuspended in red blood cell (RBC) lysis buffer containing 150 mM NH_4Cl, 10 mM $KHCO_3$, and 0.1 mM Na_2EDTA at pH 7.4 for 5 min at 4^oC before centrifugation at counting on a hemocytometer. Macrophages were further purified by adherence for 4 hrs in 100 mm dishes at 37^oC, at which point non-adherent (non-macrophage) cells were eliminated by aspiration. Cells were maintained in RPMI media.

An intraperitoneal adoptive transfer of $9x10^6$ macrophages in 0.5 mL RPMI was performed 1 day prior to the subcutaneous implantation of $2x10^6$ LLC cells.

An intratumoral adoptive transfer of $0.25x10^6$ macrophages in 0.1 mL RPMI was performed 4-days after the subcutaneous implantation of $2x10^6$ LLC cells.

2.19 Statistical analyses

All statistical calculations were performed in Prism (GraphPad Prism version 5.0). All error expressed as standard error of the mean (s.e.m.) and all Student *t*-tests performed were two-tailed, unpaired. Analysis of variance (Anova) was used to calculate the statistical significance between more than two groups.

CHAPTER 3

S100A10 DEFICIENT MICE DISPLAY IMPAIRED MACROPHAGE INVASION, IMPAIRED TUMOR GROWTH AND DECREASED TAM DENSITY

3.1 S100A10 deficiency impairs macrophage invasion

Thioglycolate elicited peritoneal macrophages were collected from both S100A10-null mice and WT mice and added to the upper reservoir of the Boyden transwell invasion chambers. The macrophages were given 48 hr to invade through a matrigel (MTG) coated membrane towards a murine Lewis lung carcinoma (LLC) monolayer in the lower chamber, after which the macrophages on the under-side of the insert were stained and counted. We observed that 40% fewer S100A10-null macrophages infiltrated through the membranes compared to WT derived macrophages (68 ± 6.7 S100A10-null and 112±11 WT macrophages per-field) (Figure 10A). The invasion was Pg dependent and migration was not affected by the loss of S100A10 (Figure 10B). In the absence of Pg, the number of invading cells decreased to approximately the same as in the S100A10-null cells with Pg. Treatment with the lys analog ε-aminocaproic acid (ACA) decreased the number of invading S100A10-null and WT macrophages to 36.9±4.6 and 29.3±4 cells per field respectively, which is below the Pg free control level. In the absence of an LLC monolayer there were very few invading macrophages (16.9±2.5 and 13.8±1.5 cells per field for S100A10-null and WT macrophages respectively). Treatment of cells with GM6001, a pan-MMP inhibitor, decreased invading S100A10-null and WT macrophages to 26.7±5.1 and 32.1±7.9 respectively. Migration was not affected for the most part, with the exception of the removal of the LLC monolayer; thereby removing the chemotactic gradient. Additionally

the ACA treatment caused a 30% decrease in cellular migration. These data show that S100A10 is utilized for Pg dependent invasion of macrophages.

Figure 10. S100A10 is required for plasminogen dependent macrophage invasion. S100A10-null and WT macrophages were added to the upper reservoir of Boyden invasion chambers with (A) Matrigel (MTG) coated transwell inserts or (B) non-coated inserts in the presence or absence of 0.5 μM plasminogen (Pg), lysine analog ε-aminocaproic acid (ACA) or a pan-MMP inhibitor (GM6001) in DMEM supplemented with 10% FBS. Cells were allowed to invade through the insert, towards the lower reservoir which contained a monolayer of LLC cells ($1x10^5$ cells seeded for 24 hr) in 10% FBS supplemented DMEM. Macrophages on the underside of the insert were stained with haematoxylin and eosin and counted. The data expressed as the means of 10 fields, representative of two independent experiments ± s.e.m and statistical significance of p=0.0019 was determined by unpaired Student's t test.

A.

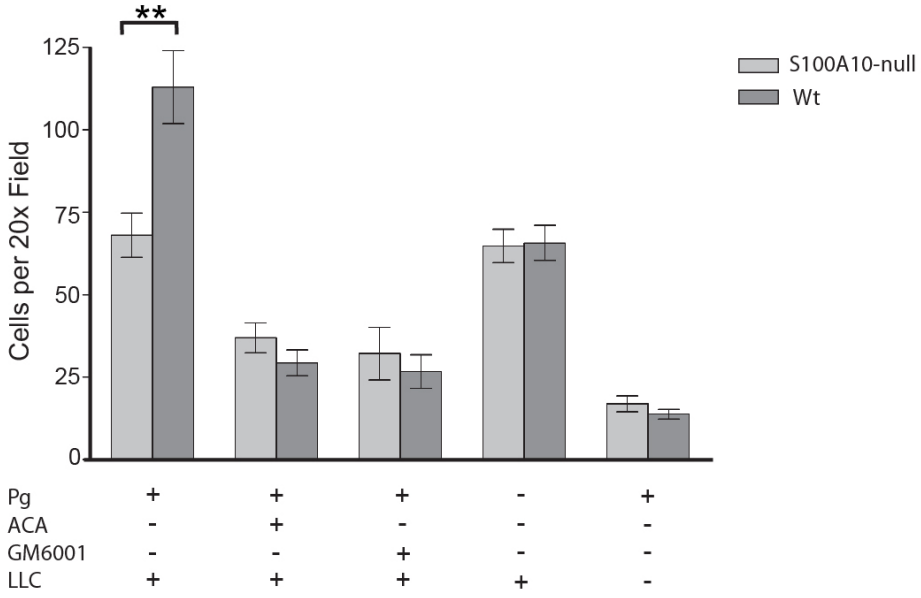
**
125
100
75
50
25
0
Cells per 20x Field
S100A10-null
Wt
Pg + + + - +
ACA - + - - -
GM6001 - - + - -
LLC + + + + -

B.

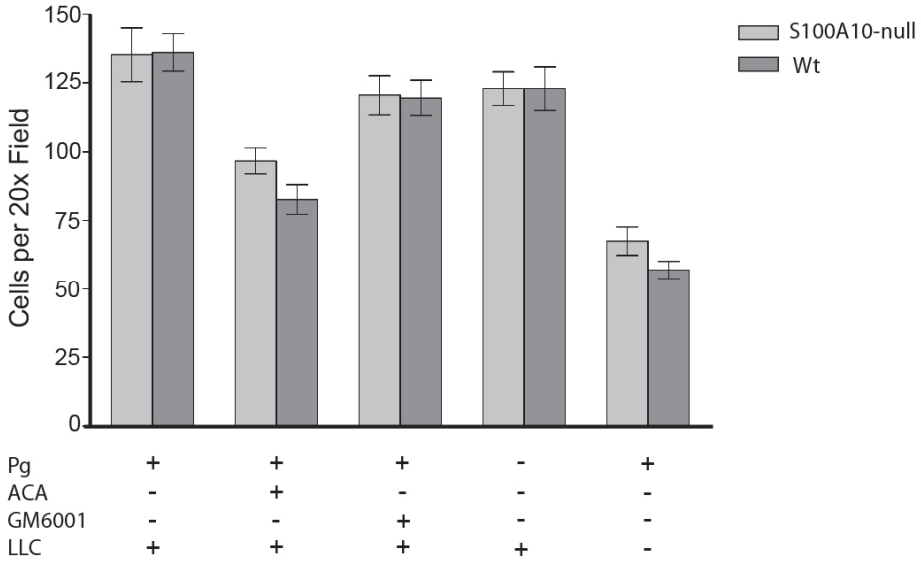
150
125
100
75
50
25
0
Cells per 20x Field
S100A10-null
Wt
Pg + + + - +
ACA - + - - -
GM6001 - - + - -
LLC + + + + -

3.2 Tumor growth in S100A10 deficient mice is severely impaired

Recruitment of macrophages to the peritoneal cavity in response to inflammatory stimuli is severely compromised in S100A10-null mice[119]. Since the tumor site is also a site of inflammation we sought to quantify the tumor-infiltrating macrophages in the S100A10-null mice. Tumors were initiated by an injection of $2x10^6$ LLC cells into the subcutaneous flank region. Surprisingly, LLC tumors in the S100A10-null mice entered growth arrest at 7 days of growth while the tumors in the WT mice grew exponentially (Figure 11A). After an 18 day growth period, the tumors grown in the S100A10-null mice were less than 10% the volume and the wet weight of tumors grown in WT mice (Figure 11B, C). In order to ensure this effect was reproducible in other tumor cell models, T241 fibrosarcoma tumors were created by an injection of $2x10^6$ T241cells into the subcutaneous flank region. Like the LLC model, the T241 tumors arrested at approximately 7 days of growth (Figure 12).

Figure 11. LLC tumor growth is impaired in S100A10-null mice. (A) Tumor growth kinetics, measured as volume, of subcutaneously established LLC tumors in both S100A10-null and WT mice. Tumor volume calculated as (length x width^2)/2. The representative data from 1 of 3 independent experiments are expressed as means of 7 tumors ± s.e.m. (B) Terminal wet weight of LLC tumors at 18 days of growth is expressed as the means of 7 tumors ± s.e.m and statistical significance of p= 0.0003 by two-tailed Student's t test. (C) Representative images of LLC tumors at 18 days of tumor growth in S100A10-null and WT mice.

A

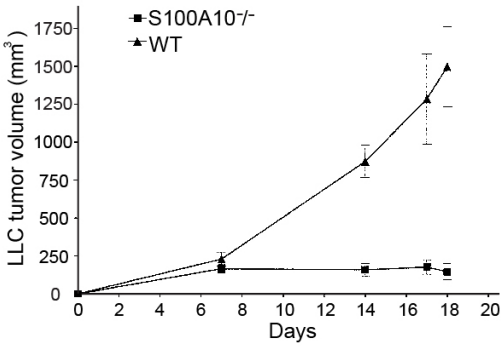
S100A10-/-
WT
LLC tumor volume (mm3)
1750
1500
1250
1000
750
500
250
0
0 2 4 6 8 10 12 14 16 18 20
Days

B

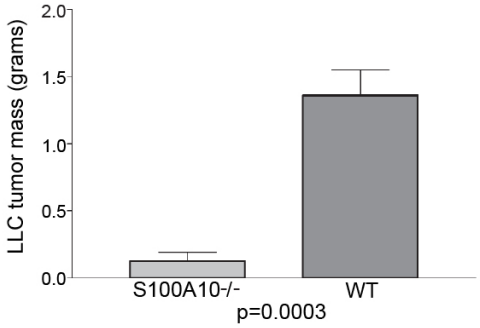
LLC tumor mass (grams)
2.0
1.5
1.0
0.5
0.0
S100A10-/-
WT
p=0.0003

C


WT
S100A10-/-
2 cm

Figure 12. T241 tumor growth is impaired in S100A10-null mice. Tumor growth kinetics, measured as volume of T241 tumors initiated by the subcutaneous implantation of $2x10^6$ T241 cells in 100 μL DMEM in both S100A10-null and WT mice. Tumor volume calculated as (length x $width^2$)/2. The representative data of two independent experiments are expressed as means of 7 tumors ± s.e.m.

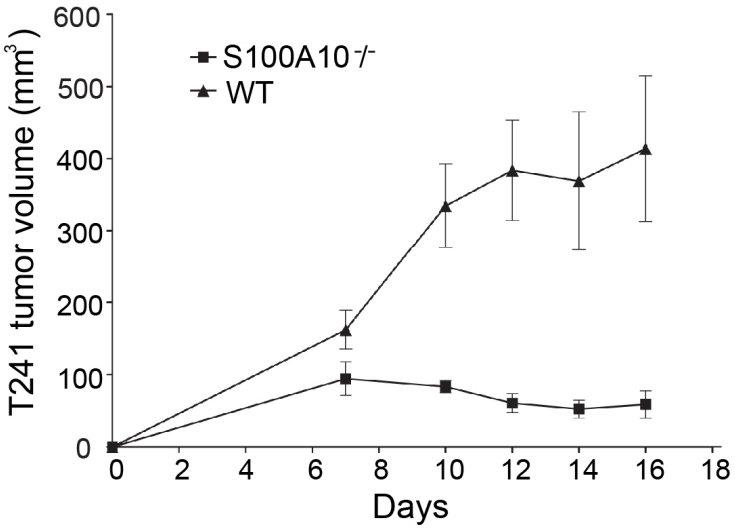
600
500
400
300
200
100
0
T241 tumor volume (mm3)
S100A10-/-
WT
0
2
4
6
8
10
12
14
16
18
Days

3.3 S100A10-null mice display drastically reduced tumor associated macrophage density

Tumors grown in the S100A10-null mice displayed a distinct inability to thrive. In order to investigate this further, an immunohistochemical detection of the F4/80 antigen was used to identify tumor infiltrating macrophages. LLC tumors grown in the S100A10-null mice displayed 12.2 ± 1.7 macrophages per 40x field whereas the tumors from the WT mice had 56.0 ± 5, representing a decrease of 78% in TAM density (Figure 13). S100A10-null macrophages could be observed in the LLC tumors along the absolute tumor tissue border whereas the WT macrophages were abundant throughout the tumor (Figure 13B).

The number of T241 tumor infiltrating macrophages in the S100A10-null mice was determined as above and found to be 21.6 ± 1.6 whereas the tumor macrophages in the WT mice was 35.1 ±1.8, representing a decrease of 39% (Figure 14).

3.3.1 Tumor cytokine level

When viewed together, these results show that the loss of S100A10 protein causes an inhibition of macrophage infiltration *in vitro,* (Section 3.1), which correlates with a decreased TAM density and a tumor growth deficiency *in vivo* (Section 3.2). In order to address whether the loss of macrophage S100A10 is responsible for the lack of TAM infiltration, we had to rule out the possibility that this TAM discrepancy could also be caused by differing levels of cytokines emanating from the tumors. A cytokine array was performed on the LLC tumors harvested from S100A10-null and WT mice and the levels of CCL-5, M-CSF, GM-CSF and MCP-1, tumor released cytokines which are associated

with macrophage recruitment and differentiation were measured[37,121,122] . The levels of tumor chemokine CCL-5 and M-CSF were significantly elevated in S100A10-null mice whereas the MCP-1 and GM-CSF levels were not significantly different (Figure 15). These results indicated that tumors grown in WT and S100A10-null mice were equally or more capable of stimulating macrophage recruitment and maturation in the tumor site compared to WT mice.

Figure 13. Reduced LLC tumor macrophage density in S100A10 deficient mice. (A) Immunohistochemical detection of F4/80 status in LLC tumors reveals the density of infiltrated tumor-associated macrophages. Tumors were harvested 18 days after the subcutaneous implantation of $2x10^6$ LLC cells in DMEM and treated to formalin fixation, OCT sucrose cryoprotection, flash frozen in liquid nitrogen and cryosectioned to 10 μM. The data expressed as the means of positive cells counted in 10 fields from 4 tumors ± s.e.m and statistical significance of $p<0.0001$ was determined by unpaired, two-tailed Student's t-test. (B) Representative tumor sections, also depicted is the increased macrophage density in the absolute tumor tissue border of a S100A10-null mouse.

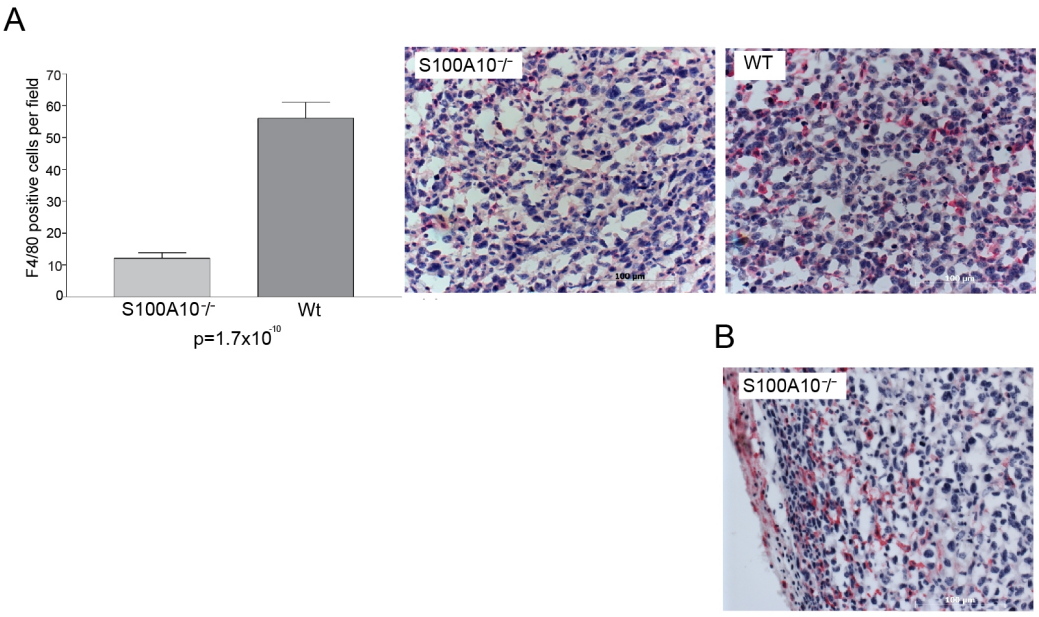
A
F4/80 positive cells per field
70
60
50
40
30
20
10
0
S100A10-/-
Wt
p=1.7x10-10
S100A10-/-
WT
B
S100A10-/-

Figure 14. Reduced T241 tumor macrophage density in S100A10 deficient mice. Immunohistochemical detection of F4/80 status in T241 tumors reveals the density of infiltrated tumor-associated macrophages. Tumors were harvested 18 days after the subcutaneous implantation of $2x10^6$ LLC cells in DMEM and treated to formalin fixation, OCT sucrose cryoprotection, flash frozen in liquid nitrogen and cryosectioned to 10 μM. The data expressed as the means of positive cells counted in 10 fields from 4 tumors ± s.e.m and statistical significance of $p<0.0001$ was determined by unpaired, two-tailed Student's t-test. Representative tumor sections shown.

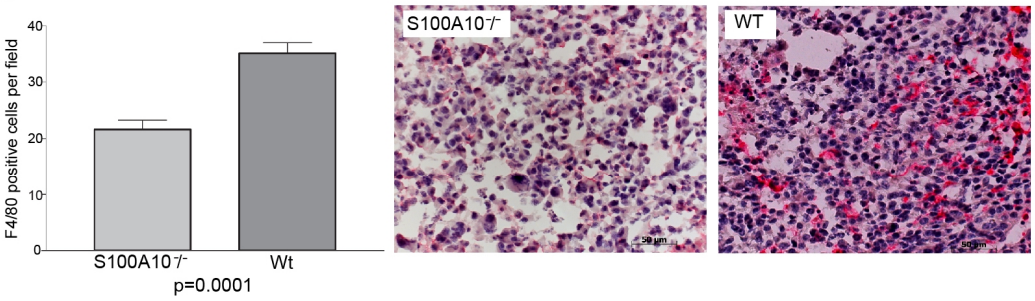
F4/80 positive cells per field
40
30
20
10
0
S100A10 -/-
Wt
p=0.0001
S100A10-/-
WT

Figure 15. LLC tumor cytokine profile from S100A10-null mice. Quantibody Cytokine array of LLC tumor showing the levels of CCL-5, M-CSF, GM-CSF and MCP-1 per tumor wet weight. CCL-5 and M-CSF levels are elevated in S100A10-null mice compared to WT, p values of 0.0353 and 0.011 respectively calculated as unpaired, two-tailed Student's t test. Levels of GM-CSF and MCP-1 in the LLC tumors are not found to be significantly different in S100A10-null mice compared to WT mice. The data expressed as the mean of cytokine levels from 8 tumors ± s.e.m and statistical significance of $p<0.0001$ was determined by unpaired, two-tailed Student's t-test.

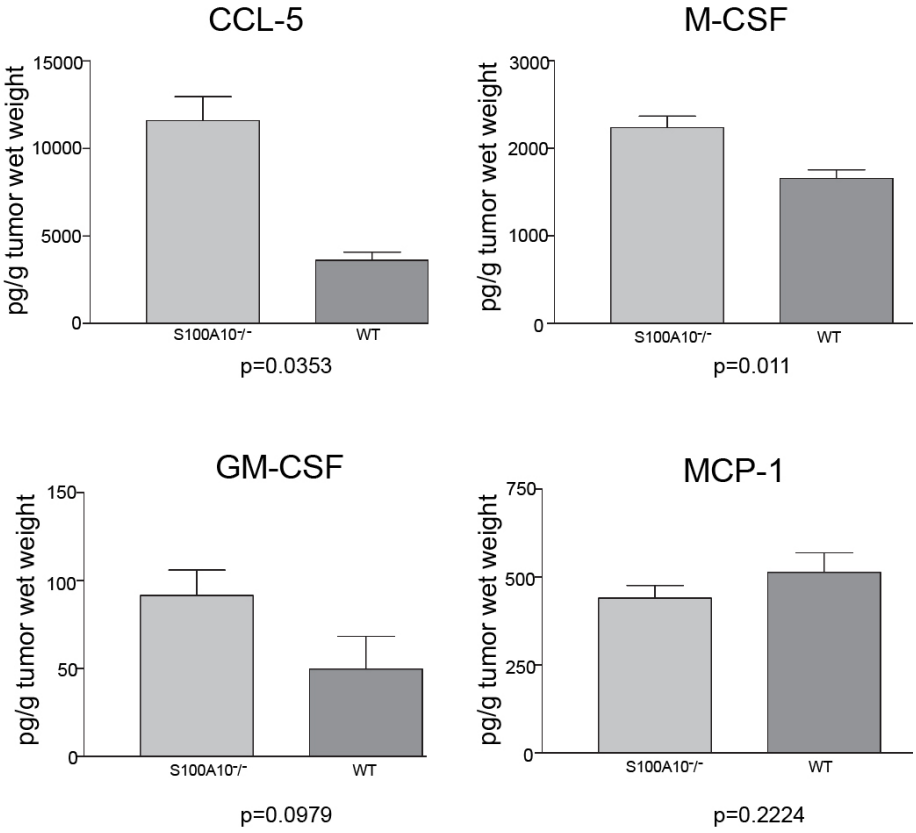
CCL-5
pg/g tumor wet weight
15000
10000
5000
0
S100A10-/-
WT
p=0.0353
M-CSF
pg/g tumor wet weight
3000
2000
1000
0
S100A10-/-
WT
p=0.011
GM-CSF
pg/g tumor wet weight
150
100
50
0
S100A10-/-
WT
p=0.0979
MCP-1
pg/g tumor wet weight
750
500
250
0
S100A10-/-
WT
p=0.2224

3.4 Quantification of the proliferative and apoptotic cells within tumors grown in the S100A10-null mice

Macrophages are known to infiltrate and support tumor growth by a number of mechanisms including the stimulation of tumor cell proliferation, immunomodulation and the stimulation of angiogenesis (see Section 1.3).

In order to address the drastic growth difference between tumors grown in S100A10-null mice and their WT counterparts, an immunohistochemical detection of the proliferating tumor cells in either mouse model was utilized. LLC tumor sections were treated with an antibody against the proliferative cell nuclear antigen (PCNA), a clamp protein expressed during DNA replication which functions to confer high processivity[123]. Quantification of the PCNA status indicated that there was an average of 808±42 cells undergoing DNA synthesis in the LLC tumors from the S100A10-null mice whereas there were 805 ±65 cells undergoing DNA synthesis in the tumors from the WT mice (Figure 16). These data, being not significantly different, indicated that there was no proliferative difference in these tumors and thus proliferating tumor cells were not the cause of the growth discrepancy.

In order to ascertain whether the tumor growth discrepancy between S100A10-null and WT mouse environments was due to unbalanced apoptosis, a TUNEL assay was performed to identify apoptotic cells within tumor sections (Figure 17). Quantification of the TUNEL positive (red) cells revealed that there was an average of 39±2 apoptotic cells per field in the S100A10-null mice and 25±2 in the WT mice, representing a 56% increase in apoptotic cells within the tumors from S100A10-null mice. As mentioned above (Section 1.3.1), TAMs have been shown to play a role in the protection of tumor cells from apoptosis induced by certain ligands. Thus, the decreased macrophage density

may be causing the increased apoptotic rate in the tumors grown in the S100A10-null mice. However in this case, the exact mechanism underlying this apoptosis is unclear.

Figure 16. Identification of proliferative cells in LLC tumors from S100A10-null and WT mice. Representative images of sections of LLC tumors, grown in S100A10-null or WT mice, treated with an antibody against the proliferative cell nuclear antigen (Brown). Tumors harvested 18 days after the subcutaneous implantation of $2x10^6$ LLC cells in DMEM and treated to formalin fixation, paraffin embedded and sectioned to 8 μM. Data from 10 fields taken across 4 tumors in two independent experiments are expressed as means ± s.e.m..These data were determined to be not significant, p=0.9683, by an unpaired, two-tailed Student's t-test

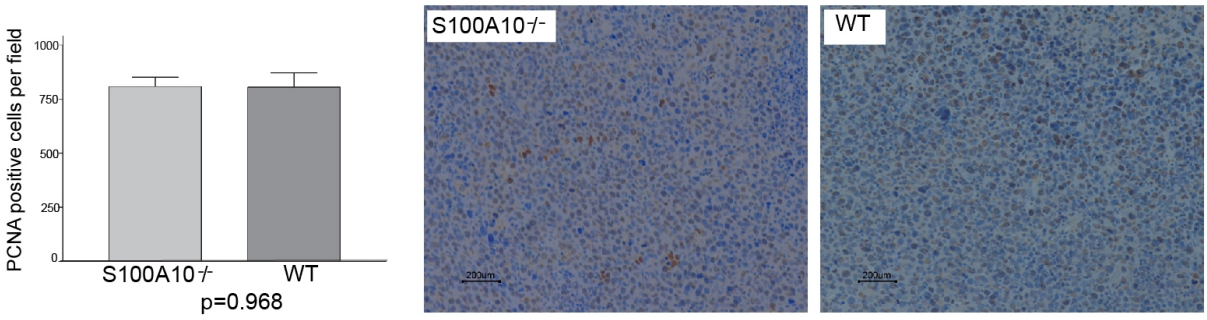
PCNA positive cells per field
1000
750
500
250
0
S100A10-/-
WT
p=0.968
S100A10-/-
WT
200um
200um

Figure 17. Identification of apoptotic cells in LLC tumors of S100A10-null mice. Representative images of LLC tumor sections, grown in S100A10-null or WT mice, treated to terminal deoxynucleotidyl transferase dUTP nick end labeling (TUNEL). Tumors harvested 18 days after the subcutaneous implantation of $2x10^6$ LLC cells in DMEM were treated to formalin fixation, paraffin embedded and sectioned to 8 μM. Sections were treated to a TUNEL assay in which double stranded DNA breaks were detected by the enzymatic addition of a fluorescein tagged dUTP residue. The fluorescein signal was amplified through the addition of an anti-fluorescein linked alkaline phosphatase enzyme. Data expressed as mean positive cells from 10 fields taken across 4 tumors in two independent experiments. Significance determined $p<0.0001$ by unpaired, two-tailed Student's t-test.

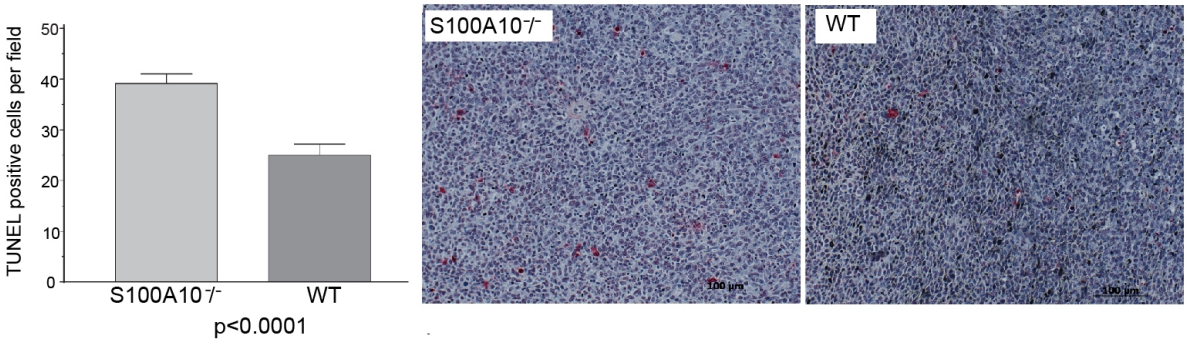
TUNEL positive cells per field
50
40
30
20
10
0
S100A10-/-
WT
p<0.0001
S100A10-/-
WT

3.5 Transient macrophage depletion reduces tumor growth in WT mice.

3.5.1 Clodrolip treatment reduces TAM density

In the S100A10-null mouse, all cells lack S100A10 therefore it is difficult to attribute the tumor growth arrest to macrophages alone. A multitude of cell types participate in cancer progression including neutrophils, fibroblasts and endothelial cells[8]. These cells may also require S100A10 to enable tumor promoting activity as S100A10 is a protein with multiple functions[107](Section 1.6). We therefore sought to address whether selective depletion of macrophages alone would inhibit tumor growth. It has been shown that macrophages may be selectively depleted in mice using liposome encapsulated clodronate[124].

LLC tumor-bearing WT mice were treated with intraperitoneal inoculations of 4 mg clodrolip/20 g mouse weight or with a liposome vehicle control (PBS-Lip) 4 days prior to subcutaneous tumor inoculation with $2x10^6$ LLC cells and 2 mg clodrolip/20 g mouse weight at day 0 and every 4 days thereafter. Fluorescence assisted cell sorting (FACS) of lysates from LLC tumors was used to quantify the extent of TAM depletion following clodrolip treatment. Typically, clodrolip treatment resulted in the depletion of approximately 75% of the F4/80 and CD11B positive TAM population, from 9% to 2%, compared to the control treated tumors (Figure 18).

3.5.2 Clodrolip treatment inhibits tumor growth

We observed that clodrolip-mediated reduction of TAMs caused a dramatic reduction in tumor growth and produced a strikingly similar tumor growth profile to that in the S100A10-null mouse (Figure 19A). The terminal wet weight of tumors grown in clodrolip treated WT mice was 0.39 ±0.09 g whereas the PBS-Lip control treated WT

mice grew tumors to 0.72 ±0.16 g, representing a 46% mass reduction (Figure 19B). The LLC tumors grown in S100A10-null mice congruently had an average wet weight of 0.3 ±0.06 g whereas the tumors in the WT mice weighed 0.9±0.2 g, representing a 67% reduction in tumor mass (Figure 19B).

In order to rule out that the reduction in tumor growth was not due to clodrolip having a cytotoxic effect on tumor cells, LLC cells and macrophages were incubated with varying concentrations of clodrolip for 4 hr and viability was assessed following a 24 hr recovery period through an 3-(4,5-dimethylthiazol-2-yl)-2,5-diphenyltetrazolium bromide (MTT) assay. Macrophages demonstrated a significant decrease in survival upon clodrolip treatment, with a mere 13.6% surviving relative to the PBS-Lip control at the highest clodrolip dose of 5mg/mL (Figure 20). The LLC cells however remained unaffected by highest dose of clodrolip, 5 mg/mL, surviving at 98% of the control treated cells.

These experiments have been undertaken to address the fact that all cells in the S100A10-null mouse lack S100A10 and it is difficult to isolate the specific tumor promoting role of macrophage S100A10. Taken together, these clodrolip experiments indicate that specifically targeting macrophages creates similar tumor results compared to those grown in the S100A10-null mouse.

Figure 18. FACS analysis of macrophage density in clodrolip treated LLC tumors
Tumors from mice treated with clodrolip or vehicle control (PBS-Lip) were harvested 16 days after the subcutaneous implantation of $2x10^6$ LLC cells in DMEM and cut into 1 mm x 1 mm cubes prior to incubation in disassociation buffer containing collagenase, DNAse and hyaluronidase. The resultant tumor slurry was applied to a cell strainer and single cells were recovered by centrifugation. Cells were incubated with antibodies against F4/80 and CD11B which were tethered to their respective secondary antibodies, phycoerythrin (PE) and fluorescein isothiocyanate (FITC). Detection of antibody binding was performed by fluorescence assisted cell sorting (FACS) on a BD FACSCalibur flow cytometer. Also depicted (below) is the isotype Igg control treated cells indicating no signal.

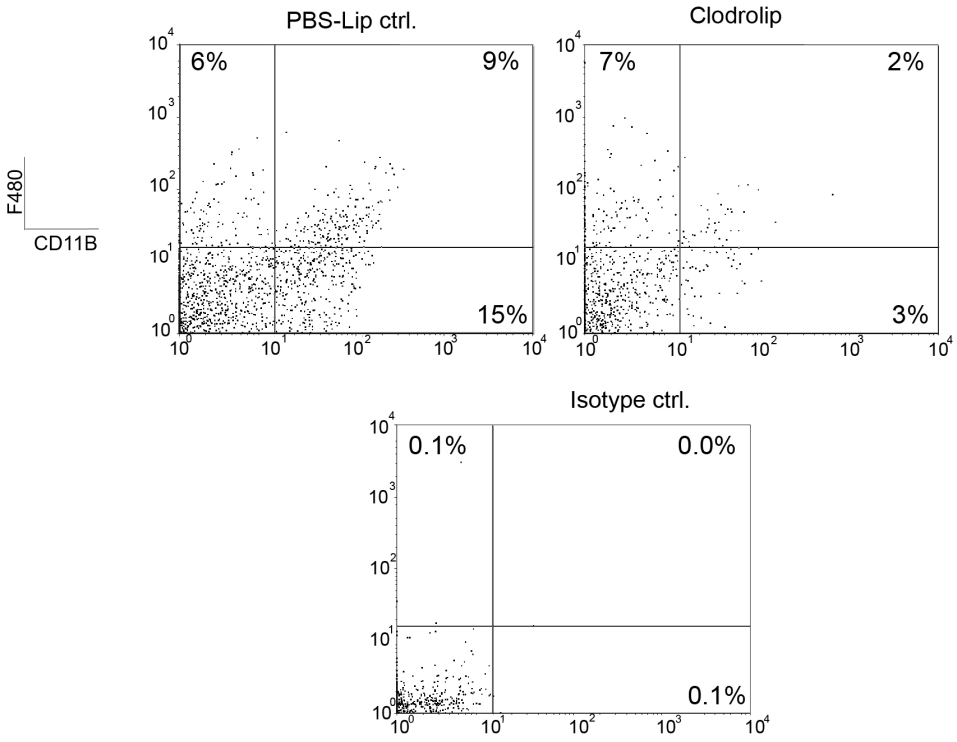
PBS-Lip ctrl.
Clodrolip
Isotype ctrl.
F480
CD11B
6%
9%
15%
7%
2%
3%
0.1%
0.0%
0.1%

Figure 19. Clodrolip treatment reduces LLC tumor growth in WT mice to S100A10-null mouse levels. (A) Tumor growth kinetics, measured as volume, of subcutaneously established LLC tumors in WT mice receiving intraperitoneal injections of either clodrolip or empty liposomes (PBS-Lip) at various points during tumor progression. Also depicted for comparison are the growth kinetics tumors in untreated WT and S100A10-null mice. (B) Terminal LLC tumor masses after 16 days of growth in a WT mouse with clodrolip or PBS-Lip treatment or no treatment (WT) or in a S100A10-null mouse. Significance values indicate two-tailed, unpaired Student's t-test and are identified as follows: *$P<0.05$, **$P<0.01$. Error bars indicate s.e.m., data shown is representative of two independent experiments, n=7.

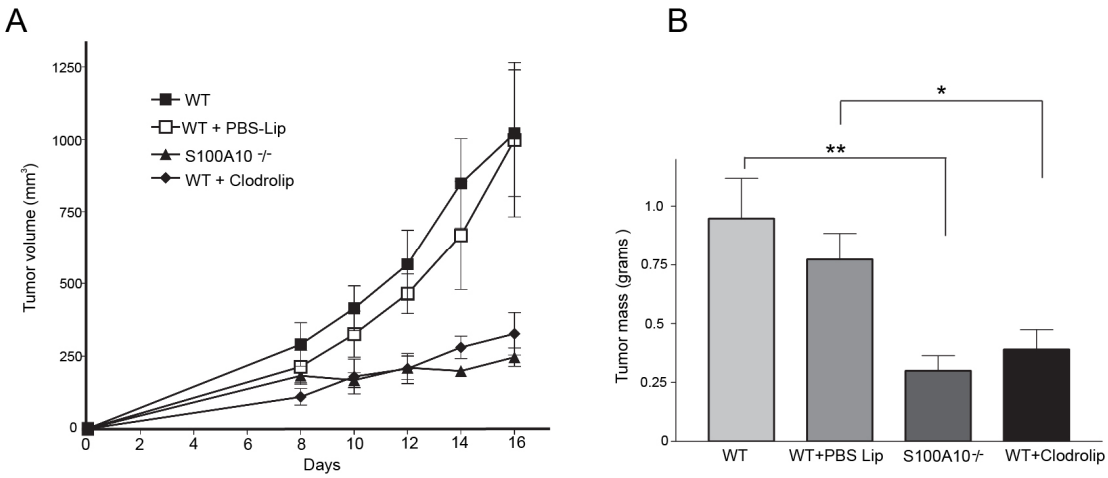
A
B
WT
WT + PBS-Lip
S100A10 -/-
WT + Clodrolip
Tumor volume (mm3)
Days
Tumor mass (grams)
WT
WT+PBS Lip
S100A10-/-
WT+Clodrolip
*
**

Figure 20. Cytotoxicity of clodrolip on macrophages and cancer cells. MTT assay of macrophage and LLC cells incubated with increasing concentrations of clodrolip for 4 hrs, followed by a 24 hr recovery period. Data expressed as mean absorbance ± s.e.m from 9 wells of clodrolip treated cells relative to treatment with an equal volume of PBS-encapsulated liposomes (PBS-Lip). Statistical significance of p= 0.0003 determined by two-tailed Student's t test

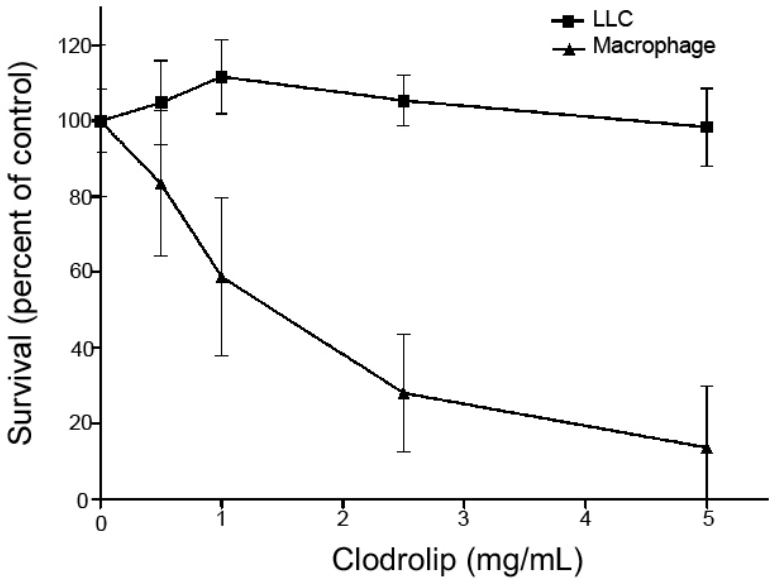
LLC
Macrophage
Survival (percent of control)
120
100
80
60
40
20
0
0
1
2
3
4
5
Clodrolip (mg/mL)

3.6 Tumor vascularity is impaired in S100A10-null mice.

3.6.1 Impaired angiogenesis

TAMs have long been implicated in the orchestration of angiogenesis (discussed in Section 1.3.3) and TAM density has been correlated with tumor vascularization and vascular hot spots within the tumor[125-128]. Therefore, we sought to quantify the vessel density within the tumors grown in the S100A10-null mouse, expecting the decreased TAM density to correlate with a decreased vessel density. LLC tumors were grown subcutaneously in mice for 18 days prior to harvesting, freezing in liquid nitrogen and subjecting the frozen tumor sections to Alexa-488 mediated CD31 immunofluorescence. As expected, the LLC tumors from the S100A10-null mouse had a decreased vessel density of 26±3 vessels per field whereas the WT grown tumors had 61±5 vessels per field. Thus a 58% reduction in vessel density was observed in associated with the S100A10-null environment (Figure 21A, B, C).

As mentioned above, this observation alone does not implicate the reduced macrophage density as the cause of the reduced angiogenesis in the S100A10-null mouse as the endothelial cells comprising the vessels are also lacking S100A10 and this might affect their angiogenic capabilities. Therefore we introduced WT macrophages, expressing normal S100A10 levels, into S100A10-null mice. The adoptive transfer of $9x10^6$ macrophages, into peritoneum of recipient mice occurred 1 day prior to subcutaneous LLC tumor cell inoculation (Adoptive transfer discussed in Section 4.6). Following an 18 day growth period, the tumors were harvested, processed and treated to immunohistochemistry, as described above. Surprisingly, the tumor vessel density in the S100A10-null mice receiving transferred WT macrophages was equivalent to the WT

vessel density; 62±5 and 61±5 respective vessels per field (Figure 21A, D). This observation indicated that the S100A10-null endothelial cells had retained the ability to vascularize the tumor; however they required the presence of S100A10 expressing macrophages. In order to ensure that this increase in tumor vascularization was specific to S100A10 expression and not a general effect of macrophage addition, WT macrophages were also adoptively transferred into WT mice bearing LLC tumors. The vessel density observed in these tumors was no different from the tumors grown in WT mice without the macrophage addition, suggesting that endogenous macrophage recruitment was sufficient to support angiogenesis to the full extent in WT mice (Figure 21A, E).

3.6.2 Impaired fibrin clearance

Multiple autofluorescent occlusions were identified within CD31 positive blood vessels in the tumors from the S100A10-null mice (Figure 22A, B), whereas the tumors from the WT mice had none (Figure 22C). Since fibrin is the main substrate of Pm, we used HRP mediated fibrin immunohistochemistry to identify the autofluorescent occlusions as fibrin depositions within the S100A10-null vessels (Figure 22E). Similarly, fibrin immunohistochemistry was used to quantify the fibrin depositions within LLC tumor sections. Tumors grown in S100A10-null mice had an average of 30±3 fibrin deposits whereas tumors from WT mice had 16±2 deposits, representing an increase of nearly 200% (Figure 23).

It is well known that tumors have an increased ability to activate fibrinogen to fibrin, forming clots which accumulate in blood vessels[129]. Vessels in the WT mice express S100A10 and can produce Pm to clear the fibrin accumulation, whereas the

S100A10-null endothelial cells do not (Figure 24). Alkaline phosphatase mediated anti-S100A10 immunohistochemistry of tumor sections was used to identify that while cancer cells express S100A10, the tumor associated endothelial cells in the S100A10-null mice do not (Figure 24). It is also of interest to note the cells circulating within the vessels, most likely lymphocytes, stain positively for S100A10 expression in the WT mice and not in the S100A10-null mice (Figure 24).

The S100A10-null endothelial cells have a reduced fibrinolytic activity, thereby causing the accumulation of fibrin in the tumor vasculature. Thus, the loss of tumor growth in the S100A10-null mice could be explained, in part, by the loss in TAM recruitment, which in turn impairs tumor angiogenesis and an inability of the existing vasculature to maintain vascular fluidity.

Figure 21. Tumor vascularization impaired in S100A10-null mice. (A) Tumors harvested 18 days after the subcutaneous implantation of $2x10^6$ LLC cells in DMEM and treated to formalin fixation, paraffin embedded and sectioned to 8 μM. Tumor sections were treated to anti-CD31 immunofluorescence, representative data from two independent experiments expressed as mean LLC tumor vessels per field ± s.e.m. from 10 fields taken across 4 tumors. Statistical significance of $p<0.0001$ was determined by one-way Anova with Tukey post-test analysis. Representative images of (B) S100A10-null mice, (C) WT mice, (D) S100A10-null mice receiving an adoptive transfer of WT macrophages or (E) WT mice receiving the same transfer are shown.

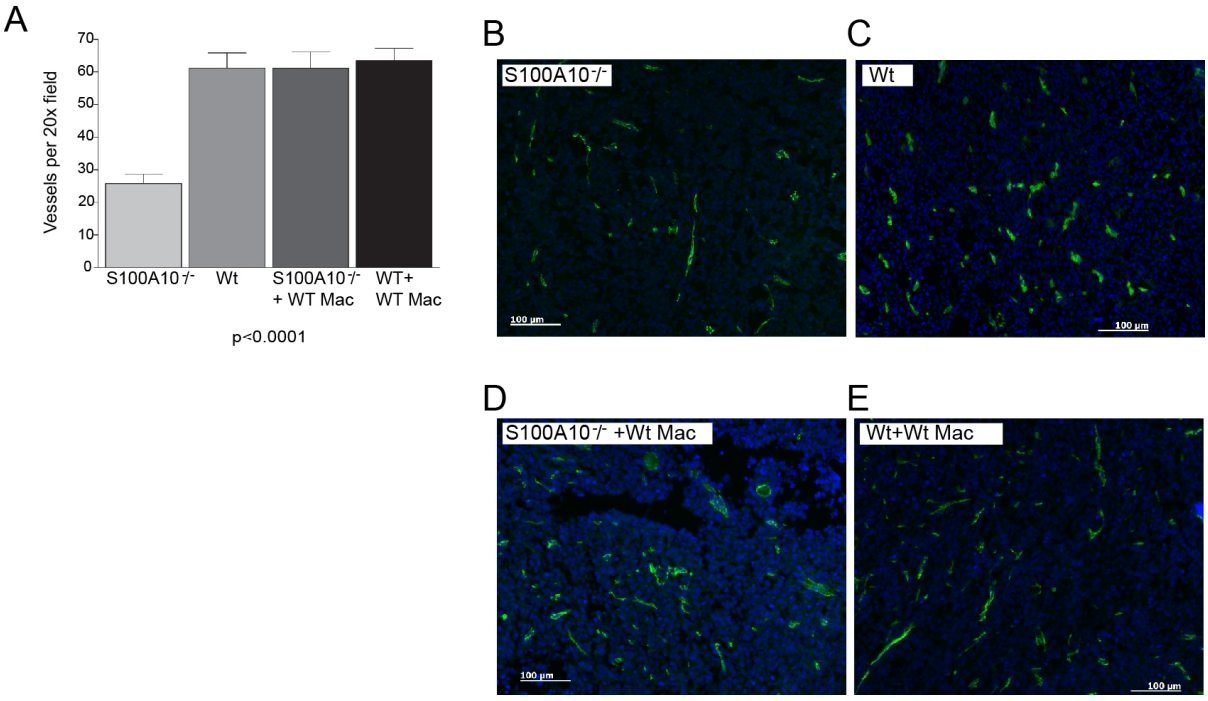
A
Vessels per 20x field
70
60
50
40
30
20
10
0
S100A10-/-
Wt
S100A10-/- + WT Mac
WT+ WT Mac
p<0.0001
B
S100A10-/-
100 µm
C
Wt
100 µm
D
S100A10-/- +Wt Mac
100 µm
E
Wt+Wt Mac
100 µm

Figure 22. Autofluorescent vessel occlusions in tumors from S100A10-null mice are comprised of fibrin. Tumors harvested 18 days after the subcutaneous implantation of $2x10^6$ LLC cells in DMEM and treated to formalin fixation, paraffin embedded, sectioned to 8 μM and treated to anti-CD31 immunofluorescence. Representative images of autofluorescent fibrin occlusions (yellow) (A, B) in CD31 positive staining vessels (green). Also depicted (C) are CD31 positive tumor vessels in tumors from WT mice. HRP mediated anti-fibrin immunohistochemistry (E) identifying a fibrin occlusion (left) within an LLC tumor from an S100A10-null mouse being associated with autofluorescence (right).

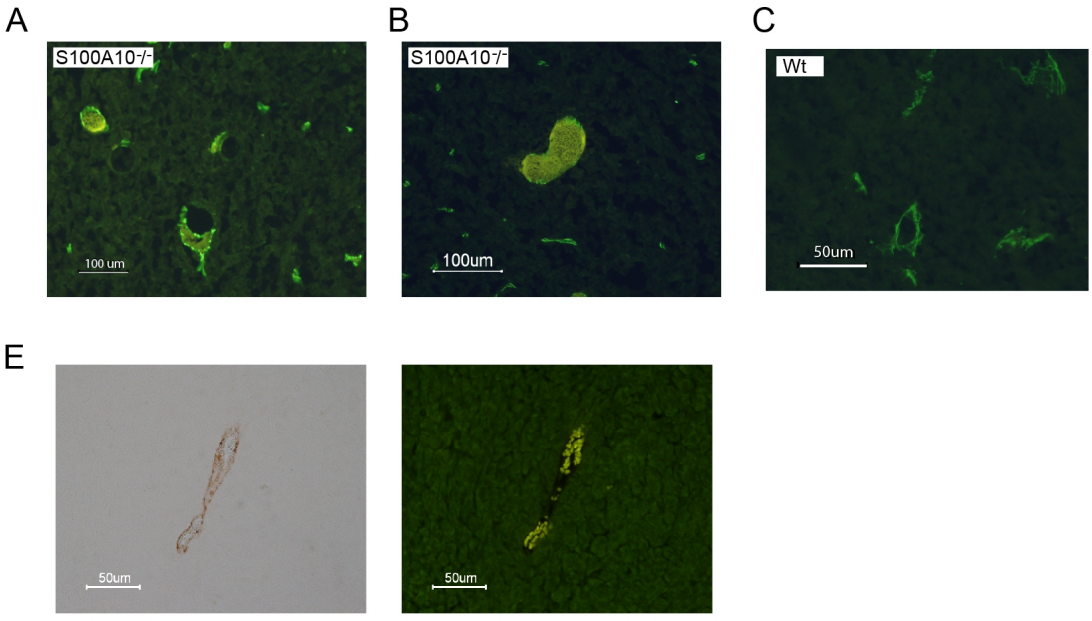
A
S100A10-/-
100 um
B
S100A10-/-
100um
C
Wt
50um
E
50um
50um

Figure 23. Increased fibrin deposition and fibrin occluded vessels in tumors from S100A10-null mice. Tumors harvested 18 days after the subcutaneous implantation of $2x10^6$ LLC cells in DMEM and treated to formalin fixation, paraffin embedded, sectioned to 8 μM and treated to horse radish peroxidase based anti-fibrin immunohistochemistry. Positive staining fibrin deposits were counted, data expressed as mean fibrin depositions per 10 fields ± s.e.m. taken across 4 tumors in two independent experiments. Representative images are shown and statistical significance of p=0.009 was determined by Student's two tailed, unpaired t-test.

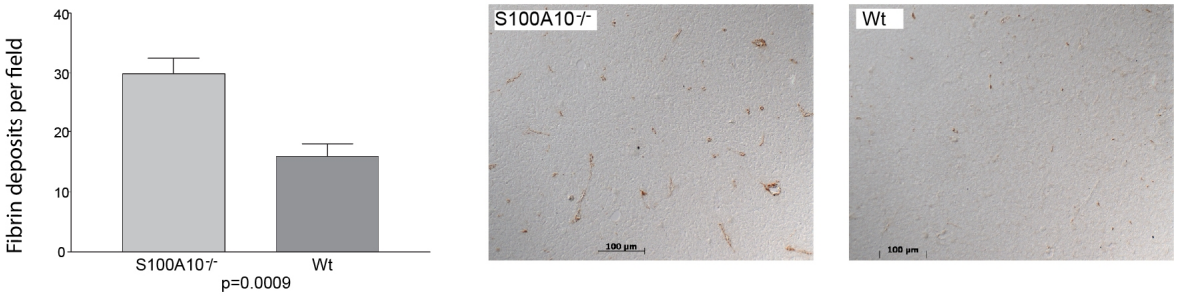
Fibrin deposits per field
40
30
20
10
0
S100A10-/-
Wt
p=0.0009
S100A10-/-
100 µm
Wt
100 µm

Figure 24. Endothelial cells forming tumor vessels express S100A10. Tumors harvested 18 days after the subcutaneous implantation of $2x10^6$ LLC cells in DMEM and treated to formalin fixation, paraffin embedded, sectioned to 8 μM. Sections were treated to anti-S100A10 immunohistochemistry linked to an alkaline phosphatase secondary antibody system. Haematoxylin counterstain allows for the histological identification of endothelial cells (arrows) lining blood vessels. Micrographs were acquired under oil-immersion at 63x magnification.

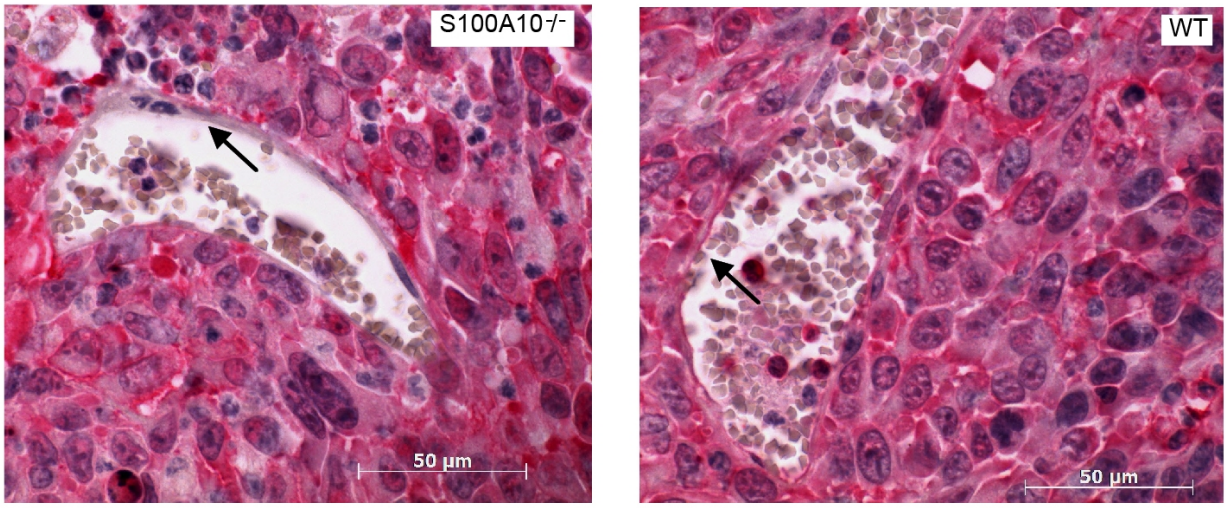
S100A10-/-
50 µm
WT
50 µm

3.7 Adoptive transfer of macrophages alters tumor growth

3.7.1 Intraperitoneal addition of macrophages

Thus far, we have established that tumors grown in the S100A10-null mice experience growth arrest and those tumors have low macrophage density. Additionally we have shown that transiently depleting macrophages creates a similar growth arrest phenotype in WT mice. To further this line of investigation, we tested whether the addition of S100A10 expressing macrophages could reverse the tumor growth arrest occurring in the S100A10-null mice via an adoptive transfer.

The initial proof of principle experiments were carried out using spleens harvested from WT mice and processed into a single cell splenocytes mixture. A murine spleen contains 8-9x10^7 cells, approximately 10% of which are macrophages, the remaining portion is mostly B and T cells and various other blood cells including neutrophils. The intraperitoneal injection of 9x10^6 splenocytes occurred 1 day prior to LLC implantation. We observed a significant boost in tumor growth to approximately half the rate of tumor growth in the WT mouse (Figure 25). These data indicating that transferred WT cells were indeed capable of altering the arrested tumor growth in the S100A10-null mice.

Macrophages, collected by thioglycolate elicitation from WT mice, were injected into the peritoneum of S100A10-null mice 1 day prior to subcutaneous tumor cell injection. We observed that after 18 days of tumor growth, the transfer of WT macrophages caused an increase in tumor volume in the S100A10-null mice by 2.5 fold, being equal to 73% of the volume of WT tumors at 18 days (Figure 26). Tumors in the S100A10-null mice not receiving the WT macrophage transfer were only 28% the

volume of WT grown tumors at day 18 (Figure 26). The intraperitoneal addition of WT macrophages to WT mice did not alter the tumor growth profile (Figure 26). Similarly, the addition of S100A10-null macrophages to S100A10-null mice via the peritoneum also had no effect on tumor growth.

3.7.2 Intratumoral addition of macrophages

We have established that S100A10-null macrophages have a deficit in proteolysis and therefore have a decreased ability to reach the tumor site, causing diminished tumor growth. However, we have yet to address whether or not S100A10-null macrophages retain tumor promoting functionality, had they the ability to reach the tumor site. To this end, S100A10-null macrophages were directly injected intratumorally into LLC-bearing S100A10-null mice at 4 days after tumor cell inoculation. In contrast to the intraperitoneal injection, we observed that the direct tumor injection of S100A10-null macrophages stimulated tumor growth in the S100A10-null mice to similar levels to that in WT mice (Figure 27).

These results indicate that the tumor growth deficit in the S100A10-null mouse could be overcome by S100A10 expressing WT macrophages infiltrating into the tumor from the peritoneum, or by the direct intratumoral delivery of S100A10-null macrophages. Thus, macrophages lacking S100A10 are capable of stimulating tumor growth; but lack the ability to transit into the tumor. Additionally, the transfer of WT macrophages by either route had no effect on tumor growth in the WT mice, suggesting that endogenous macrophage recruitment was sufficient to support tumor growth in WT mice.

Figure 25. Intraperitoneal adoptive transfer of WT splenocytes effects tumor growth in S100A10-null mice. S100A10-null mice receiving an intraperitoneal injection of of $9x10^6$ WT splenocytes were subcutaneously injected with $2x10^6$ LLC cells on the following day. The growth kinetics of the resultant LLC tumors are represented as mean tumor volume ± s.e.m. relative to time of 5 tumors. Also depicted for comparison are the typical LLC growth profiles of tumors grown in WT and S100A10-null mice. Volumes calculated as (length x width^2)/2. Data expressed as mean volume ± s.e.m. of 7 tumors from two independent experiments.

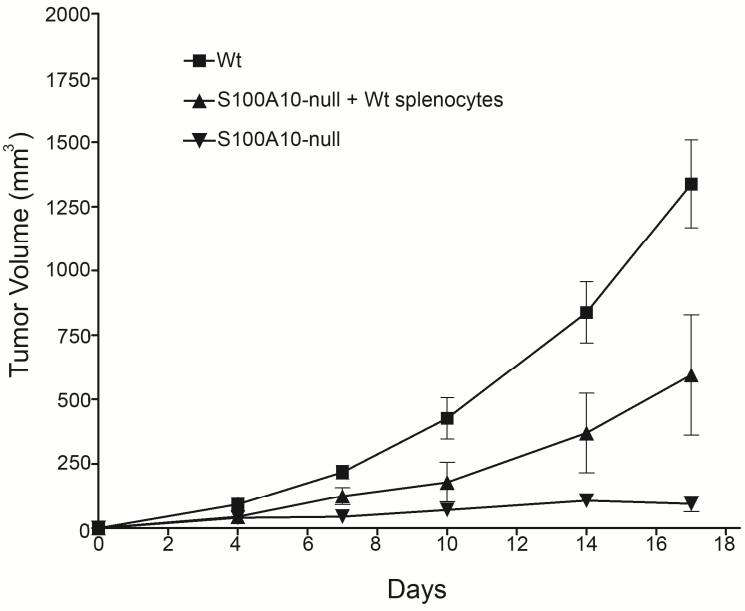
Wt
S100A10-null + Wt splenocytes
S100A10-null
Tumor Volume (mm3)
Days
2000
1750
1500
1250
1000
750
500
250
0
0
2
4
6
8
10
12
14
16
18

Figure 26. Intraperitoneal adoptive transfer of macrophages effects tumor growth in S100A10-null mice. (A) S100A10-null or WT mice receiving an intraperitoneal injection of $9x10^6$ S100A10-null or WT macrophages were subcutaneously injected with $2x10^6$ LLC cells on the following day. The growth kinetics of the resultant LLC tumors are represented as mean tumor volume ± s.e.m. relative to time of 7 tumors per treatment. Volumes calculated as (length x width^2)/2. (B) The corresponding terminal LLC tumor masses after 18 days of tumor growth are expressed as mean ± s.e.m. of 7 tumors. Statistical significance calculated by two-tailed, unpaired Student's t-test relative to $S100A10^{-/-}$ identified as follows: *P<0.05, **P<0.01, ***P<0.001, NS= Not significant.

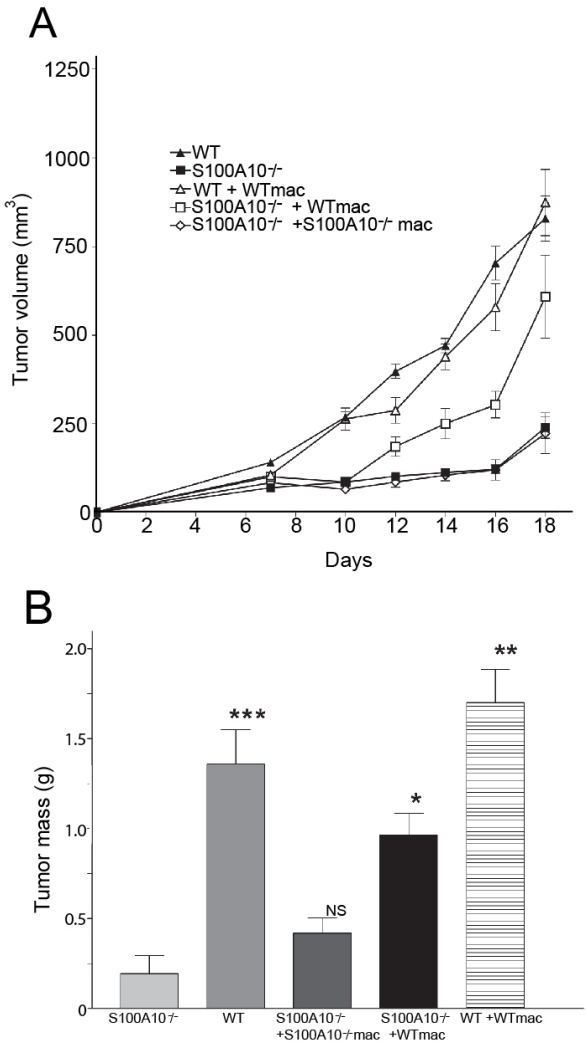
A
1250
1000
750
500
250
0
Tumor volume (mm3)
WT
S100A10-/-
WT + WTmac
S100A10-/- + WTmac
S100A10-/- +S100A10-/- mac
0 2 4 6 8 10 12 14 16 18
Days
B
2.0
1.5
1.0
0.5
0
Tumor mass (g)
***
**
*
NS
S100A10-/-
WT
S100A10-/- +S100A10-/-mac
S100A10-/- +WTmac
WT +WTmac

Figure 27. Intratumoral adoptive transfer of macrophages effects tumor growth in S100A10-null mice. (A) S100A10-null or WT mice subcutaneously injected with $2x10^6$ LLC cells were intratumorally injected with $0.25x10^6$ WT or S100A10-null macrophages after 4 days of tumor growth. The growth kinetics of the LLC tumors are represented as mean tumor volume ± s.e.m. relative to time of 7 tumors per treatment. Volumes calculated as (length x width^2)/2. (B) The corresponding terminal LLC tumor masses after 18 days of tumor growth are expressed as mean ± s.e.m. of 7 tumors. Statistical significance calculated by two-tailed, unpaired Student's t-test relative to S100A10$^{-/-}$, identified as follows: *P<0.05, **P<0.01.

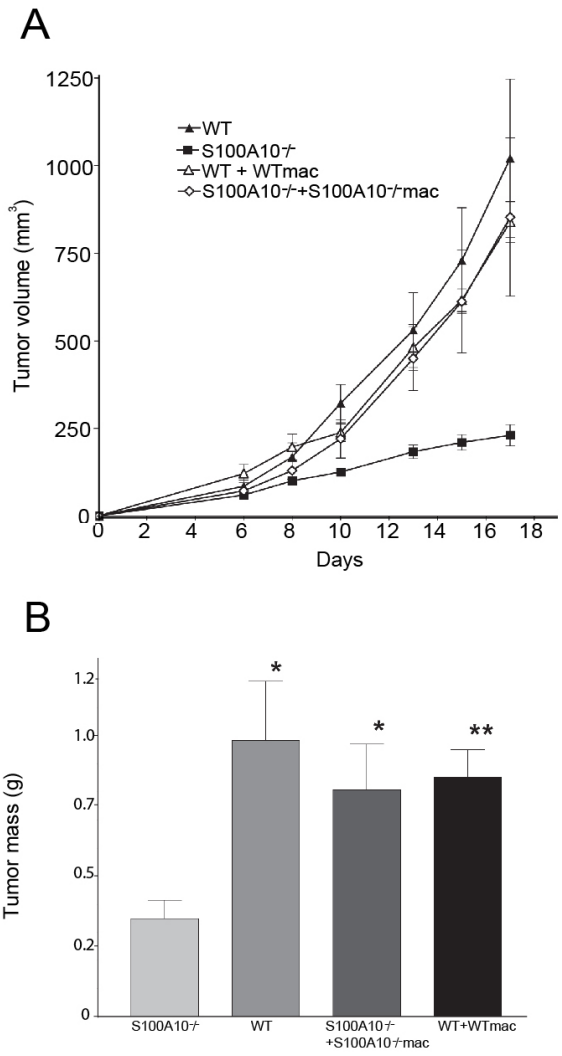
A
1250
1000
750
500
250
0
Tumor volume (mm3)
WT
S100A10-/-
WT + WTmac
S100A10-/-+S100A10-/-mac
0 2 4 6 8 10 12 14 16 18
Days
B
1.2
1.0
0.7
0.5
0.2
0
Tumor mass (g)
*
*
**
S100A10-/-
WT
S100A10-/-
+S100A10-/-mac
WT+WTmac

CHAPTER 4

ROLE OF S100A10 IN PLASMIN GENERATION AND CELLULAR INVASION

4.1 RNAi mediated depletion of cellular S100A10 levels

We have shown that macrophages mediated tumor promotion is facilitated by S100A10 expression which enables Pg activation and cellular invasion. In order to establish the role of S100A10 in Pg dependent cellular invasion in cancer cells, we utilized RNAi constructs to deplete S100A10 levels in human HT1080 and murine LLC cancer cells. Following the application of the RNAi constructs and antibiotic selection, Western blot analysis was used to confirm diminished levels of the S100A10 protein in HT1080 (Figure 28A) and LLC (Figure 28B) cells, using the respective human and murine targeted plasmid constructs. Infrared signal was utilized for quantification on a Licor Odyssey (Licor Biosciences) and the depletion was found to be greater than 90% in both cases. We also observed that the annexin 2 levels were affected by the S100A10 depletion in the HT1080 cells but not in the LLC cells.

Figure 28. RNAi mediated depletion of S100A10. Human HT1080 fibrosarcoma cells (A) and murine LLC cells (B) were transduced with a retroviral delivery system (pSUPER.retro.puro) causing the expression of RNAi constructs which caused the specific depletion of S100A10 levels; RNAi1 and RNAiD respectively. The unaltered levels of S100A10 are demonstrated by the treatment with RNAi scramble constructs (RNAi1 Sc and RNAiD Sc) and the level of the S100A10 binding partner, annexin A2, is also depicted. The recombinant annexin A2 is depicted as a size standard (Std) and actin is shown as a load control.

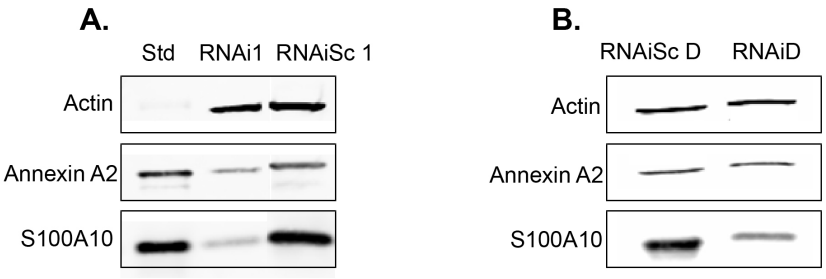
A.
Std
RNAi1
RNAiSc 1
Actin
Annexin A2
S100A10
B.
RNAiSc D
RNAiD
Actin
Annexin A2
S100A10

4.2 S100A10 is required for plasminogen activation

The rate of Pg activation was determined in the S100A10 depleted cells as the ability to cleave S2251, a chromogenic plasmin substrate. Cleavage of the colorless S2251 reagent results in the release of a yellow para-nitro-analine (pNA) product, whose appearance is quantifiable on a spectrophotometer at 405 nm. The rate of pNA formation is proportional to the enzymatic activity.

In the presence of Pg we observed that RNAi1 treatment of HT1080 cells caused a 53% reduction in the rate of Pg activation from $20x10^{-5}\Delta405$ nm/min^2 in RNAi1 Sc treated cells to 9.33 ± 0.33 x$10^{-5}\Delta405$ nm/min^2 in RNAi1 treated cells (Figure 29). The addition of uPA to the system resulted in a similar rate reduction of 56% from $20x10^{-5}\Delta405$ nm/min^2 in RNAiSc treated cells to $8.83 \pm 0.54x10^{-5}\Delta405$ nm/min^2 in RNAi1 treated cells (Figure 29).

A strikingly similar reduction in the rate of Pg activation was observed in S100A10 depleted murine cancer cells. In the presence of Pg we observed that RNAiD treatment of LLC cells caused a 56% reduction in the rate of Pg activation from 3.2 ± 0.2 x$10^{-5}\Delta405$ nm/min^2 in RNAiD Sc treated cells to 1.4 ± 0.24 x$10^{-5}\Delta405$ nm/min^2 in RNAi1 treated cells (Figure 30). The addition of uPA to the system also resulted in a similar rate reduction of 41% from 3.4 ± 0.24 x$10^{-5}\Delta405$ nm/min^2 in RNAiD Sc treated cells to 2 x$10^{-5}\Delta405$ nm/min^2 in RNAiD treated cells (Figure 30).

Figure 29. Depletion of S100A10 in human HT1080 cells decreases plasminogen activation. $1x10^5$ human HT1080 fibrosarcoma cells were seeded in 96 well plates and allowed 12 hr to acclimate in FBS free DMEM. Cells incubated with or without uPA (50 nM) for 10 min at RT were washed twice in PBS before the addition of the S2251 (100 μM) plasmin substrate. The reaction was initiated by the addition of Pg (0.5 μM) and followed by the appearance of the S2251 cleavage product at 405 nm by a spectrophotometer, reading every min for 2 hr. The representative data from two independent experiments are expressed as the means ± s.e.m., n=4 and statistical significance of $p<0.0001$ was determined by one-way anova with Tukey post-test analysis.

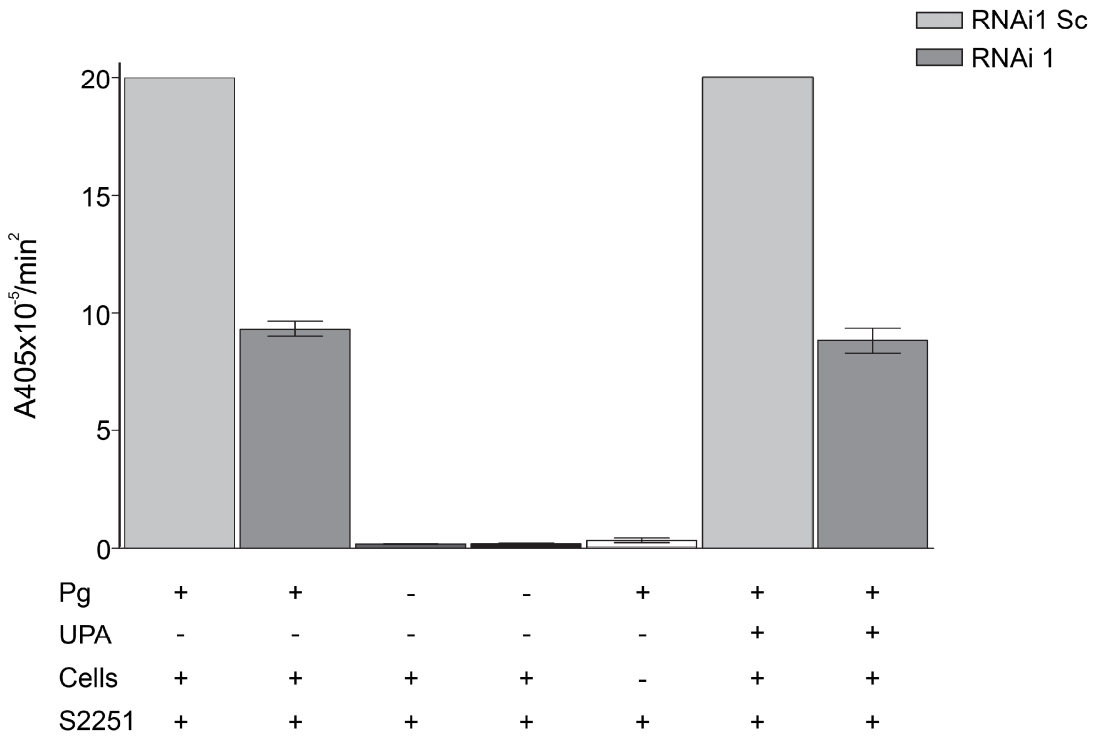
RNAi1 Sc
RNAi 1
A405x10^{-5}/min^{2}
20
15
10
5
0
Pg + + - - + + +
UPA - - - - - + +
Cells + + + + - + +
S2251 + + + + + + +

Figure 30. Depletion of S100A10 in murine LLC cells decreases plasminogen activation. $1x10^5$ murine LLC cells were seeded in 96 well plates and allowed 12 hr to acclimate in FBS free DMEM. Cells incubated with or without uPA (50 nM) for 10 mins at RT were washed twice in PBS before the addition of the S2251 (100 μM) plasmin substrate. The reaction was initiated by the addition of plasminogen (0.5 μM) and followed by the appearance of the S2251 cleavage product at 405 nm by a spectrophotometer, reading every min for 2 hr. The representative data from two independent experiments are expressed as the means ± s.e.m, n=4 and statistical significance of $p<0.0001$ was determined by one-way anova with Tukey post-test analysis.

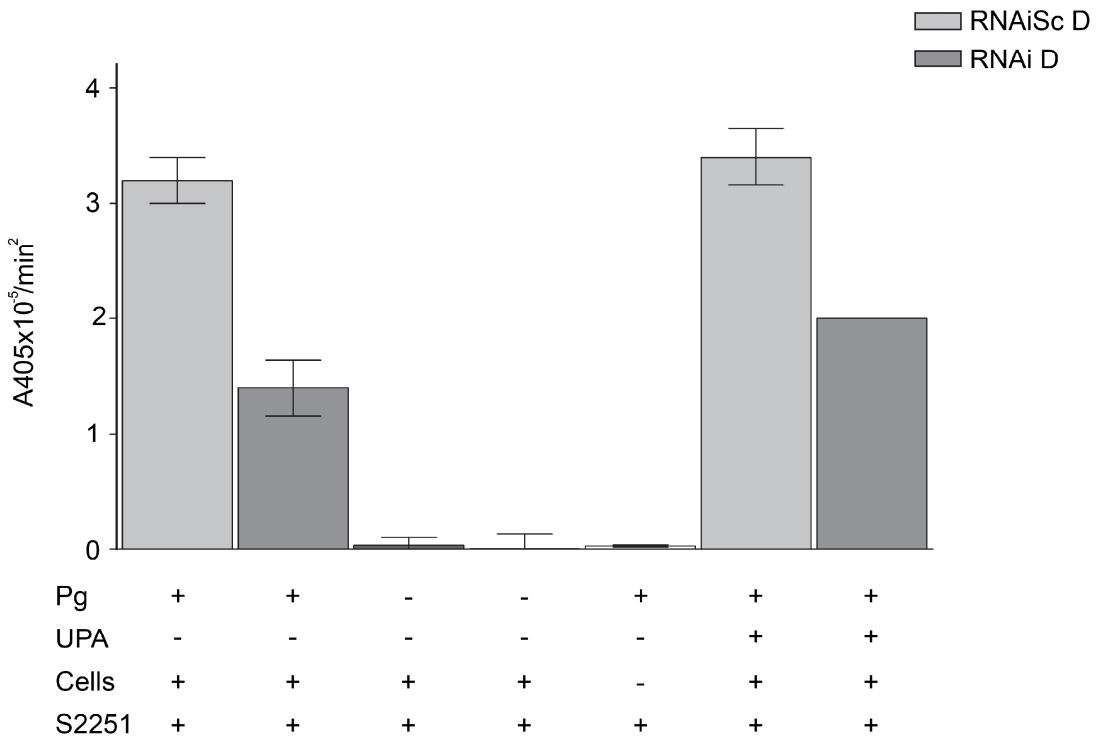
RNAiSc D
RNAi D
A405x10^5/min^2
4
3
2
1
0
Pg + + - - + + +
UPA - - - - - + +
Cells + + + + - + +
S2251 + + + + + + +

4.3 S100A10 is required for plasminogen dependent cancer cell invasion

The conversion of Pg to Pm is thought to confer proteolytic ability, which is the basis for an invasive cellular phenotype. We tested whether the deficiency in the ability to activate Pm, observed in the S100A10 depleted cancer cells, would translate into a deficiency in cellular invasiveness. Human HT1080 cells were given a 24 hr period to invade through a Matrigel (MTG) coated trans-well barrier, after which an average of 279 ±32 cells treated with RNAi1 and 650±41 cells treated with the scramble control per field, had invaded to the underside of the barrier (Figure 31). Thus a 56% reduction in invading cells was observed in association with S100A10 depletion.

Similarly, LLC cells were given a 48 hr period to infiltrate through a MTG coated barrier, after which 138 ± 12 LLC cells treated with RNAiD had invaded through as compared to 239 ± 9 LLC cells treated with the RNAiD Sc control construct (Figure 32). Thus the S100A10 depleted LLCs correlated with a 48% decrease in infiltrating cells relative to the RNAiD Sc control treated cells (Figure 32). This disparity of invading cells was abolished when cells were added to the non-MTG coated control membranes, indicating that cellular motility was unaffected. Additionally, when Pg was not added to the system, the number of invading cells dropped off significantly. These data indicate that S100A10 contributes to Pg dependent cellular invasion of cancer cells.

Figure 31. S100A10 is required for human plasminogen dependent cellular invasion. $5x10^5$ HT1080 cells with or without S100A10 RNAi mediated depletion (RNAi1 and RNAi1 Sc respectively), were added to the upper reservoir of Boyden invasion chambers with Matrigel (MTG) coated transwell inserts or to non-coated migration chambers in the presence of 0.5 μM plasminogen (Pg) in serum free DMEM. Cells were allowed to invade through the insert, towards the lower reservoir containing DMEM supplemented with 10% FBS (Pg depleted) for 24 hr. Cells invading through to the underside of the insert were stained with haematoxylin and eosin and counted. The data expressed as the means of 10 fields from 1 of 3 independent experiments ± s.e.m and statistical significance of $p<0.0001$ was determined by one-way Anova with Tukey post-test analysis.

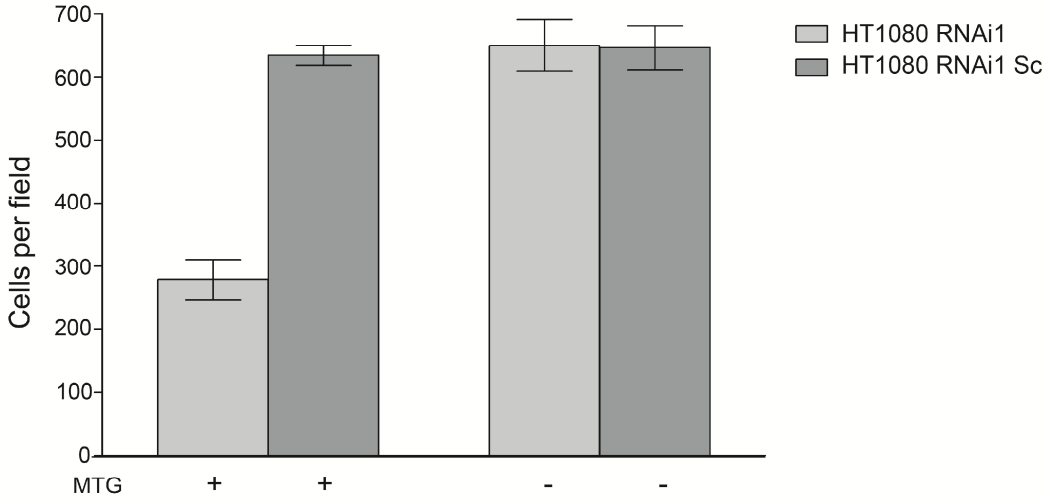
700
600
500
400
300
200
100
0
Cells per field
MTG
+
+
-
-
HT1080 RNAi1
HT1080 RNAi1 Sc

Figure 32. S100A10 is required for murine plasminogen dependent cellular invasion. $1x10^5$ LLC cells with or without S100A10 RNAi mediated depletion (RNAiD and RNAiD Sc respectively), were added to the upper reservoir of Boyden invasion chambers with Matrigel (MTG) coated transwell inserts or to non-coated migration chambers in the presence or absence of 0.5 μM plasminogen (Pg) in serum free DMEM. Cells were allowed to invade through the insert, towards the lower reservoir containing DMEM supplemented with 10% FBS (Pg depleted) for 48 hr. Cells invading through to the underside of the insert were stained with haematoxylin and eosin and counted. The data are expressed as the means of 10 fields from two independent experiments ± s.e.m and statistical significance of $p<0.0001$ was determined by one-way anova with Tukey post-test analysis.

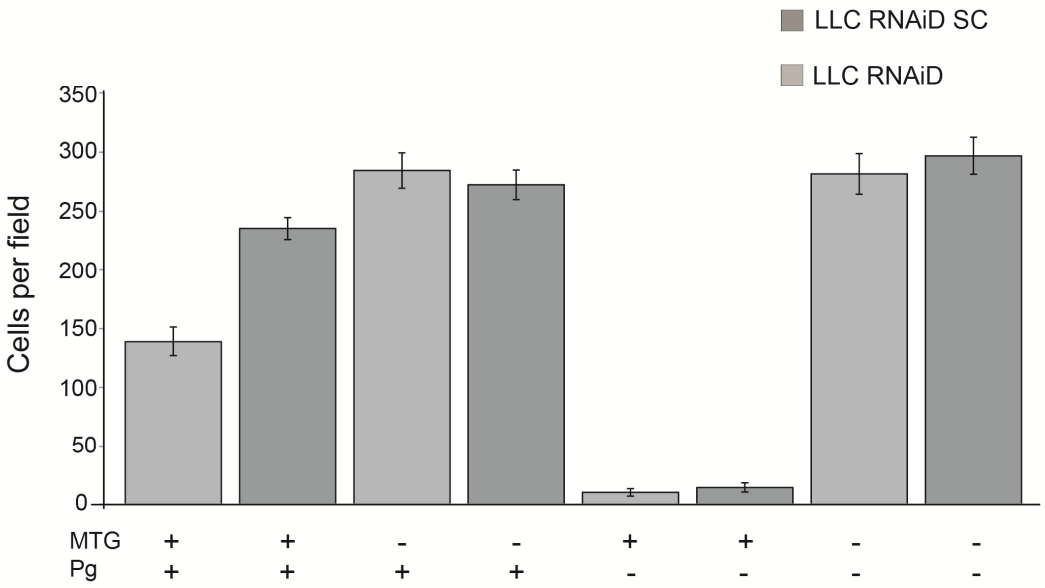
LLC RNAiD SC
LLC RNAiD
Cells per field
350
300
250
200
150
100
50
0
MTG + + - - + + - -
Pg + + + + - - - -

CHAPTER 5

DISCUSSION

5.1 S100A10 regulates plasmin mediated macrophage invasion

The concept on macrophage co-option by tumor cells is only now becoming an accepted view, it is however a very old idea, first proposed in 1863 by Rudolf Virchow[130]. Recent works have addressed the fundamental and varied roles macrophages play in tumor promotion. Despite this new fervor in the field, the mechanism by which macrophages reach the tumor site has yet to be identified and characterized.

Previous work on the Pg-deficient mouse has shown that Pm generation and subsequent MMP-9 activation is a requirement for macrophage recruitment[131]. Thus, Pm facilitates invasion by both direct degradation of ECM components and by the Pm-activated MMP-9 mediated ECM degradation. Several Pg receptors may be responsible for the activation of Pm at the macrophage cell surface. Previous work in our laboratory has established S100A10 as a key Pg receptor in cancer cells and most recently in macrophages[51,82,119]. Additionally, work by our laboratory with the S100A10-null mouse has shown S100A10 to be responsible for 50% of macrophage generated plasmin and 53% of peritoneal infiltrating macrophages in response to a thioglycolate stimulus as well as more than 85% of macrophages infiltrating into a subcutaneously implanted matrigel (MTG) plug[119]. The objective of the current study is to address whether macrophages utilize S100A10 to transit to the tumor site.

Macrophages collected from S100A10-null mice also displayed a 40% decrease in their ability to invade through MTG, towards a cancer cell monolayer. In the absence of Pg, the number of invading macrophages drops to approximately the same number as in

the S100A10-null cells with Pg, indicating that S100A10 is used to activate all the Pg to Pm and to allow subsequent invasion. As previously reported by our laboratory, the invasion was inhibited by the addition of the lysine analog ε-aminocaproic acid (ACA)[74,75, 76]. It is of interest to note that the ACA treatment, which functions to competitively inhibit Pg through competitive binding of kringle domains, decreased the number of invading cells below the Pg-free control. This may be due to ACA inhibiting other proteases, as it has been shown to inhibit trypsin[77]. Additionally, the same mechanism of inhibition allows ACA to inhibit uPA, which plays a role in anchoring the plasma membrane to the cytoskeletal network and Jak/Stat signal transduction, associated with the cytoskeleton remodeling occurring during cellular motility[77-79]. Cellular invasion is dependent upon both proteolysis and cellular motility. Supporting the possibility that impaired cellular motility was occurring is the observation that ACA was the only treatment to effect cellular migration and did so by ~30% inhibition (Figure 10B). The pericellular proteolytic ability conferred upon plasmin activation is through both direct substrate degradation and through activation of latent MMPs. Treatment of cells with GM6001, a pan-MMP inhibitor also caused a drastic decrease in invasion, indicating that plasmin is most likely functioning through MMP activation and subsequent MTG proteolysis. Recent work from our laboratory with antibody-blocking has identified MMP-9 as the major contributor to this Pg dependent proteolysis[119]. Thus, we have shown that macrophages require S100A10 to facilitate invasion through synthetic ECM membranes in a Pg dependent manner, which may be facilitated through MMP activation.

5.2 S100A10 facilitates TAM infiltration and subsequent tumor growth

We have, for the first time, reported that tumor growth in mice lacking S100A10 is severely compromised. This inability to sustain tumor growth may be attributable to multiple causes as all cells of these mice lack S100A10 and S100A10 has multiple functions. We have identified that the tumor growth inhibition is correlated with diminished TAM infiltration. We have hypothesized that the lack of S100A10 impedes the association of TAMs with tumor cells by curtailing the TAM invasive capability and thus, their ability to transit to the tumor site. In order to ensure that both macrophages from WT and S100A10-null mice were receiving a comparable level of cytokine stimulation from the tumor, a cytokine array was performed and found that the levels of macrophage specific cytokine per tumor wet weight were either the same or elevated in the S100A10-null mice. Although the cytokine levels were measured per tumor wet weight, the tumors grown in the S100A10-null mice are significantly smaller at 14 days of tumor growth. Therefore, the level of chemokine with respect to the entire mouse may be less in the S100A10-null environment as compared to the WT counterparts. However, the tumors from both environments were initially the same size and remained comparable until ~7 days of tumor growth. Therefore, the initial release of macrophage specific chemokines during the first 7 days of growth would be expected to be the same in both WT and S100A10-null mice, with respect to both the tumor and entire mouse.

There are several cell types which become co-opted by tumors to further tumor progression. We employed two strategies to identify macrophages as the cause of the observed tumor growth deficiency in the S100A10-null mouse. First, macrophages were transiently depleted using liposome encapsulated clodronate. Clodronate, a

bisphosphonate, is a cytotoxic compound which becomes metabolized intracellularly to an analog of ATP, which inhibits the mitochondrial ADP/ATP translocase[124,132]. Clodronate has been approved as an osteoporosis treatment in Canada (marketed as Bonefos) as free clodronate will bind hydroxyapatite and kill osteoclasts, thereby inhibiting bone resorption. This mechanism of action also makes clodronate useful in targeting bone metastases.

Clodronate encapsulated within a liposome (termed clodrolip) becomes a target for circulating phagocytotic monocytes, as their function is to remove debris from circulation. Upon engulfment, the liposome is degraded and the released clodronate causes monocyte cell death. As discussed in Section 1.4, monocytes exit circulation in response to the tumor chemotactic signals which causes differentiation into the macrophage. Depleting a monocyte population has the effect of depleting the macrophage population available to enter the tumor site.

An intraperitoneal clodrolip injection is well tolerated by mice and is able to decrease circulating macrophages/monocytes for 4 days[124]. FACS analysis was used to confirm the clodrolip mediated reduction in TAMs. Interestingly, the clodrolip mediated macrophage depletion caused a similar tumor growth reduction as that observed in the S100A10-null mice. This may be due to similar mechanisms of action, being that tumors from both environments have decreased TAM infiltrate. As it is possible that the clodrolip injections were having a cytotoxic effect on the tumors themselves, macrophages and cancer cells were subjected to incubations with increasing concentrations of clodrolip *in vitro*, which caused significant decreases in macrophage survival and left the cancer cells unaffected.

Secondly, to establish that macrophages were the lacking component in the S100A10-null growth arrested tumors, we employed a macrophage transfer to tumor bearing mice. Initial experiments proved promising as a peritoneal transfer of WT splenocytes, of which 10% of cells are macrophages, caused an intermediate increase in tumor growth. Similarly, the tumor growth arrest could be reversed by adding WT macrophages to the S100A10-null mice, also via the peritoneal route.

The intraperitoneal addition of WT macrophages to WT mice did not alter the tumor growth profile, indicating that there are sufficient endogenous macrophages present at the WT tumor site. Similarly, the addition of S100A10-null macrophages to S100A10-null mice via the peritoneum also had no effect on tumor growth, suggesting that S100A10 expression is a requisite for the increased tumor growth observed upon addition of WT macrophages. Presumably, transferred WT macrophages are able to transit from the peritoneum to the S100A10-null tumor site, whereas S100A10-null macrophages are not.

Most unexpectedly, we observed that the addition of WT macrophages via the peritoneum of S100A10-null mice increased the impaired tumor vascular density to the normal levels observed in tumors from WT mice. These observations, along with the increases in tumor growth indicate that WT macrophages were capable of stimulating both angiogenesis and subsequent tumor growth in the S100A10-null mice, whereas S100A10-null macrophages were not.

We have also found that the addition of S100A10-null macrophages directly to a growth arrested tumor on a S100A10-null mouse is able to initiate tumor growth. This finding indicates that although the S100A10-null macrophages are unable to transit to the

tumor site, they retain the ability to promote tumor growth and will do so when artificially placed in the tumor environment. As in the intraperitoneal experiment, the intratumoral addition of WT macrophages to the tumors on the WT mice did not cause an alteration in tumor growth. Presumably the tumors from the WT mice have sufficient TAM density and a macrophage increase, either systematically through peritoneal transfer, or at the tumor site, does not alter tumor growth.

Macrophages have been reported to promote several aspects of tumor growth, including direct stimulation of tumor cell proliferation, inhibition of tumor cell apoptosis, immunomodulation which allows tumor cells to evade the immune system and the orchestration of angiogenesis. As the macrophage/tumor relationship is so diverse and complex, a TAM deficiency may inhibit several facets of tumor growth. Of these we have observed two such mechanisms. We have found TAM deficiency to be correlated with increased apoptosis within the tumor. The mechanism for this apoptosis was not identified, however previous studies have reported that macrophages are able to block TRAIL induced apoptosis though IL-1β stabilization of the Snail transcription factor. mechanisms of cancer cell apoptosis[41]. Although the density of proliferating cells within the tumors grown in S100A10-null mice appeared to be no different than in tumors grown in WT mice, the altered apoptotic rate may contribute to tumor growth arrest.

We have found that TAM deficiency correlates with a substantial decrease in tumor vascular density. This vascular deficiency may be due to the lack of macrophages, causing a lack of angiogenic stimuli or conversely, by the S100A10-null endothelial cells lacking the ability to form tumor vasculature. The cause of decreased vascular density was elucidated through the observation that tumors within the S100A10-null environment

experienced a vascular increase to WT levels upon receiving transferred WT macrophages; thereby indicating that S100A10-null endothelial cells retained the ability to vascularize the tumor upon stimulation by S100A10-expressing TAMs.

Interestingly, the tumor blood vessels within the S100A10-null mice were often occluded by an autofluorescent material. A side by side immunofluorescent and anti-fibrin immunohistochemistry allowed for the identification of the deposits as fibrin. This observation may be explained by the fact that tumor endothelium in the S100A10-null mice lack S100A10 and thus lack the ability to activate plasmin to clear fibrin deposits. This observation supports recent findings from our laboratory of fibrin accumulation in several tissues from the S100A10-null mouse including; lung, liver, kidney and spleen (Surette *et. al. Blood.* 2011 in press). Additionally, Surette has identified deficiencies in Pg binding and Pm activation by S100A10 depleted endothelial cells.

Thus, the loss of tumor growth in the S100A10-null mice could be explained, in part, by the loss in TAM recruitment causing decreased angiogenesis and increased apoptotic rates or by an inability of the tumor vasculature to maintain vascular fluidity.

Tumor growth requires an intimate relationship between macrophages and cancer cells, the current study demonstrates that the recruitment of macrophages to the tumor site is mediated, in part, by the S100A10 dependent generation of plasmin by the macrophage.

CHAPTER 6

CONCLUSION

6.1 S100A10 facilitates the association of macrophages with tumor cells.

The work presented herein demonstrates that the S100A10 protein enables the plasmin mediated infiltration of macrophages to the tumor site. We report that the S100A10-null mouse is incapable of sustaining tumor growth due to a decrease in TAM infiltrate leading to both inadequate tumor vascularization and an increased tumor apoptotic rate. We also report that a selective, drug mediated depletion of WT macrophages caused a similar reduction in tumor growth. Tumor growth in S100A10-null mice could be restored by intraperitoneal injection of WT macrophages; S100A10-null macrophages only restored tumor growth when directly injected into the tumor.

Together, these results highlight the absolute requirement of S100A10 in the association of macrophages with tumors and demonstrate a potential therapeutic strategy in which the tumor associated cells may be targeted. If S100A10 were to be used as a therapeutic target, the intervention could occur after tumor identification and prior to surgical removal in order to curtail further tumor development. Additionally, an anti S100A10 therapy may be a beneficial adjacent approach, limiting macrophage association while chemotherapy is applied.

6.2 Future Directions

The present body of work establishes the role of S100A10 in enabling macrophage transit to the primary tumor site. Secondary tumors, or metastatic tumors, are the cause of the majority of cancer related deaths and have been recently reported to rely

upon macrophage recruitment. Pollard and colleagues have compared the macrophage populations in primary tumors to those in metastatic tumors and found a distinct sub-population of macrophages of $CD11b^{+}$ $Gr1^{-}$ macrophages associated with metastatic tumors[133]. It would be interesting to investigate if these metastatic associated TAMs require S100A10 expression. Currently, we are attempting to address this through a spontaneously metastatic tumor cell line, and by creating a new mouse model which exhibits a high incidence of metastasis (discussed below).

We have observed that S100A10 enables macrophage transition through physiological barriers. S100A10 may also play a role facilitating the escape of disseminated cancer cells from the primary tumor and their establishment at a secondary site. Several steps in the metastatic cascade require the dissolution of the ECM and other barriers, most notably extravasation and intravasation. Thus an overexpression of S100A10 and annexin 2 would enable increased plasmin activation and proteolysis. Supporting this is the observation that invasive MDA-MB-435 human melanoma cells overexpress S100A10 and annexin 2[134]. Investigating the manner in which cancer cells utilize S100A10 is best done by removing the protein. However RNA mediated depletion of S100A10 within *in vivo* tumor systems is problematic. Introducing RNA depleted cells to novel cellular environments or allowing them prolonged periods without antibiotic selection, as they would be subjected to in mice, is likely to cause protein expression to return to normal levels. Therefore, a knock-out system is desirable in which S100A10 expression cannot occur regardless of external stress. To this end we have set about creating a polyoma middle T (PyMT) spontaneous breast tumor mouse model on a S100A10-null environment. The goal is to create spontaneous tumors which arise in the

total absence of S100A10. The PyMT protein activates the Src tyrosine kinase which results in the activation of multiple signaling cascades such as phosphoinositide 3-kinase, phospholipase C and the Ras–Raf–MAP kinase pathway[89]. The activation of one or more of these cascades is thought to contribute to the oncogenic properties of PyMT[135]. The PyMT expression remains localized to the mammary fat pad due to the mammary tumor virus (MMTV) promoter. The MMTV-PyMT mouse is an excellent model as all mice develop mammary tumors with a short latency period, independent of pregnancy and express a high incidence of lung metastasis. Within 20 weeks multiple large palpable tumors are present in the MMTV-PyMT mice (Figure 33). This model will allow us to better investigate the role of the S100A10 protein in the progression from transformed cell to occult primary tumor to the metastatic form of the disease. This work will most likely take be approached through immunohistochemical analyses to identify tumor progression, invasion into surrounding tissue and the association of host cells, such as leukocytes and endothelial cells.

Additionally, this mouse model will allow for the study of the role of S100A10 in early events in cancer progression, a draw-back in our current model. Currently, tumors are established through the injection of millions of transformed cells. This does not accurately model the natural initiation of cancer, originating from defective cell cycle control. The MMTV-PyMT mouse will allow us to follow cancer progression from inappropriate genetic signals to primary tumor growth to metastasis in the complete absence of S100A10.

Additionally the MMTV-PyMT S100A10-null model will allow us to again examine macrophages, but with regard to secondary tumors. The Pollard group has

created an MMTV-PyMT mouse which lacks CSF1 ($CSF1^{op/op}$) thereby disabling a key factor involved in macrophage recruitment[24,136]. Unlike our observations with the LLC and T241 tumors, the primary breast tumor incidence and tumor growth rate was reported to be unaffected by the lack of CSF1 and TAMs. Interestingly, the occurrence of metastatic tumors is greatly decreased in the MMTV-PyMT $CSF1^{op/op}$ mice. Therefore the PyMT-MMTV S100A10-null mouse will allow us to identify if this sub-population of macrophages also requires S100A10.

Figure 33. Multiple spontaneous mammary tumors in the MMTV-PyMT mouse. Several large tumors localized to the mammary fat pad were identified in a 20 week old female MMTV-PyMT mouse.

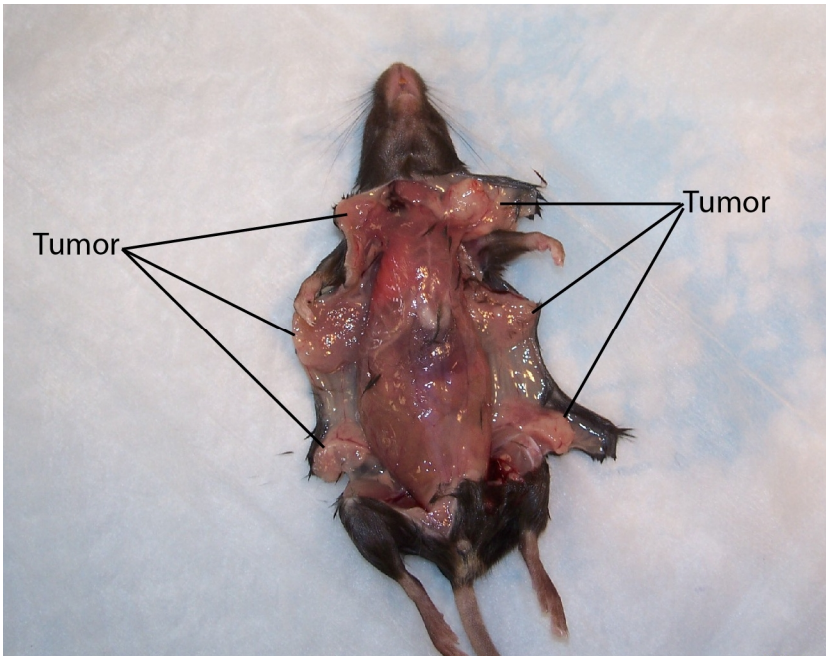
Tumor
Tumor

APPENDIX A: UTILIZATION OF THE KATUSHKA PROTEIN FOR NON-INVASIVE *IN VIVO* TUMOR IMAGING

This appendix contains work on the adaptation of the Katushka protein for non-invasive *in vivo* tumor imaging.

ABSTRACT

Non-invasive *in vivo* imaging is a powerful tool which promises to provide much to the field of cancer research. I report the adaptation of the newly discovered Katushka protein to a lentiviral expression system for use in tumor imaging. Katushka has much potential for *in vivo* imaging as it is the brightest, farthest red-shifted protein discovered thus far. I show that Katushka expression is ideal for labeling cells *in vitro* and that it is bright enough for tumor monitoring *in vivo.* Unfortunately, Katushka expression severely limits tumor growth in immunocompetant but not immunocompromised mice. This finding suggests that Katushka may be immunogenic, however more work is required to ascertain the exact effect Katushka is having on tumor growth.

CHAPTER A1

NON-INVASIVE *IN VIVO* TUMOR IMAGING

INTRODUCTION

A1.1 Katushka and *in vivo* tumor imaging

In vivo tumor imaging is a powerful tool in the field of cancer research, however a strategy for deep tissue penetrating imaging has yet to be developed. Deep tissue imaging requires a high wavelength optical window such as the far-red shifted spectra. Far-red wavelengths are able to penetrate animal tissues due to a relative low absorption by biological molecules. Melanin and hemoglobin scatter light of lower wavelengths as they absorb in both ultraviolet (UV;330–400 nm) and in the visible (400–600 nm) ranges of the spectrum[137]. Far-red and near infrared wavelengths are therefore better for deep tissue penetration. A far-red fluorescent protein, named Katushka, derived from the brilliant red sea anemone (*Entacmaea quadricolo*), was reported by Shcherbo and colleagues, in 2007[138]. Katushka is a pH stable, dimeric protein which emits light at 635nm when excited at 588nm. It was reported to be seven to tenfold brighter than any fluorescent protein known to date[138]. We therefore sought to adapt this technology to tumor tracking within mice, with the ultimate goal of identifying specifics about the growth arrested tumors in the S100A10-null mice.

METHODS

A2.1 Katushka cloning

A DNA fragment containing the Katushka coding sequence, the preceding Kozak consensus sequence and tata-box region was amplified by PCR from the pTurboFP635 plasmid (Evrogen) and inserted into the pLenti6⁄V5-D-TOPO plasmid (Invitrogen) through a topoisomerase mediated reaction as per the manufacturer's instructions. The plasmid produced, termed p.lenti topo katushka, allows for Katushka expression to be tethered to a lentiviral expression system.

A2.2 Katushka transfection and infection

The plasmids described above were transfected into Phoenix cells, HEK293-T cells modified for viral packaging, using Lipofectamine 2000 transfection reagent (Invitrogen) as per the manufacturer's protocol. The expression of Katushka in the Phoenix cells was confirmed with an MVX10 stereoscope (Olympus) using an ex560/em585lp filter set. Following a 48 hr incubation period the Phoenix cell media was collected, cleared of cells through centrifugation and 0.45 μM filtration and introduced to the LLC and HT1080 target cells. Selection for the LLC and HT1080 cells expressing the blasticidin resistance cassette of the plasmid was initiated by the addition of 2 μg/mL blasticidin 72 hr after the addition of the Phoenix infection media.

A2.3 Katushka expressing tumor imaging

Tumor micrographs were acquired on a MVX10 stereoscope (Olympus) using an ex560/em585lp filter set, a Retiga Exi monochromatic digital camera and Q-capture pro-imaging software. Removal of all hair down to the epidermis was essential for clear

imaging and was accomplished by a single treatment with hair removal cream (Nair; Church & Dwight Co., Inc).

RESULTS

A3.1 Adaptation of Katushka to a lentiviral expression system

A new plasmid construct, called p.lenti topo katushka, was created to incorporate the Katushka sequence into a lentiviral expression system (Figure 34). The p.lenti topo Katushka plasmid contained a blasticidin resistance gene for cell selection, a strong cytomegalovirus (CMV) promoter driving Katushka expression and a ψ sequence, which identifies the plasmid as a target for packaging into viral particles by the Phoenix cell (described in Section 2.3). It was found that the Phoenix cells packaging the lentiviral Katushka also expressed the protein. This was not entirely unexpected, as plasmids awaiting packaging within the Phoenix cell would have operational promoters. This effect allowed for simple quantification of transfection, by imaging the Phoenix cells using a far-red filter set (Figure 35). It should be noted that the red observed in these photomicrographs is pseudo color, as the camera used is monochromatic.

As described in Section 3.1, the Phoenix cell media, containing the viral particles, was applied to the target LLC cell lines. The rate of infection was determined to be >90% through observation of Katushka expression in the far-red optical window (Figure 36). The Katushka expressing LLC cells (LLC^{Kat}) were kept under antibiotic selection while in tissue culture.

Figure 34. Plasmid map of p.lenti topo Katushka. A representative map of the p.lenti topo Katushka plasmid which was produced from combining elements of the p.TurboFP635 plasmid into the p.Lenti6/V5-D-TOPO plasmid. Key features are depicted including restriction sites.

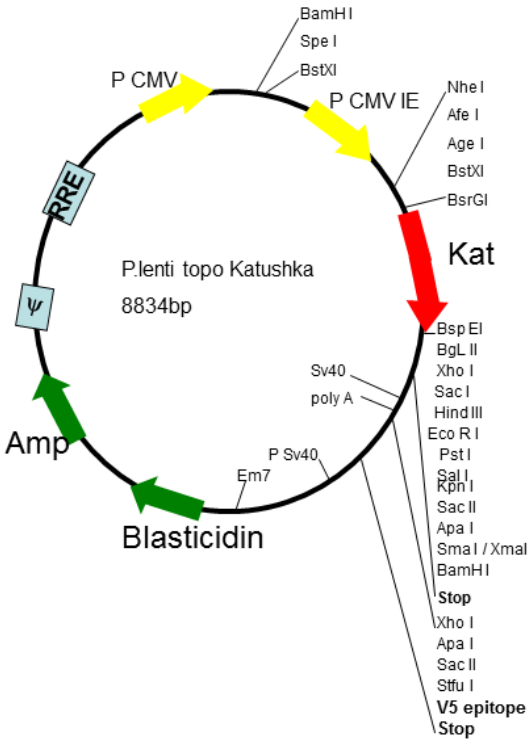
BamH I
Spe I
BstXI
P CMV
P CMV IE
Nhe I
Afe I
Age I
BstXI
BsrGI
RRE
Kat
P.lenti topo Katushka
8834bp
Ψ
Bsp EI
BgL II
Xho I
Sac I
Hind III
Eco R I
Pst I
Sal I
Kpn I
Sac II
Apa I
Sma I / Xmal
BamH I
Stop
Xho I
Apa I
Sac II
Stfu I
V5 epitope
Stop
Sv40
poly A
P Sv40
Em7
Amp
Blasticidin

Figure 35. Phoenix packaging cells express Katushka. Transfection of Phoenix viral packaging cells with the p.lenti topo Katushka plasmid causes Katushka expression and signal in the far-red optical window, observed through use of a 585lp filter set.

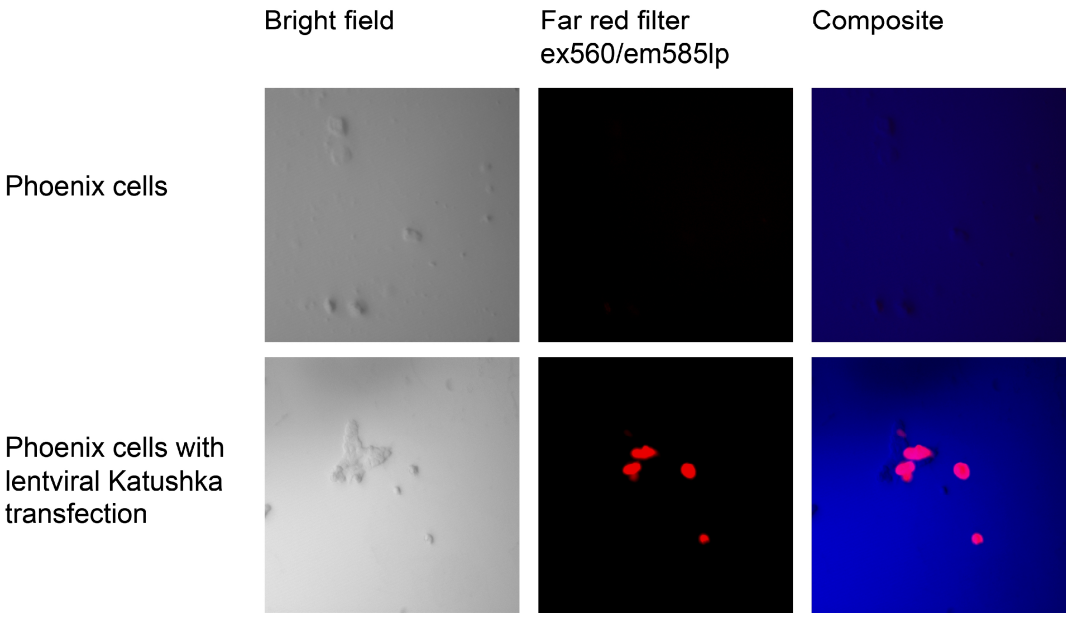
Bright field
Far red filter ex560/em585lp
Composite
Phoenix cells
Phoenix cells with lentviral Katushka transfection

Figure 36. LLC cells express Katushka. Katushka expression confirmed through far-red signal observation in LLC cells incubated with lentiviral Katushka infection media. The infection media was produced by p.lenti topo Katushka transfected Phoenix cells.

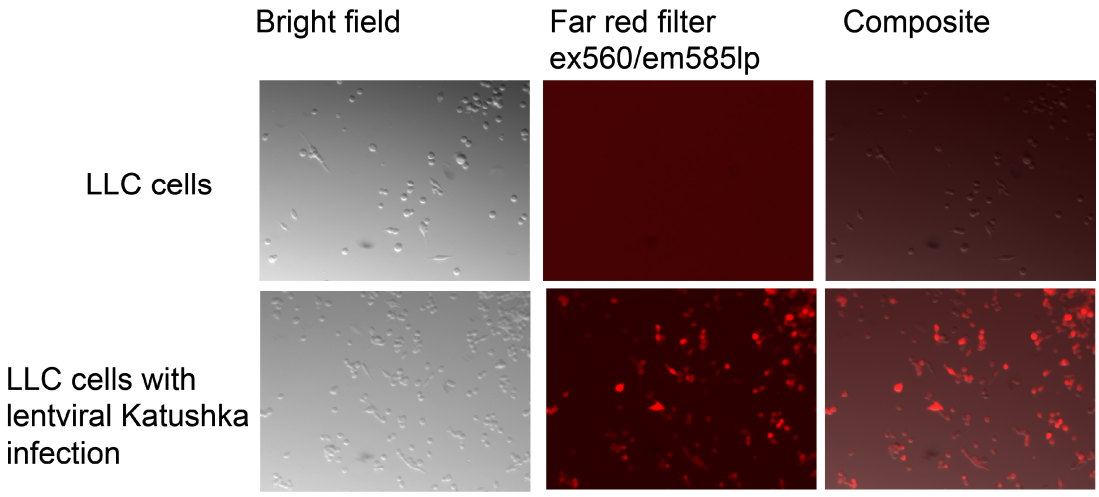
Bright field
Far red filter ex560/em585lp
Composite
LLC cells
LLC cells with lentviral Katushka infection

A3.2 Katushka mediated imaging *in vivo*

Katushka expression status in the LLC^{Kat} cells was reconfirmed immediately prior to injection into mice and had remained stable (Figure 37). Tumors were initiated by a subcutaneous flank injection of $2x10^6$ LLC^{Kat} cells into WT and S100A10-null mice. Tumors were palpable after 4 days of growth and could be imaged in the far-red window (Figure 38). It is interesting to note that at day 4, LLC^{Kat} cells can be observed, in far-red, migrating away from the lower border of the tumor mass, perhaps draining into a lymphatic vessel (Figure 38). Tumor micrographs could be acquired throughout the tumor growth period without any notable drop in signal.

Surprisingly, LLC^{Kat} tumors failed to thrive in both S100A10-null and WT mice (Figure 39). After an 18 day growth period in WT mice, the LLC^{Kat} were less than 30% of the volume of LLC cells without Katushka expression. In order to ascertain if Katushka affected tumor growth in general, HT1080 human fibrosarcoma were made to express Katushka, as described with the LLC cells. Tumors were initiated by the injection of $2x10^6$ $HT1080^{Kat}$ cells into the subcutaneous flank region of immunocompromised C57BL/6 $RAG1^{-/-}$ (*C57BL/6* 129-*RAG1*tm1 *Mom*/j) mice. The $HT1080^{Kat}$ tumors displayed exponential growth and maintained a strong Katushka signal up to day 16 at which point the experiment was terminated (Figure 40). The ability of Katushka to penetrate tissue is demonstrated through a comparison of the signal with (Figure 40A) and without (Figure 40B) the dermal layer.

Figure 37. Confirmation of Katushka signal prior to mouse injection. Final confirmation of Katushka expression was accomplished by the observation of the far-red signal of a droplet at the tip of a needle prior to injection (Right). LLC cells not expressing Katushka (Left) do not display a signal under the far red filter conditions.

Bright field

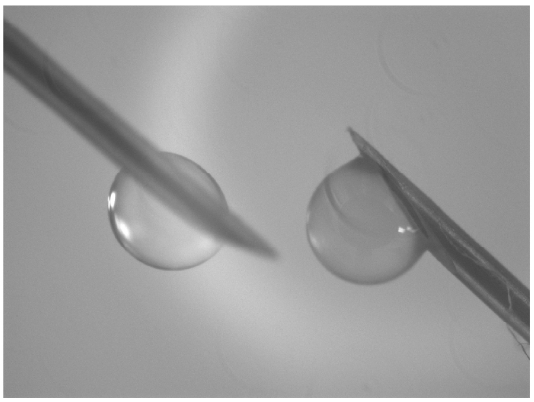

Far red filter
ex560/em585lp

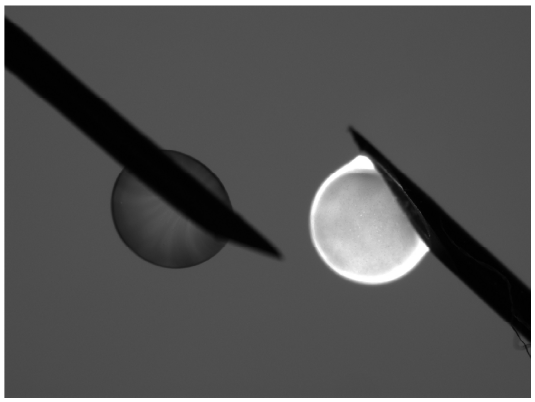

Figure 38. *In vivo* tumor imaging of LLC^{Kat}. Tumors, imaged 4-days after a subcutaneous flank injection of $2x10^6$ LLC^{Kat} cells, display a robust signal in the far-red range.

Bright field

Far red filter
ex560/em585lp

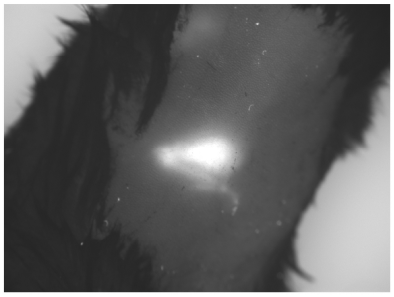

Far red filter
ex560/em585lp
with pseudo color

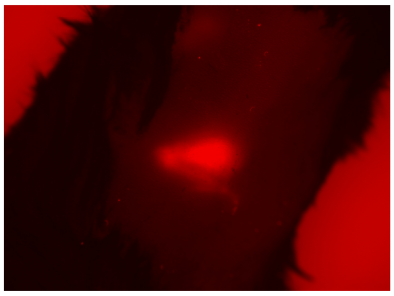

Figure 39. Katushka expression reduces LLC tumor growth in mice. Tumor growth kinetics, represented as mean volume ± s.e.m. of 7 tumors from subcutaneously established LLC and LLC^{Kat} tumors in WT mice. Tumor volume calculated as (length x $width^2$)/2.

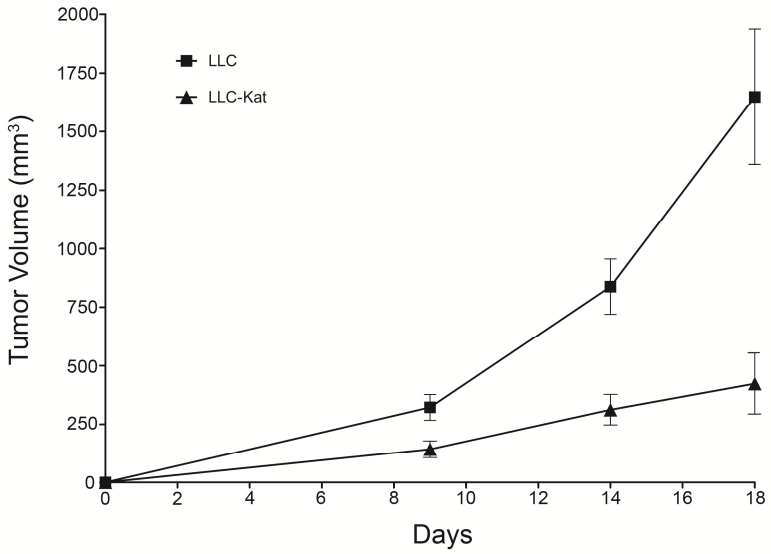
LLC
LLC-Kat
Tumor Volume (mm3)
Days
0
250
500
750
1000
1250
1500
1750
2000
0
2
4
6
8
10
12
14
16
18

Figure 40. *In vivo* tumor imaging of HT1080^{Kat}. (A)Tumors, imaged 16-days after a subcutaneous flank injection of 2x10^{6} HT1080^{Kat} cells, display a robust signal in the far-red range. (B) A demonstration of the tissue penetration of Katushka produced light was carried out through the removal of the dermal layer. A comparable far-red signal is observed upon direct visualization of the uncovered tumor relative to the tumor beneath the dermal layer.

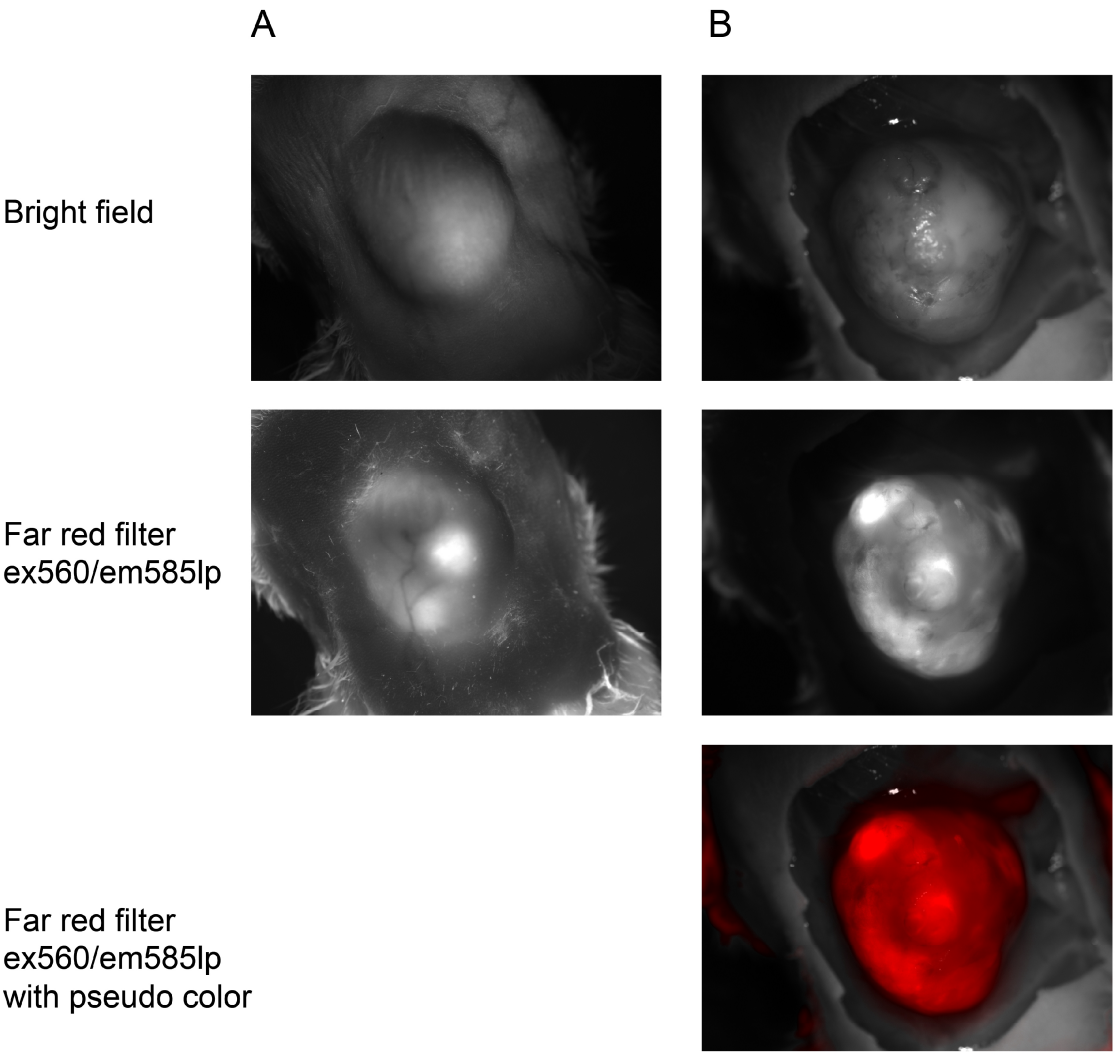
A
B
Bright field
Far red filter
ex560/em585lp
Far red filter
ex560/em585lp
with pseudo color

DISCUSSION

A4.1 Katushka; a milestone for *in vivo* imaging

The discovery and development of GFP from the *Aequorea victoria* jellyfish in the 1960s began a revolution in cellular biology research. The far-reaching impacts of GFP discovery is in the enormous breadth of research it has fostered and it is because of this that its discoverers earned the Nobel Prize in Chemistry in 2008[139,140]. While GFP is ideal for observations within the *in vitro* realm of cellular biology, its emission peak at 509nm is not high enough to allow for the tissue penetration required for animal imaging. The discovery and use of higher wavelength proteins began with the purification of DsRed from the *Discosoma* sp coral in 1999[141]. DsRed was reported to have emission maxima of 583 nm[142]. It was later reported in 2004 that mutagenesis of DsRed produced a series of higher wavelength proteins which were termed mCherry, mRasberry, mPlum and mTomato some of which displayed emission spectra as long as 649nm[143]. Although these wavelengths are suitably red-shifted, the DsRed based mutant proteins displayed relatively low quantum yields, being the ratio of emitted photons to absorbed photons, and were therefore not adequately bright for *in vivo*[144].

The extraction of Katushka from the sea anemone *Entacmaea quadricolor* was first described in *Nature Methods*, in 2007 by Shcherbo *et al*[138]. Katushka displayed a far-red shifted emission spectra of 635 nm, as well as other useful traits including a rapid 20 min maturation time, no observed cellular toxicity, a high extinction coefficient of 65 000 $M^{-1}cm^{-1}$ and a sufficient quantum yield of 0.34[138]. Shcherbo and colleagues created transgenic *Xenopus laevis* frogs in which Katushka expression was driven by the cardiac actin promoter. Non-invasive imaging of the Katushka transgenic frogs revealed that the

heart rudiment was easily observed whereas no heart-signal was found in frogs expressing DSRed or mPlum transgenes from the cardiac promoter[138]. Thus in 2007, Katushka appeared to be the next revolution in the field of non-invasive animal imaging and therefore we set out to adapt the technology to our S100A10-null mouse tumor model.

We, for the first time, have reported adapting Katushka to a lentiviral expression system for use in tumor cell tracking *in vivo*. Our observation that Katushka expression greatly diminishes tumor growth in immunocompetant but not immunocompromised animals was unexpected and suggests that the protein may be immunogenic.

It has been reported that GFP is minimally immunogenic, however several studies utilize the protein for *in vivo* studies[145,146,93,94]. A recent observation by Hojman in 2009 has identified that Katushka has a lower *in vivo* stability and therefore brightness compared to GFP. This is unexpected as the *in vitro* results show Katushka to be far brighter with better tissue penetrance than GFP. Hojman and colleagues suggest the reason for this discrepancy between *in vitro* and *in vivo* observations may be due to either some intrinsic protein features, the types of which they do not speculate, or due to an immunogenic response[147]. Our results support Hojman's later hypothesis rather than the former. If there were some intrinsic features which kept Katuhska expressing tumor cells from thriving in immunocompetant mice, then they would also reduce growth in the immunocompromised model. Our results are explained easily by a Katushka mediated immune response. If this were the case then the initial characterization of the transgenic Katushka expressing frogs would have not identified immunogenicity, as the Katushka gene presence in the frog germ-line would ensure the encoded protein was recognized as

"self". The exact mechanism by which the presence of an intracellular sea anemone protein would trigger immune response is unclear. However, cancer cells do exist in an environment in which the availability of nutrients and oxygen is quite transient, therefore tumors exhibit a higher degree of cell turn-over. If lysed tumor cells release the foreign protein into the tumor microenvironment it would cause a shift of the recruited macrophages towards an M1 tumoricidal phenotype, or cause a xenograph rejection response[148]. In either case, T-cells would identify the foreign antigen and would recruit macrophages by MCP-1 and other chemokines and release stimulatory factors such as IFN-γ to promote M1 macrophage infiltration and tumor destruction. Alternatively graph rejection has been shown to occur in a T-cell independent manner by macrophages alone[148]. The T-cell independent model is unlikely to be the mechanism at play in this case as Katushka expressing tumors thrive in Rag1 deficient mice, which lack mature B and T cells but have macrophages. There is also the possibility that the macrophages from the C57BL/6 $RAG1^{-/-}$ immunodeficient mice are altered in some way, however that has yet to be reported.

Despite these observations, one report by Nunez-Cruz *et al.* has utilized Katushka for imaging orthotopic ovarian cancer[149]. In this study, an ovarian Katushka expressing tumor is made from a lentiviral Katushka infected cell line (called $MOV1^{Kat}$), which originated from a spontaneous ovarian tumor forming mouse. Although tumor growth is readily observed in the recipient mouse, the authors do not compare tumor growth with tumors not expressing Katushka[149]. Therefore it is unclear whether or not the tumor growth is reduced by Katushka expression in this case.

CONCLUSION

A5.1 The use of Katushka for *in vivo* tumor imaging studies

We had set out to utilize the far-red Katushka protein to image tumors thereby complementing the previously described work with tumors grown in the S100A10-null mouse model. Although cellular labeling and *in vivo* detection functioned as expected, an unfortunate effect of Katushka expression was hampered tumor growth in immunocompetant mice. These findings suggest that Katushka may be immunogenic, however further studies are required for such a determination.

A5.2 Future directions

In light of Katushka's short comings in our experimental model we next sought to employ magnetic resonance imaging (MRI) as a means of non-invasive, deep tissue animal imaging. MRI functions by creating a powerful magnetic field (B_o), aligning the atomic nuclei within the animal, and systematically altering that alignment by a second radio frequency (RF) field operating in pulses[150]. The RF field is oriented at 90^o from the B_o field causing an alteration in the alignment of the nuclei from the B_o field to the RF field until the pulse is stopped and the nuclei re-align with the B_o field[151]. The system causes the nuclei to produce a rotating magnetism which is detectable by a scanner. MRI produces images with high contrast between different soft tissues on the body at resolution of tens of microns[151]. We have used MRI to create an image of a spontaneous MMTV-PyMT breast tumor in a mouse (Figure 41). This technique ideal for longitudinal tumor tracking studies of the MMTV-PyMT/S100A10-null mice allowing us to better investigate the growth inhibition occurring in the absence of S100A10. Additionally,

MRI is useful in tracking tagged cells. We plan to repeat the macrophage adoptive transfer studies with macrophages that have engulfed 0.9 μm polymer beads containing iron oxide. The iron oxide will show up as dark points on the MRI, allowing for the confirmation that transferred WT macrophages are indeed infiltrating into the tumor site.

Figure 41. MRI image of a MMTV-PyMT breast tumor. 150μm^3 isotropic images of transverse (left) and axial (right) slices of a mouse showing unilateral MMTV-PyMT breast tumor formation. Green arrow indicates tumor mass whereas blue arrow indicates tumor free tissue mammary fat pad. All MRI scans were performed at 3.0 T. *In vivo* images were obtained using a 3D true-FISP (balanced steady-state free precession, b-SSFP) imaging sequence (T2/T1 weighting). Repetition time (T_R), echo time (T_E), flip angle and bandwidth (BW) were optimized for best image quality. The sequence consisted of T_R/T_E = 8/4 ms, flip angle = 30° and BW = 50 kHz. A field of view (FOV) of 38.4 × 25.5 × 25.5 with matrix dimensions 256 × 170 × 170 was used to acquire (150-μm)^3 isotropic spatial resolution images with 6 signal averages (~48 minutes per MRI scan).

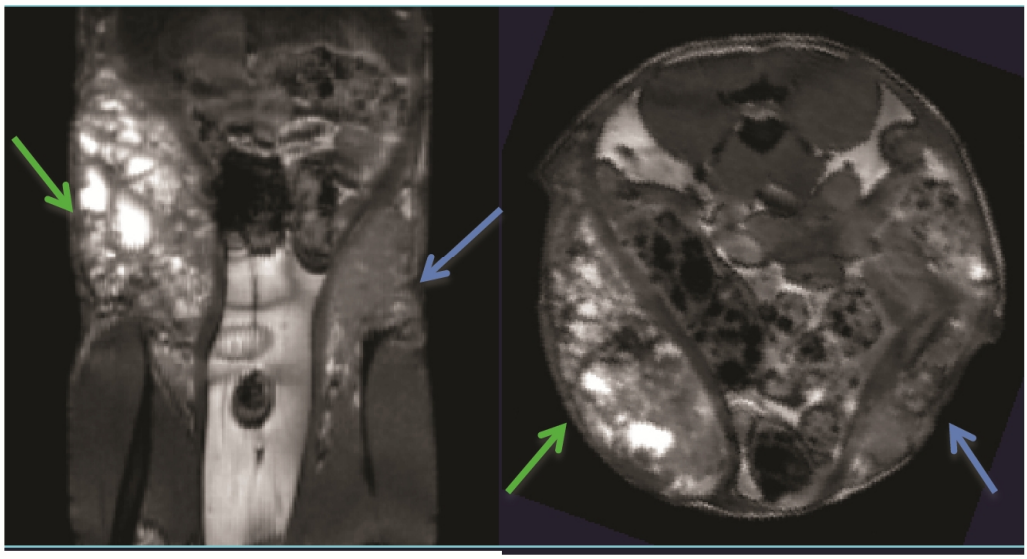

APPENDIX B: MANUSCIPT IN REVISION

The following appendix contains the first manuscript in revision featuring some of the work presented in this thesis. The references have not been included with the manuscript.

A catastrophic collaboration; S100A10 facilitates the tumor promoting association of macrophages with tumor cells.

Kyle D. Phipps, Alexi P. Surette and David M. Waisman
Department of Biochemistry and Molecular Biology, Dalhousie University, Halifax, NS

Corresponding Author:
David Waisman
1459 Oxford Street
Dalhousie University
Halifax, Nova Scotia
Canada B3H 4R2
TEL (902) 494-1803
FAX: (902) 494-1355

Running Head: Tumor-associated macrophage utilization of S100A10

Keywords: Tumor Associated Macrophage, S100A10, Plasminogen, Plasmin, Annexin A2

Grant Support: Authors supported by a grant from the Canadian Cancer Society Research Institute and Canadian Institutes of Health Research.

The authors declare no competing interests.

Manuscript Details
Abstract = 197 words
Main text = 2,118 words
Fig legends = 675 words
References = 20
Figs
4 figs
4 sup figs

ABSTRACT

Macrophages play a fundamental role as mediators of tumor growth, invasion and metastasis. The movement of macrophages across the basement membrane and through the extracellular matrix to the tumor site requires the activation of proteases, such as plasmin, at their cell surface. In the present study we report that the growth of murine Lewis lung carcinoma or T241 fibrosarcoma is dramatically reduced in S100A10$^{-/-}$ (S100A10-null) mice compared to WT mice. The tumor growth deficit corresponded with a decrease in macrophage density, suggesting that macrophages required S100A10 to migrate to the tumor site. Although the tumor growth deficit observed in S100A10-null mice was restored by intraperitoneal injection of WT macrophages, S100A10-null macrophages only restored tumor growth when directly injected into the tumor, suggesting a loss in migratory capability by S100A10-null macrophages. Lastly, selective depletion of macrophages from a WT mouse resulted in similar tumor growth deficits to that in the S100A10-null mouse. These results show that S100A10-dependent plasmin generation is required for macrophage migration to the tumor site and that this represents a rate limiting step in tumor progression. Our results highlight a new role for the S100A10 protein in the recruitment of macrophages to the tumor site.

B1 INTRODUCTION

There is an increasingly large body of evidence correlating tumor-associated macrophage (TAM) density with poor prognosis in a varied number of solid tumors (1, 2). TAM density is directly dependent upon the recruitment of monocytic precursor cells from circulation in response to varied chemotactic signals from the tumor (3). The tumor cytokine milieu, including M-CSF, IL-4, IL-13 and IL-10, causes the recruited monocytes/macrophages to differentiate into the alternatively activated, M2 macrophage phenotype rather than the tumoricidal M1 phenotype (4-6). The M2 TAMs promote tumor growth by mediating inflammation, stimulating angiogenesis, suppressing anti-tumor immunity and by matrix remodeling (6-8). Little is known however about the mechanism by which monocytes/macrophages move through tissue barriers in order to arrive at the tumor site. Plow *et al.* hypothesized that upon activation, circulating monocytes mobilize cell surface plasminogen receptors to generate plasmin, facilitating their movement out of the vessel, through the basement membrane and interstitial space and into the tumor site (9-11). Several activators have been proposed to mediate cellular plasmin generation, most recently the plasminogen receptor S100A10 has been shown to mediate the recruitment of macrophages to an inflammatory stimulus (12).

S100A10, also known as p11, is a member of the S100 family of small, EF hand containing, dimeric proteins. It is present on the cell surface in a heterotetrameric form in which two annexin A2 monomers secure the S100A10 dimer to the cell surface. S100A10 binds both plasminogen and tissue plasminogen activator, facilitating the conversion of plasminogen to plasmin (13). Active plasmin both degrades fibrin directly and activates members of the matrix metalloproteases family, creating a localized

proteolytic hub (14, 15). Recent work by our laboratory has shown that S100A10 is responsible for the conversion of plasminogen to plasmin by many transformed and normal cells, including macrophages (12, 16, 17). Here, we show that compared to WT mice, tumor cells injected into S100A10-null mice fail to thrive because of a loss of macrophage recruitment to the tumor site. Thus, we demonstrate for the first time that macrophages utilize S100A10 to migrate to the tumor site and that this recruitment is the rate limiting step in tumor growth.

B2 MATERIALS AND METHODS

B2.1 Cell lines and reagents. The LLC cell line was obtained from and authenticated by ATCC in 2006. The T241 cell line was obtained from Dr. Y. Cao (Karolinska Instiute). Both LLC and T241 have been found negative for mycoplasma as well as negative for a panel of murine pathogens (Charles River Comprehensive Mouse Panel 1). Cell lines were maintained in complete DMEM (Gibco) with 10% FCS (Hyclone) and penicillin/streptomycin (Hyclone).

B2.2 *In vivo* tumor growth and macrophage addback. Mouse experiments were performed under the approval of the Dalhousie University Carlton Animal Care Facility and mice were maintained in pathogen-free facilities. Tumors were established by subcutaneous injection of $2x10^6$ cells in the right flank of female 6-8week old mice. Volume calculated as (length x width^2)/2. Intraperitoneal transfer of $9x10^6$ macrophages was performed 1-day prior to tumor cell inoculation while intratumoral transfer of $0.25x10^6$ macrophages was performed 4-days after tumor cell inoculation.

B2.3 Macrophage collection. Macrophages were collected by peritoneal lavage with RPMI (Gibco) 4-days after intraperitoneal injection of 2.5 ml of 4% brewers thioglycolate (Sigma).

B2.4 Immunofluorescence and immunohistochemistry. Tumors were snap-frozen for immunostaining with F4/80 (Abcam), alkaline phosphatase secondary (Biocare Medical); CD31 (Abcam), Alexa-488 secondary; anti-Fibrin (ADI), horseradish peroxidase secondary (HRP). Tumors were fixed in 10% formalin and paraffin embedded for PCNA (Abcam) immunostaining with HRP secondary.

B2.5 Terminal deoxynucleotidyl transferase dUTP nick end labeling (TUNEL) assay. TUNEL was performed on snap frozen, cryosectioned tumors as per the manufacturer's instructions with an alkaline phosphatase converter (*In situ* cell death detection Roche).

B2.6 Liposomes. Clodronate (Sigma) was encapsulated in liposomes as in Zeisberger *et al*. 2006.

B2.7 Cytokine array. Array performed by RayBiotech inc. (Norcross G.A.)

B2.8 Invasion assay. $1x10^5$ WT and S100A10-null peritoneal macrophages were added to the upper reservoir of Matrigel (MTG) coated invasion chambers (BD 8 μm pore) in the presence or absence of 0.5 μM plasminogen (PG). Macrophages were allowed to invade towards $1x10^5$ LLC cells in the lower reservoir for 48 hrs.

B2.9 Survival assay. $1x10^5$ Macrophages and $0.2x10^5$LLC cells plated for 24hr prior to a 4-hr incubation with varying levels of clodrolip. Following a 24-hr recovery period, cells were subjected to an MTT assay (CellTiter 96 Promega) to assess viability.

B2.10 MTT assay. MTT was performed on macrophages and LLC cells as per the manufacturer's instructions (CellTiter 96 Promega).

B2.11 Statistical analyses. All statistical calculations were performed in Prism (GraphPad Prism version 3.0 Software). All error expressed as standard error of the mean and all Student *t*-tests performed were two-tailed. ANOVA with Tukey post analysis was used to calculate the statistical significance between more than two groups.

B3 RESULTS AND DISCUSSION

Our previous studies had shown that macrophage migration in response to thioglycollate-induced peritonitis was dramatically diminished in S100A10-null mice. The inability of these macrophages to respond to this inflammatory stimulus was due to the reduced capability of the S100A10-null macrophages to convert plasminogen to plasmin. Since the site of tumor growth is also a site of inflammation, we tested the possibility that S100A10 might be required for the recruitment of macrophages to the tumor site. Therefore, we inoculated WT and S100A10-null mice with Lewis lung carcinoma (LLC) cells and measured the kinetics of tumor growth. Surprisingly, we found that S100A10-null tumor growth ceased at approximately 7-days, whereas tumors in the WT controls displayed nearly exponential growth (Fig. 1A). Eighteen days after the initiation of tumor growth we observed LLC tumors in WT mice were greater than 10-fold the weight of those in the S100A10-null mice (Fig. 1A). To rule out the

possibility that the tumor growth deficit was limited to LLC, we examined another tumor model system and observed that the tumor growth rate from T241 murine fibrosarcoma cells was also dramatically reduced in the S100A10-null mice (Fig. 1A). Imunohistochemical assessment of the proliferative cell nuclear antigen status indicated that there was no difference in the proliferative rates of the tumor cells in either mouse type (Fig. 1B). There was however, a moderate increase in apoptotic cells in the tumors on S100A10-null mice, identified by terminal deoxynucleotidyl transferase dUTP nick end labeling (Fig. 1C). Taken together these observations suggest that apoptosis contributes to the tumor growth inhibition in the S100A10-null environment, although the apoptotic mechanism is unclear.

Immunohistochemical analysis indicated that the tumors grown in the S100A10-null mice contained much fewer macrophages than the WT tumors, suggesting that the S100A10-null macrophages failed to colonize the LLC and T241 tumors (Fig. 1D). S100A10-null macrophages could only be observed along the absolute tumor tissue border whereas the WT macrophages were abundant throughout the tumor (Fig. 1D). Macrophages are known to infiltrate and support tumor growth (13). Therefore, these results suggested that S100A10 plays a key role in the recruitment of macrophages to the tumor site and that the inability of S100A10-null macrophages to reach the tumor site might result in a tumor growth deficit, although we could not rule out the possibility that S100A10 played a role in the function of other tumor-associated cells.

We had also considered the possibility that the difference in macrophage density could also result from lower levels of the cytokines emanating from the tumor cells in the S100A10-null mice. However, the MCP-1, CCL5, GM-CSF and M-CSF levels were

either the same or elevated in the S100A10-null environment, indicating that tumors grown in WT and S100A10-null mice were equally capable of stimulating macrophage recruitment to the tumor site (Supplementary Fig. 1).

To test the possibility that the tumor growth deficit observed in the S100A10-null mice was due to an inability of the macrophages to enter the tumor stroma, we performed an invasion assay in which macrophages invaded through a synthetic basement membrane (Matrigel) towards a LLC monolayer in the presence of plasminogen. Macrophages isolated from S100A10-null mice displayed an impaired ability to invade through the Matrigel coated membrane compared to the WT macrophages (Supplementary Fig. 2), suggesting that the difference in invasion was due to an inability to stimulate protease activity to cleave and penetrate the Matrigel barrier (6).

Angiogenesis, the formation of new blood vessels from pre-existing vessels, is commonly associated with TAM function (4, 18). We observed that, compared to tumors grown in the WT mice, tumors from the S100A10-null mice had a 58% decrease in vessel density (Fig. 2A). Additionally, multiple fibrin occluded vessels were identified in the vasculature of the tumors grown in the S100A10-null mice (Fig. 2B, C). Tumors have an increased ability to activate fibrinogen to fibrin, forming clots which accumulate in blood vessels (19). Vessels in the WT mice express S100A10 and can produce plasmin to clear the fibrin accumulation (Supplementary Fig. 3). The S100A10-null endothelial cells have a reduced fibrinolytic activity, thereby causing the accumulation of fibrin in the tumor vasculature. Thus, the loss of tumor growth in the S100A10-null mice could be explained, in part, by the loss in TAM recruitment, the loss in tumor angiogenesis and an inability of the existing vasculature to maintain vascular fluidity.

In order to directly access the role that macrophages played in our tumor model system, we tested the effect of injecting macrophages, collected from WT mice, into the peritoneum of S100A10-null mice prior to subcutaneous tumor implantation. We observed that the WT macrophages stimulated tumor growth (Fig. 3A,C) and produced an increase in tumor vascular density to that observed in tumors grown in WT mice (Fig. 2A). However, WT macrophages injected into the peritoneum of WT mice had no effect on tumor vascular density (Fig. 2A) or tumor growth in these WT mice (Fig. 3A,C). Importantly, an intraperitoneal injection of macrophages isolated from S100A10-null mice had no effect on tumor growth in S100A10-null mice (Fig. 3A, C). These results indicate that the WT macrophages but not S100A10-null macrophages were capable of stimulating both angiogenesis and subsequent tumor growth in the S100A10-null mice. In contrast we observed that the direct injection of either WT or S100A10-null macrophages into the tumors growing in S100A10-null mice stimulated tumor growth to similar levels to that of WT mice (Fig. 3B,D). These results indicate that the tumor growth deficit could be overcome by S100A10 expressing, WT macrophages infiltrating into the tumor from the peritoneum, or by the direct intratumoral delivery of S100A10-null macrophages. Thus, macrophages lacking S100A10 are capable of stimulating tumor growth, but lack the ability to transit into the tumor. Additionally, the transfer of WT macrophages by either route had no effect on tumor growth in the WT mice, suggesting that endogenous macrophage recruitment was sufficient to support tumor growth in WT mice.

Tumor growth is promoted by macrophages as well as by other cells including neutrophils and fibroblasts, all of which lack S100A10 in our model (6). We therefore sought to address whether selective depletion of macrophages would also inhibit tumor

growth. It has been shown that macrophages may be selectively depleted in mice using liposome encapsulated clodronate (20). We treated LLC tumor bearing WT mice with intraperitoneal inoculations of clodrolip or with an empty liposome control at various points throughout tumor progression. Typically, this approach resulted in the depletion of approximately 75% of the tumor macrophage population compared to the control treated tumors (Fig. 4C). We observed that clodrolip-mediated reduction of TAMs also caused a dramatic reduction in tumor growth and produced a strikingly similar tumor growth profile to that in the S100A10-null mouse (Fig. 4A,B). To rule out that the reduction in tumor growth was not due to clodrolip having a cytotoxic effect on tumor cells, we incubated LLC cells and macrophages with varying concentrations of clodrolip. Macrophages demonstrated a significant decrease in survival relative to clodrolip concentration while LLC survivability remained unaffected (Supplementary Fig. 4).

Tumor growth and metastasis require an intimate relationship between macrophages and cancer cells, the current study demonstrates that the recruitment of macrophages to the tumor site is mediated, in part, by the S100A10 dependent generation of plasmin at the macrophage cell surface. These findings highlight a new therapeutic modality in which tumor progression may be controlled by targeting tumor-associated macrophages.

B4 ACKNOWLEDGEMENTS

S100A10-null mice were donated by P. Svenningsson (Karolinska Institute), and P. Greengard (Rockefeller University). We thank the Dalhousie University Carleton Animal Care Facility for animal support, R. De Antueno (Dalhousie University) for liposome

technical support, Pat Colp (Histology Research Services, Dalhousie University) for immunohistochemical technical support and M. Taboski (Dalhousie University) for helpful comments.

B5 FIGURE LEGENDS

Figure 1. Primary tumor growth is impaired in S100A10-null mice. (**A**), Tumor growth kinetics, terminal weight and representative images of LLC tumors, 18-days after subcutaneous injection of $2x10^6$ LLC cells. Three independent experiments were performed with n=7 mice. Also depicted (lower left) is the tumor growth kinetics of $2x10^6$ subcutaneously injected T241 fibrosarcoma cells. Two independent experiments were performed with n=7 mice. (**B**) LLC tumor proliferative cell nuclear antigen (PCNA) status shown by horse radish peroxidase staining positive staining. Positive cells per 20x s field shown in histogram. (**C**) LLC tumor apoptotic index shown as positive staining terminal deoxynucleotidyl transferase dUTP nick end labeling (TUNEL) cells per field. Staining identified by positive alkaline phosphatase signal and counted per 20x field. (**D**) LLC tumor (upper) and T241 (lower) tumor macrophage density, determined as positive F4/80 staining cells per field by positive alkaline phosphatase staining. (Far right) F4/80 staining cells along the LLC tumor border in a S100A10-null mouse. Histograms display counts of positive cells per 40x field. All error bars signify standard error of the mean and p values are indicative of Student's two tailed, unpaired t-test.

Figure 2. Tumor vascularization impaired in S100A10-null mice. (**A**) Vascular density quantified by Alexa-488 mediated CD31 immunofluorescence of LLC tumors from WT or S100A10-null mice or on mice receiving adoptive transfer of WT macrophages. Histogram displays positive staining vessels per 20x field. (**B**) Fibrin depositions in LLC tumors depicted by anti-fibrin horse-radish peroxidase immunohistochemistry. Histogram displays positive fibrin plaques per 20x field. (**C**) Representative images of autofluorescent (yellow) fibrin occlusions in CD31 positive staining vessels (green) at 40x. Error bars signify standard error of the mean and p values are indicative of (**A**) single variable ANOVA with Tukey post-test analysis or (**B**) Student's two tailed, unpaired t-test.

Figure 3. Adoptive transfer of macrophages effects tumor growth in S100A10-null mice. LLC tumor growth kinetics of mice receiving either (**A**) intraperitoneal or (**B**) intratumoral transfer of WT or S100A10-null macrophages. Terminal LLC tumor masses after (**C**) intraperitoneal or (**D**) intratumoral transfer of WT or S100A10-null macrophages. Volumes calculated as (length x $width^2$)/2. Error bars represent standard error of the mean, p values indicate two-tailed, unpaired Student's t-test and are identified as follows: *P<0.05, **P<0.01, ***P<0.001, NS= Not significant. Experiment was performed three times with n=7 mice.

Figure 4. Macrophage depletion reduces tumor growth. (**A**) LLC tumor growth kinetics of mice receiving intraperitoneal injections of either clodrolip or empty liposomes (PBS-Lip) at various points during tumor progression. Also depicted for comparison are tumor growth kinetics of WT and S100A10-null mice. Experiment was performed twice with n=8 mice. (**B**) Terminal LLC tumor masses after 16 days of growth in a WT mouse with clodrolip or PBS-Lip treatment or no treatment (WT) or on a S100A10-null ($S100A10^{-/-}$) background. (**C**) FACS analysis of F4/80 and CD11B macrophage markers in LLC tumors treated with PBS-Lip or with clodrolip. Macrophages appear in the upper right quadrant. Error bars represent standard error of the mean, p values indicate two-tailed, unpaired Student's t-test and are identified as follows: *P<0.05, **P<0.01, ***P<0.001.

Supplementary Figure 1. Cytokine array of LLC tumors. Chemokine levels of CCL-5, M-CSF, GM-CSF and MCP-1 as Pg/g tumor wet weight from WT and S100A10-null tumors at 14 days after initiation by subcutaneous injection of $2x10^6$ LLC cells. Error bars represent standard error of the mean, p values indicate two-tailed, unpaired Student's t-test.

Supplementary Figure 2. S100A10 mediates macrophage invasion. WT and S100A10-null macrophages which had invaded through Matrigel coated membranes towards LLC cells were stained and counted per 20x field.

Supplementary Figure 3. S100A10 expression on tumor vessels. Alkaline phosphatase mediated anti-S100A10 (R&D Systems) immunohistochemistry used to identify S100A10 expression on endothelial cells lining vessels within snap-frozen LLC tumor sections. Arrows indicate endothelial cells lining vessels. Micrographs were acquired under oil-immersion at 63x magnification.

Supplementary Figure 4. Effect of clodrolip on macrophages and tumor cells. MTT assay of macrophages and LLC cells subjected to increasing concentrations of clodrolip. Results are displayed relative to incubation with an equal volume of PBS-encapsulated liposomes (PBS-Lip). Error bars represent standard error of the mean.

Figure 1

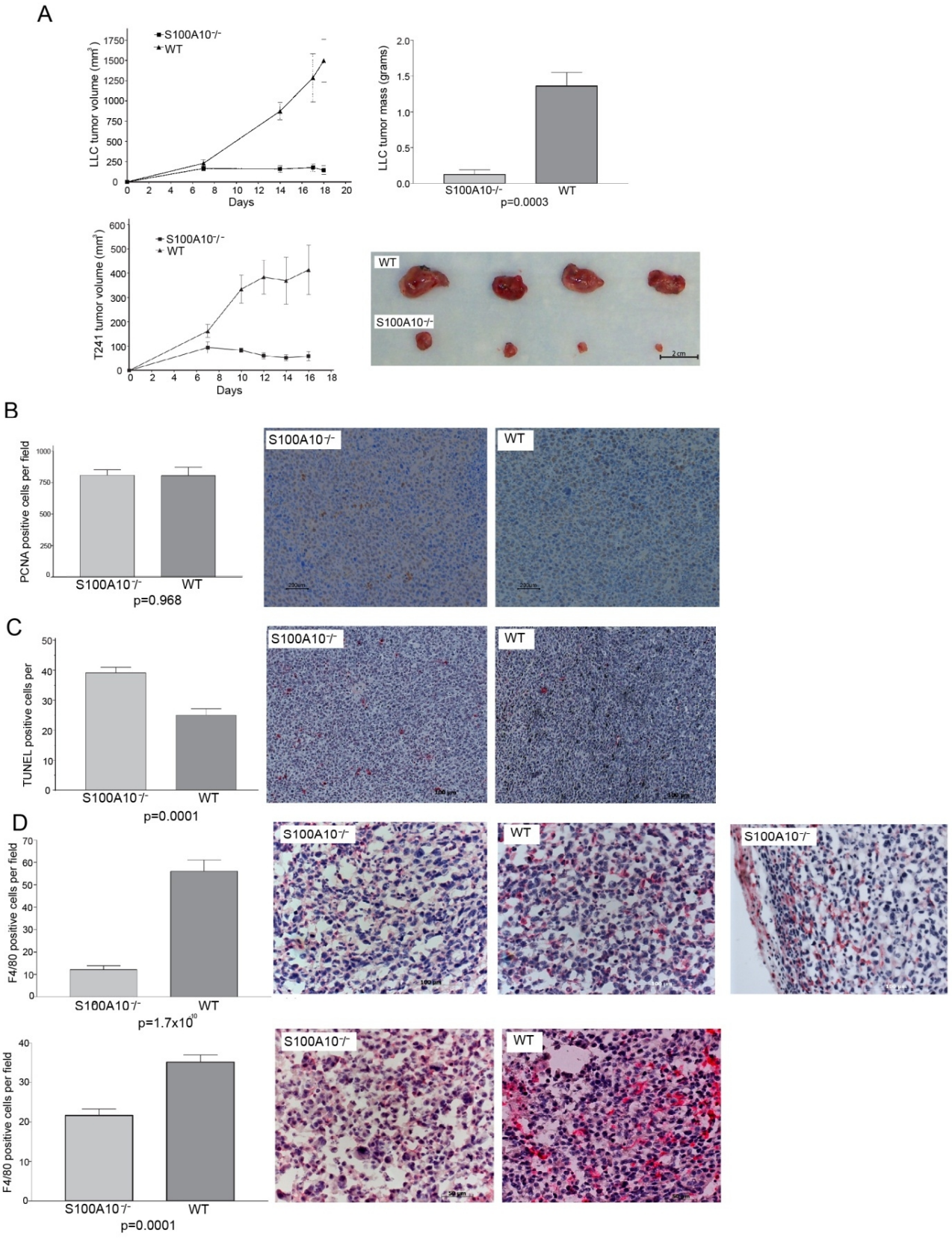
A
S100A10-/-
WT
LLC tumor volume (mm3)
Days
LLC tumor mass (grams)
S100A10-/-
WT
p=0.0003
T241 tumor volume (mm3)
Days
WT
S100A10-/-
2cm
B
PCNA positive cells per field
S100A10-/-
WT
p=0.968
C
TUNEL positive cells per
S100A10-/-
WT
p=0.0001
D
F4/80 positive cells per field
S100A10-/-
WT
p=1.7x10
F4/80 positive cells per field
S100A10-/-
WT
p=0.0001

Figure 2

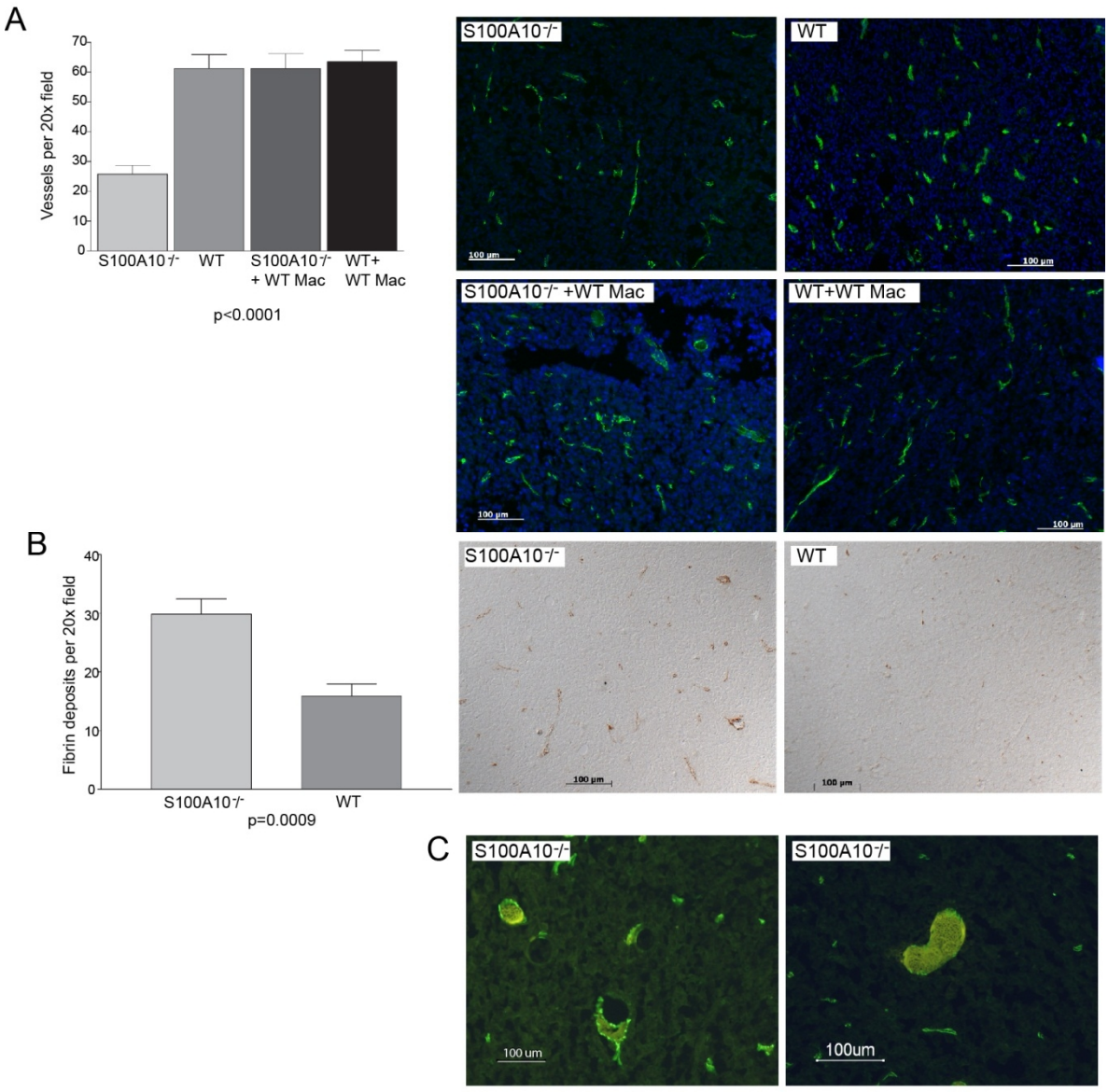
A
Vessels per 20x field
70
60
50
40
30
20
10
0
S100A10-/-
WT
S100A10-/- + WT Mac
WT+ WT Mac
p<0.0001
S100A10-/-
WT
S100A10-/- +WT Mac
WT+WT Mac
100 µm
B
Fibrin deposits per 20x field
40
30
20
10
0
S100A10-/-
WT
p=0.0009
S100A10-/-
WT
C
S100A10-/-
S100A10-/-
100 um
100um

Figure 3

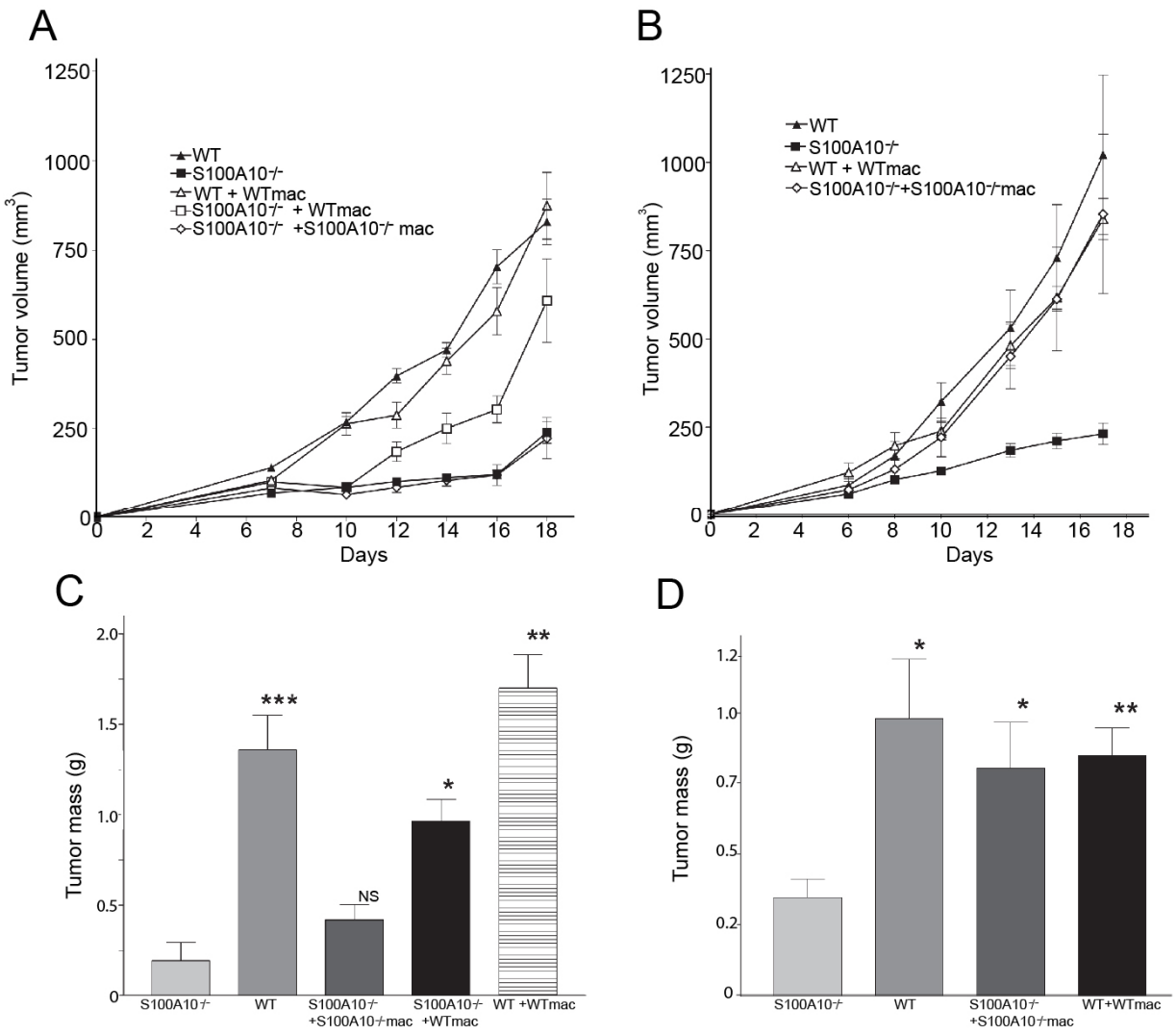
A
Tumor volume (mm3)
Days
WT
S100A10-/-
WT + WTmac
S100A10-/- + WTmac
S100A10-/- +S100A10-/- mac
B
Tumor volume (mm3)
Days
WT
S100A10-/-
WT + WTmac
S100A10-/-+S100A10-/-mac
C
Tumor mass (g)
***
*
NS
*
**
S100A10-/-
WT
S100A10-/- +S100A10-/-mac
S100A10-/- +WTmac
WT +WTmac
D
Tumor mass (g)
*
*
**
S100A10-/-
WT
S100A10-/- +S100A10-/-mac
WT+WTmac

Figure 4

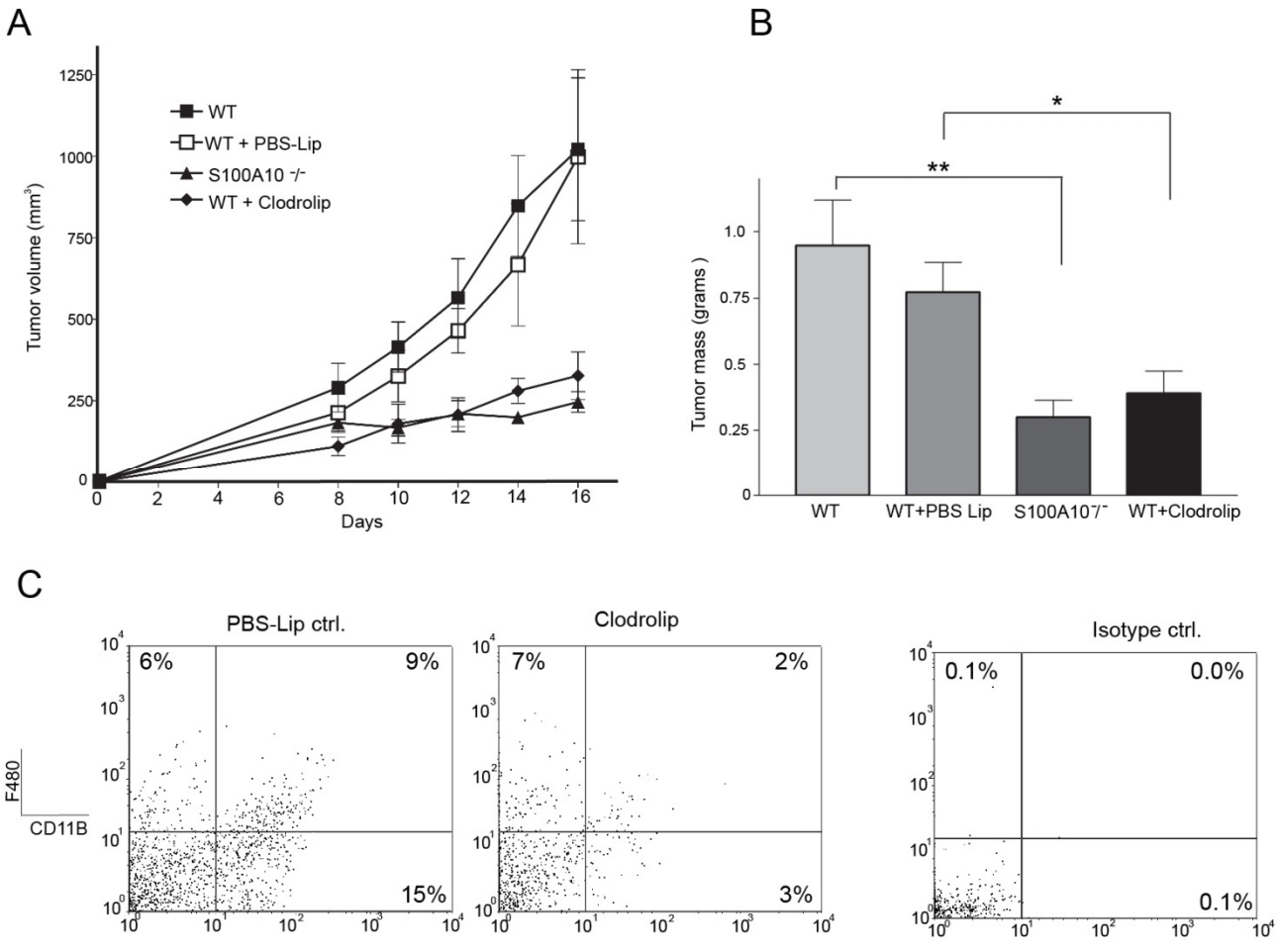
A
Tumor volume (mm3)
1250
1000
750
500
250
0
0
2
4
6
8
10
12
14
16
Days
WT
WT + PBS-Lip
S100A10 -/-
WT + Clodrolip
B
Tumor mass (grams)
1.0
0.75
0.5
0.25
0
*
**
WT
WT+PBS Lip
S100A10-/-
WT+Clodrolip
C
PBS-Lip ctrl.
Clodrolip
Isotype ctrl.
F480
CD11B
6%
9%
15%
7%
2%
3%
0.1%
0.0%
0.1%

Supplementary Figure 1

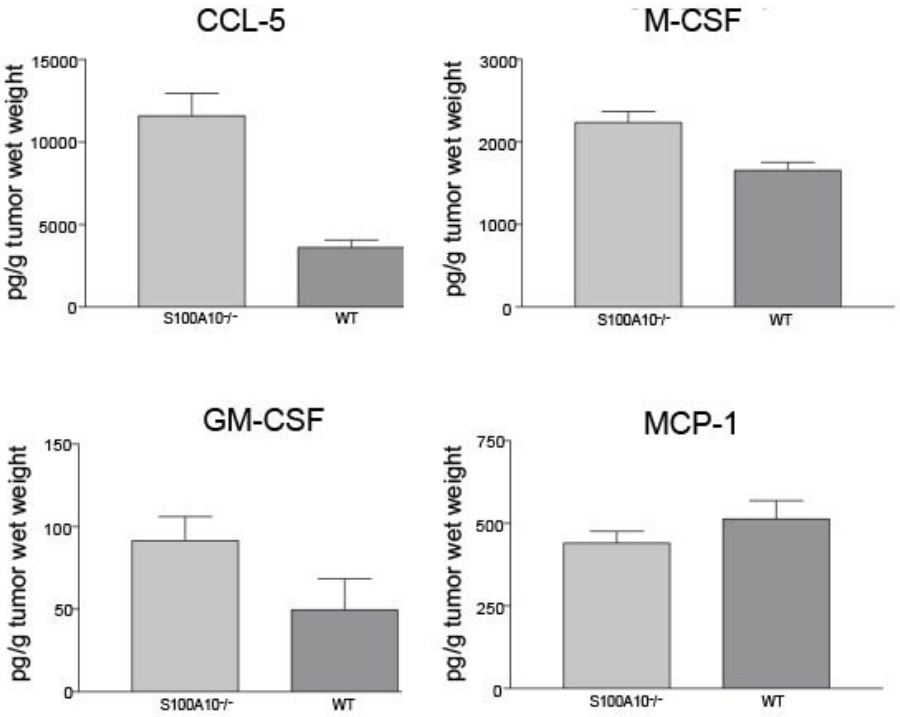

Supplementary Figure 2

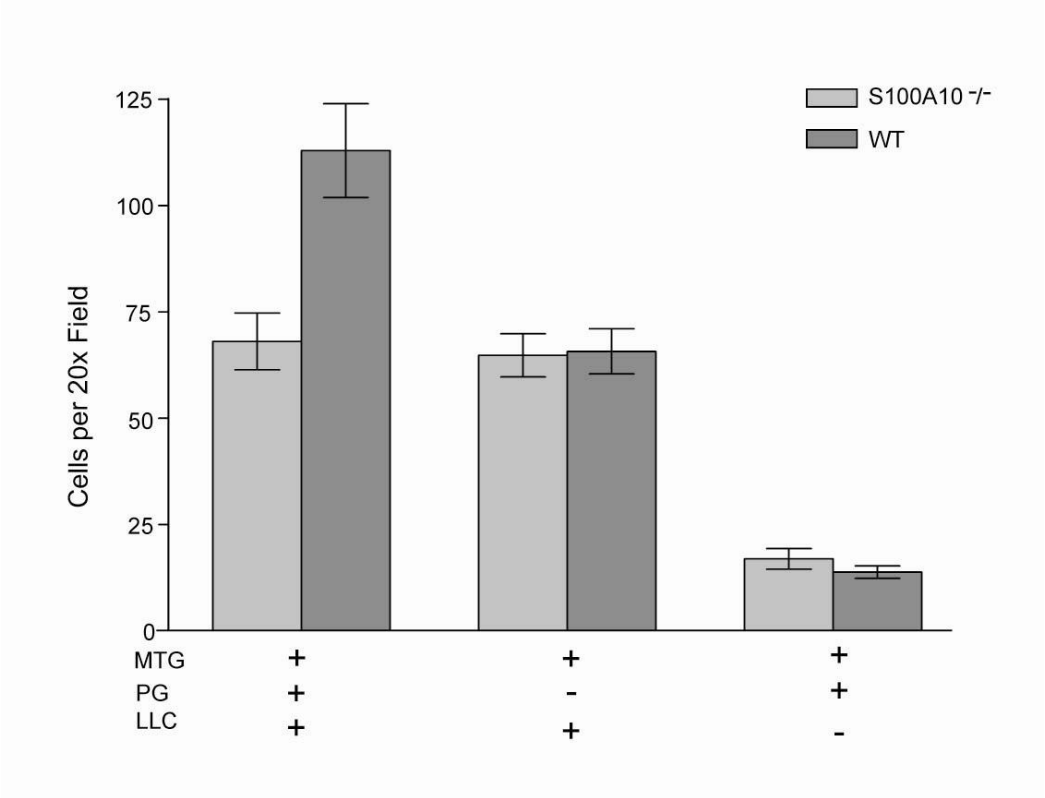

Supplementary Figure 3

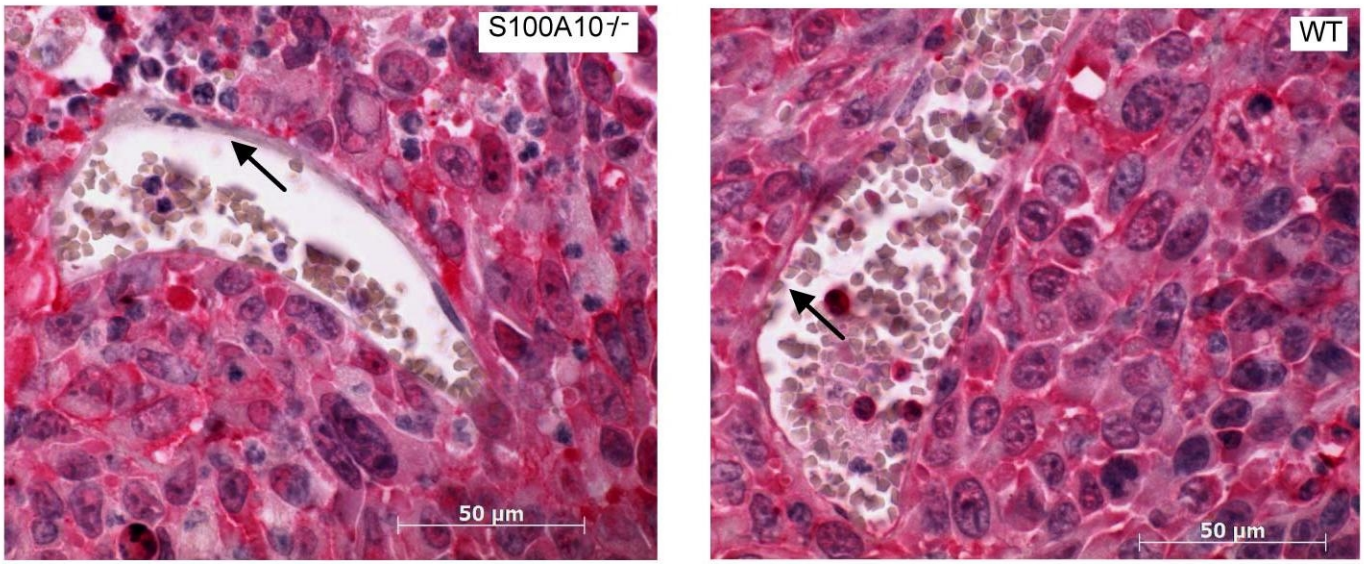

Supplementary Figure 4

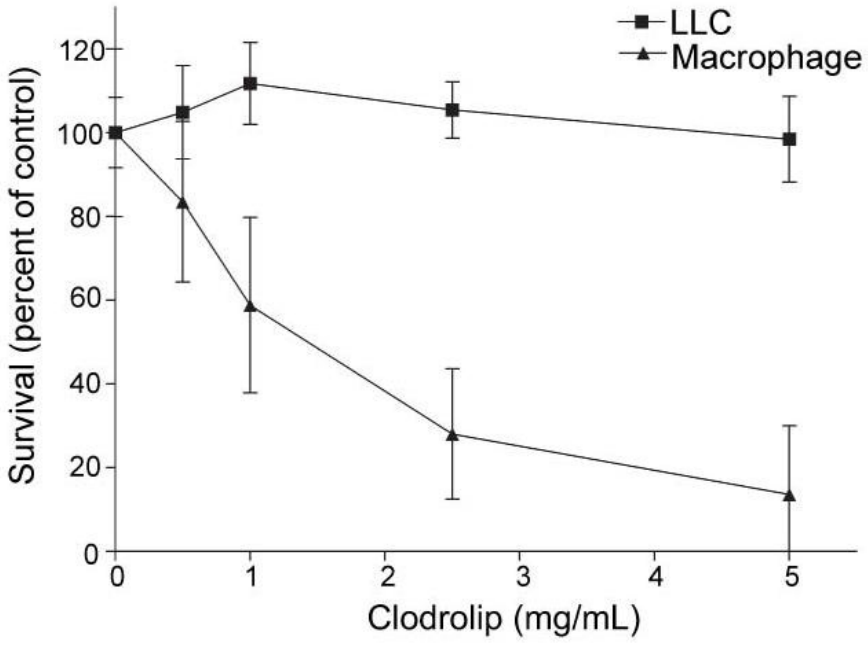

REFFERENCES

1. Geissmann F, Manz MG, Jung S, et al. Development of Monocytes, Macrophages, and Dendritic Cells. *Science*. 2010;327(5966):656 -661.

2. Geissmann F, Jung S, Littman DR. Blood Monocytes Consist of Two Principal Subsets with Distinct Migratory Properties. *Immunity*. 2003;19(1):71-82.

3. Hume DA. The mononuclear phagocyte system. *Current Opinion in Immunology*. 2006;18(1):49-53.

4. Geissmann F, Jung S, Littman DR. Blood Monocytes Consist of Two Principal Subsets with Distinct Migratory Properties. *Immunity*. 2003;19(1):71-82.

5. Sunderkötter C, Nikolic T, Dillon MJ, et al. Subpopulations of Mouse Blood Monocytes Differ in Maturation Stage and Inflammatory Response. *The Journal of Immunology*. 2004;172(7):4410 -4417.

6. Mantovani A, Sozzani S, Locati M, Allavena P, Sica A. Macrophage polarization: tumor-associated macrophages as a paradigm for polarized M2 mononuclear phagocytes. *Trends in Immunology*. 2002;23(11):549-555.

7. Pollard JW. Tumour-educated macrophages promote tumour progression and metastasis. *Nat Rev Cancer*. 2004;4(1):71-78.

8. Sica A, Bronte V. Altered macrophage differentiation and immune dysfunction in tumor development. *J. Clin. Invest*. 2007;117(5):1155-1166.

9. Grakoui A, Bromley SK, Sumen C, et al. The immunological synapse: a molecular machine controlling T cell activation. *Science*. 1999;285(5425):221-227.

10. Quiding-Järbrink M, Raghavan S, Sundquist M. Enhanced M1 Macrophage Polarization in Human Helicobacter pylori-Associated Atrophic Gastritis and in Vaccinated Mice. *PLoS ONE*. 2010;5(11):e15018.

11. Fenton M, Golenbock D. LPS-binding proteins and receptors. *Journal of Leukocyte Biology*. 1998;64(1):25 -32.

12. Murray HW, Nathan CF. Macrophage Microbicidal Mechanisms In Vivo: Reactive Nitrogen versus Oxygen Intermediates in the Killing of Intracellular Visceral Leishmania donovani. *J Exp Med*. 1999;189(4):741-746.

13. Sindrilaru A, Peters T, Wieschalka S, et al. An unrestrained proinflammatory M1 macrophage population induced by iron impairs wound healing in humans and mice. *J. Clin. Invest.* 2011;121(3):985-997.

14. Challen GA, Boles NC, Chambers SM, Goodell MA. Distinct hematopoietic stem cell subtypes are differentially regulated by TGF-beta1. *Cell Stem Cell*. 2010;6(3):265-278.

15. Cassol E, Cassetta L, Alfano M, Poli G. Macrophage polarization and HIV-1 infection. *Journal of Leukocyte Biology*. 2010;87(4):599 -608.

16. Chang CI, Liao JC, Kuo L. Arginase modulates nitric oxide production in activated macrophages. *Am. J. Physiol*. 1998;274(1 Pt 2):H342-348.

17. Chang C-I, Liao JC, Kuo L. Macrophage Arginase Promotes Tumor Cell Growth and Suppresses Nitric Oxide-mediated Tumor Cytotoxicity. *Cancer Research*. 2001;61(3):1100 -1106.

18. Ding T, Xu J, Wang F, et al. High tumor-infiltrating macrophage density predicts poor prognosis in patients with primary hepatocellular carcinoma after resection. *Hum. Pathol*. 2009;40(3):381-389.

19. Wongkham. Tissue invasive macrophage density is correlated with prognosis in cholangiocarcinoma. *Mol Med Rep*. 2010;3(4).

20. Takanami I, Takeuchi K, Kodaira S. Tumor-Associated Macrophage Infiltration in Pulmonary Adenocarcinoma: Association with Angiogenesis and Poor Prognosis. *Oncology*. 1999;57(2):138-142.

21. Clear AJ, Lee AM, Calaminici M, et al. Increased angiogenic sprouting in poor prognosis FL is associated with elevated numbers of CD163+ macrophages within the immediate sprouting microenvironment. *Blood*. 2010;115(24):5053-5056.

22. Ryder M, Ghossein RA, Ricarte-Filho JCM, Knauf JA, Fagin JA. Increased density of tumor-associated macrophages is associated with decreased survival in advanced thyroid cancer. *Endocr Relat Cancer*. 2008;15(4):1069-1074.

23. Salvesen HB, Akslen LA. Significance of tumour-associated macrophages, vascular endothelial growth factor and thrombospondin-1 expression for tumour angiogenesis and prognosis in endometrial carcinomas. *Int. J. Cancer*. 1999;84(5):538-543.

24. Lin EY, Nguyen AV, Russell RG, Pollard JW. Colony-Stimulating Factor 1 Promotes Progression of Mammary Tumors to Malignancy. *The Journal of Experimental Medicine*. 2001;193(6):727 -740.

25. Duluc D, Delneste Y, Tan F, et al. Tumor-associated leukemia inhibitory factor and IL-6 skew monocyte differentiation into tumor-associated macrophage-like cells. *Blood*. 2007;110(13):4319 -4330.

26. Duluc D, Corvaisier M, Blanchard S, et al. Interferon γ reverses the immunosuppressive and protumoral properties and prevents the generation of human tumor associated macrophages. *International Journal of Cancer*. 2009;125(2):367-373.

27. Melancon MP, Lu W, Huang Q, et al. Targeted imaging of tumor-associated M2 macrophages using a macromolecular contrast agent PG-Gd-NIR813. *Biomaterials*. 2010;31(25):6567-6573.

28. Sica A, Saccani A, Mantovani A. Tumor-associated macrophages: a molecular perspective. *International Immunopharmacology*. 2002;2(8):1045-1054.

29. Lauber K, Bohn E, Kröber SM, et al. Apoptotic cells induce migration of phagocytes via caspase-3-mediated release of a lipid attraction signal. *Cell*. 2003;113(6):717-730.

30. Leek RD, Harris AL. Tumor-associated macrophages in breast cancer. *J Mammary Gland Biol Neoplasia*. 2002;7(2):177-189.

31. Brigati C, Noonan DM, Albini A, Benelli R. Tumors and inflammatory infiltrates: friends or foes? *Clin. Exp. Metastasis*. 2002;19(3):247-258.

32. Sica A, Schioppa T, Mantovani A, Allavena P. Tumour-associated macrophages are a distinct M2 polarised population promoting tumour progression: Potential targets of anti-cancer therapy. *European Journal of Cancer*. 2006;42(6):717-727.

33. Lewis C, Hughes R. Inflammation and breast cancer. Microenvironmental factors regulating macrophage function in breast tumours: hypoxia and angiopoietin-2. *Breast Cancer Research*. 2007;9(3):209.

34. Lewis CE, Pollard JW. Distinct Role of Macrophages in Different Tumor Microenvironments. *Cancer Research*. 2006;66(2):605 -612.

35. Luo Y. Targeting tumor-associated macrophages as a novel strategy against breast cancer. *Journal of Clinical Investigation*. 2006;116(8):2132-2141.

36. Allavena P, Chieppa M, Bianchi G, et al. Engagement of the Mannose Receptor by Tumoral Mucins Activates an Immune Suppressive Phenotype in Human Tumor-Associated Macrophages. *Clinical and Developmental Immunology*. 2010;2010:1-10.

37. Allavena P, Sica A, Solinas G, Porta C, Mantovani A. The inflammatory micro-environment in tumor progression: The role of tumor-associated macrophages. *Critical Reviews in Oncology/Hematology*. 2008;66(1):1-9.

38. Yañez R, Oviedo A, Aldea M, Bueren JA, Lamana ML. Prostaglandin E2 plays a key role in the immunosuppressive properties of adipose and bone marrow tissue-derived mesenchymal stromal cells. *Experimental Cell Research*. 2010;316(19):3109-3123.

39. Kobie JJ, Akporiaye ET. Immunosuppressive role of transforming growth factor beta in breast cancer. *Clinical and Applied Immunology Reviews*. 2003;3(6):277-287.

40. Walczak H, Degli-Esposti MA, Johnson RS, et al. TRAIL-R2: a novel apoptosis-mediating receptor for TRAIL. *EMBO J*. 1997;16(17):5386-5397.

41. Kaler P, Galea V, Augenlicht L, Klampfer L. Tumor Associated Macrophages Protect Colon Cancer Cells from TRAIL-Induced Apoptosis through IL-1β- Dependent Stabilization of Snail in Tumor Cells. *PLoS ONE*. 2010;5(7):e11700.

42. Wang F-Q, So J, Reierstad S, Fishman DA. Matrilysin (MMP-7) promotes invasion of ovarian cancer cells by activation of progelatinase. *Int. J. Cancer*. 2005;114(1):19-31.

43. Hamada I, Kato M, Yamasaki T, et al. Clinical effects of tumor-associated macrophages and dendritic cells on renal cell carcinoma. *Anticancer Res*. 2002;22(6C):4281-4284.

44. O'Sullivan C, Lewis CE, McGee JO, Harris AL. Secretion of epidermal growth factor by macrophages associated with breast carcinoma. *The Lancet*. 1993;342(8864):148-149.

45. Goswami S, Sahai E, Wyckoff JB, et al. Macrophages Promote the Invasion of Breast Carcinoma Cells via a Colony-Stimulating Factor-1/Epidermal Growth Factor Paracrine Loop. *Cancer Research*. 2005;65(12):5278 -5283.

46. Tsutsui S, Yasuda K, Suzuki K, et al. Macrophage infiltration and its prognostic implications in breast cancer: the relationship with VEGF expression and microvessel density. *Oncol. Rep*. 2005;14(2):425-431.

47. Chai C-Y, Chen W-T, Hung W-C, et al. Hypoxia-inducible factor-1α expression correlates with focal macrophage infiltration, angiogenesis and unfavourable prognosis in urothelial carcinoma. *Journal of Clinical Pathology*. 2008;61(5):658 -664.

48. Mantovani A, Schioppa T, Porta C, Allavena P, Sica A. Role of tumor-associated macrophages in tumor progression and invasion. *Cancer Metastasis Rev*. 2006;25(3):315-322.

49. Dirkx AEM, oude Egbrink MGA, Wagstaff J, Griffioen AW. Monocyte/macrophage infiltration in tumors: modulators of angiogenesis. *Journal of Leukocyte Biology*. 2006;80(6):1183 -1196.

50. Muller WA, Weigl SA, Deng X, Phillips DM. PECAM-1 is required for transendothelial migration of leukocytes. *J. Exp. Med*. 1993;178(2):449-460.

51. Zhang L, Fogg DK, Waisman DM. RNA interference-mediated silencing of the S100A10 gene attenuates plasmin generation and invasiveness of Colo 222 colorectal cancer cells. *J. Biol. Chem*. 2004;279(3):2053-2062.

52. De Petro G, Barlati S. Characterisation of fibronectin fragments and plasminogen activators released by RSV-transformed cells. *Fibrinolysis*. 1987;1(3):183-187.

53. Horowitz JC, Rogers DS, Simon RH, Sisson TH, Thannickal VJ. Plasminogen Activation Induced Pericellular Fibronectin Proteolysis Promotes Fibroblast Apoptosis. *Am. J. Respir. Cell Mol. Biol.* 2008;38(1):78-87.

54. Moser TL, Enghild JJ, Pizzo SV, Stack MS. The extracellular matrix proteins laminin and fibronectin contain binding domains for human plasminogen and tissue plasminogen activator. *J. Biol. Chem*. 1993;268(25):18917-18923.

55. DePoli P, Bacon-Baguley T, Kendra-Franczak S, Cederholm MT, Walz DA. Thrombospondin interaction with plasminogen. Evidence for binding to a specific region of the kringle structure of plasminogen. *Blood*. 1989;73(4):976-982.

56. Chapman Jr. HA, Vavrin Z, Hibbs Jr. JB. Macrophage fibrinolytic activity: Identification of two pathways of plasmin formation by intact cells and of a plasminogen activator inhibitor. *Cell*. 1982;28(3):653-662.

57. Ramos-DeSimone N, Hahn-Dantona E, Sipley J, et al. Activation of Matrix Metalloproteinase-9 (MMP-9) via a Converging Plasmin/Stromelysin-1 Cascade Enhances Tumor Cell Invasion. *Journal of Biological Chemistry*. 1999;274(19):13066 - 13076.

58. Das R, Pluskota E, Plow EF. Plasminogen and Its Receptors as Regulators of Cardiovascular Inflammatory Responses. *Trends in Cardiovascular Medicine*. 2010;20(4):120-124.

59. Hashizume H, Baluk P, Morikawa S, et al. Openings between defective endothelial cells explain tumor vessel leakiness. *Am. J. Pathol*. 2000;156(4):1363-1380.

60. Kang HM, Choi KS, Kassam G, et al. Role of annexin II tetramer in plasminogen activation. *Trends Cardiovasc. Med*. 1999;9(3-4):92-102.

61. Hasumi K, Yamamichi S, Harada T. Small-molecule modulators of zymogen activation in the fibrinolytic and coagulation systems. *FEBS J*. 2010;277(18):3675-3687.

62. Waisman DM. *Plasminogen: structure, activation, and regulation*. Springer; 2003.
63. Castellino FJ, McCance SG. The kringle domains of human plasminogen. *Ciba Found. Symp*. 1997;212:46-60; discussion 60-65.

64. REJANTE MR, LLINÁS M. 1H NMR assignments and secondary structure of human plasminogen kringle 1. *European Journal of Biochemistry*. 1994;221(3):927-937.

65. Nowak P, Zgirski A. Effects of Metal Ions on Activity of Plasmin. *BTER*. 2003;93(1-3):87-94.

66. Bohnsack RN, Patel M, Olson LJ, Twining SS, Dahms NM. Residues Essential for Plasminogen Binding by the Cation-Independent Mannose 6-Phosphate Receptor. *Biochemistry*. 2010;49(3):635.

67. Ellis V, Scully MF, Kakkar VV. Plasminogen activation initiated by single-chain urokinase-type plasminogen activator. Potentiation by U937 monocytes. *J. Biol. Chem*. 1989;264(4):2185-2188.

68. Petersen LC. Kinetics of reciprocal pro-urokinase/plasminogen activation--stimulation by a template formed by the urokinase receptor bound to poly(D-lysine). *Eur. J. Biochem*. 1997;245(2):316-323.

69. Kwak S-H, Mitra S, Bdeir K, et al. The kringle domain of urokinase-type plasminogen activator potentiates LPS-induced neutrophil activation through interaction with {alpha}V{beta}3 integrins. *J. Leukoc. Biol*. 2005;78(4):937-945.

70. Mauro MA, Murphy K, Thomson K, Zollikofer CL. *Image-Guided Intervention*. Elsevier Health Sciences; 2008.

71. Ichinose A, Takio K, Fujikawa K. Localization of the binding site of tissue-type plasminogen activator to fibrin. *J Clin Invest*. 1986;78(1):163-169.

72. Runge MS, Bode C, Matsueda GR, Haber E. Antibody-enhanced thrombolysis: targeting of tissue plasminogen activator in vivo. *Proc Natl Acad Sci U S A*. 1987;84(21):7659-7662.

73. Sitrin RG, Johnson DR, Pan PM, et al. Lipid Raft Compartmentalization of Urokinase Receptor Signaling in Human Neutrophils. *Am. J. Respir. Cell Mol. Biol.* 2004;30(2):233-241.

74. Gerke V, Moss SE. Annexins: From Structure to Function. *Physiological Reviews*. 2002;82(2):331 -371.

75. Longstaff C, Thelwell C, Williams SC, et al. The interplay between tissue plasminogen activator domains and fibrin structures in the regulation of fibrinolysis: kinetic and microscopic studies. *Blood*. 2011;117(2):661 -668.

76. McClatchey KD. *Clinical laboratory medicine*. Lippincott Williams & Wilkins; 2002.

77. Janciauskiene S. Conformational properties of serine proteinase inhibitors (serpins) confer multiple pathophysiological roles. *Biochimica et Biophysica Acta (BBA) - Molecular Basis of Disease*. 2001;1535(3):221-235.

78. Boncela J, Przygodzka P, Papiewska-Pajak I, et al. Plasminogen activator inhibitor type 1 interacts with alpha3 subunit of proteasome and modulates its activity. *J. Biol. Chem*. 2011;286(8):6820-6831.

79. Colman RW. *Hemostasis and thrombosis: basic principles and clinical practice*. Lippincott Williams & Wilkins; 2006.

80. Kapadia C, Yousef GM, Mellati AA, et al. Complex formation between human kallikrein 13 and serum protease inhibitors. *Clin. Chim. Acta*. 2004;339(1-2):157-167.

81. Miles LA, Hawley SB, Baik N, et al. Plasminogen receptors: the sine qua non of cell surface plasminogen activation. *Front. Biosci*. 2005;10:1754-1762.

82. Kwon M, MacLeod TJ, Zhang Y, Waisman DM. S100A10, annexin A2, and annexin a2 heterotetramer as candidate plasminogen receptors. *Front. Biosci*. 2005;10:300-325.

83. Félez J, Miles LA, Fábregas P, et al. Characterization of cellular binding sites and interactive regions within reactants required for enhancement of plasminogen activation by tPA on the surface of leukocytic cells. *Thromb. Haemost*. 1996;76(4):577-584.

84. Miles LA, Plow EF. Receptor mediated binding of the fibrinolytic components, plasminogen and urokinase, to peripheral blood cells. *Thromb. Haemost*. 1987;58(3):936-942.

85. Andronicos NM, Chen EI, Baik N, et al. Proteomics-based discovery of a novel, structurally unique, and developmentally regulated plasminogen receptor, Plg-RKT, a major regulator of cell surface plasminogen activation. *Blood*. 2010;115(7):1319 -1330.

86. Miles LA, Dahlberg CM, Plescia J, et al. Role of cell-surface lysines in plasminogen binding to cells: identification of alpha-enolase as a candidate plasminogen receptor. *Biochemistry*. 1991;30(6):1682-1691.

87. Das R, Burke T, Plow EF. Histone H2B as a functionally important plasminogen receptor on macrophages. *Blood*. 2007;110(10):3763 -3772.

88. Anon. Identification of Histone H2B as a Regulated Plasminogen Receptor† - Biochemistry (ACS Publications).

89. Waisman DM. Annexin A2 may not play a role as a plasminogen receptor. *Br. J. Haematol*. 2005;131(4):553-554; author reply 554-556.

90. Kwon M, Yoon C-S, Jeong W, Rhee SG, Waisman DM. Annexin A2-S100A10 heterotetramer, a novel substrate of thioredoxin. *J. Biol. Chem*. 2005;280(25):23584-23592.

91. Waisman DM. Annexin II tetramer: structure and function. *Mol. Cell. Biochem*. 1995;149-150:301-322.

92. Miles LA, Dahlberg CM, Plescia J, et al. Role of cell-surface lysines in plasminogen binding to cells: identification of .alpha.-enolase as a candidate plasminogen receptor. *Biochemistry*. 1991;30(6):1682-1691.

93. MacLeod TJ, Kwon M, Filipenko NR, Waisman DM. Phospholipid-associated annexin A2-S100A10 heterotetramer and its subunits: characterization of the interaction with tissue plasminogen activator, plasminogen, and plasmin. *J. Biol. Chem*. 2003;278(28):25577-25584.

94. Kim J, Hajjar KA. Annexin II: a plasminogen-plasminogen activator co-receptor. *Front. Biosci*. 2002;7:d341-348.

95. Redlitz A, Plow EF. Receptors for plasminogen and t-PA: an update. *Baillieres Clin. Haematol*. 1995;8(2):313-327.

96. Hembrough TA, Li L, Gonias SL. Cell-surface cytokeratin 8 is the major plasminogen receptor on breast cancer cells and is required for the accelerated activation of cell-associated plasminogen by tissue-type plasminogen activator. *J. Biol. Chem*. 1996;271(41):25684-25691.

97. Semov A, Moreno MJ, Onichtchenko A, et al. Metastasis-associated Protein S100A4 Induces Angiogenesis through Interaction with Annexin II and Accelerated Plasmin Formation. *Journal of Biological Chemistry*. 2005;280(21):20833 -20841.

98. Silverstein RL, Leung LL, Harpel PC, Nachman RL. Platelet thrombospondin forms a trimolecular complex with plasminogen and histidine-rich glycoprotein. *J Clin Invest*. 1985;75(6):2065-2073.

99. Miles LA, Andronicos NM, Baik N, Parmer RJ. Cell-Surface Actin Binds Plasminogen and Modulates Neurotransmitter Release from Catecholaminergic Cells. *The Journal of Neuroscience*. 2006;26(50):13017 -13024.

100. Chapman HA, Wei Y. Protease crosstalk with integrins: the urokinase receptor paradigm. *Thromb. Haemost*. 2001;86(1):124-129.

101. Wei Y, Czekay R-P, Robillard L, et al. Regulation of alpha5beta1 integrin conformation and function by urokinase receptor binding. *J. Cell Biol*. 2005;168(3):501-511.

102. Tarabykina S, Scott DJ, Herzyk P, et al. The Dimerization Interface of the Metastasis-associated Protein S100A4 (Mts1). *Journal of Biological Chemistry*. 2001;276(26):24212 -24222.

103. Donato R. S100: a multigenic family of calcium-modulated proteins of the EF-hand type with intracellular and extracellular functional roles. *Int. J. Biochem. Cell Biol*. 2001;33(7):637-668.

104. Zimmer DB, Cornwall EH, Landar A, Song W. The S100 protein family: history, function, and expression. *Brain Res. Bull*. 1995;37(4):417-429.

105. Réty S, Sopkova J, Renouard M, et al. The crystal structure of a complex of p11 with the annexin II N-terminal peptide. *Nat. Struct. Biol*. 1999;6(1):89-95.

106. Sopkova-de Oliveira Santos J, Oling FK, Réty S, et al. S100 protein-annexin interactions: a model of the (Anx2-p11)(2) heterotetramer complex. *Biochim. Biophys. Acta*. 2000;1498(2-3):181-191.

107. Rescher U, Gerke V. S100A10/p11: family, friends and functions. *Pflugers Arch*. 2008;455(4):575-582.

108. Johnsson N, Marriott G, Weber K. p36, the major cytoplasmic substrate of src tyrosine protein kinase, binds to its p11 regulatory subunit via a short amino-terminal amphiphatic helix. *EMBO J*. 1988;7(8):2435-2442.

109. Harder T, Gerke V. The subcellular distribution of early endosomes is affected by the annexin II2p11(2) complex. *The Journal of Cell Biology*. 1993;123(5):1119 -1132.

110. Chasserot-Golaz S, Vitale N, Umbrecht-Jenck E, et al. Annexin 2 Promotes the Formation of Lipid Microdomains Required for Calcium-regulated Exocytosis of Dense-Core Vesicles. *Mol. Biol. Cell*. 2005;16(3):1108-1119.

111. Yamada A, Irie K, Hirota T, et al. Involvement of the Annexin II-S100A10 Complex in the Formation of E-cadherin-based Adherens Junctions in Madin-Darby Canine Kidney Cells. *Journal of Biological Chemistry*. 2005;280(7):6016 -6027.

112. Girard C, Tinel N, Terrenoire C, et al. p11, an annexin II subunit, an auxiliary protein associated with the background K+ channel, TASK-1. *EMBO J*. 2002;21(17):4439-4448.

113. Hayes MJ, Rescher U, Gerke V, Moss SE. Annexin–Actin Interactions. *Traffic*. 2004;5(8):571-576.

114. Hayes MJ, Shao D, Bailly M, Moss SE. Regulation of actin dynamics by annexin 2. *EMBO J*. 2006;25(9):1816-1826.

115. Miles LA, Parmer RJ. S100A10: a complex inflammatory role. *Blood*. 2010;116(7):1022 -1024.

116. Fogg DK, Bridges DE, Cheung KK-T, et al. The p11 subunit of annexin II heterotetramer is regulated by basic carboxypeptidase. *Biochemistry*. 2002;41(15):4953-4961.

117. Kassam G, Le BH, Choi KS, et al. The p11 subunit of the annexin II tetramer plays a key role in the stimulation of t-PA-dependent plasminogen activation. *Biochemistry*. 1998;37(48):16958-16966.

118. Choi K-S, Fogg DK, Yoon C-S, Waisman DM. p11 regulates extracellular plasmin production and invasiveness of HT1080 fibrosarcoma cells. *FASEB J*. 2003;17(2):235-246.

119. O'Connell PA, Surette AP, Liwski RS, Svenningsson P, Waisman DM. S100A10 regulates plasminogen-dependent macrophage invasion. *Blood*. 2010;116(7):1136-1146.

120. Hou Y, Yang L, Mou M, et al. Annexin A2 regulates the levels of plasmin, S100A10 and Fascin in L5178Y cells. *Cancer Invest*. 2008;26(8):809-815.

121. Schmid MC, Varner JA. Myeloid cells in the tumor microenvironment: modulation of tumor angiogenesis and tumor inflammation. *J Oncol*. 2010;2010:201026.

122. Munn DH, Armstrong E. Cytokine Regulation of Human Monocyte Differentiation in Vitro: The Tumor-Cytotoxic Phenotype Induced by Macrophage Colony-stimulating Factor Is Developmentally Regulated by γ-Interferon. *Cancer Research*. 1993;53(11):2603 -2613.

123. Bowman GD, O'Donnell M, Kuriyan J. Structural analysis of a eukaryotic sliding DNA clamp-clamp loader complex. *Nature*. 2004;429(6993):724-730.

124. Zeisberger SM, Odermatt B, Marty C, et al. Clodronate-liposome-mediated depletion of tumour-associated macrophages: a new and highly effective antiangiogenic therapy approach. *Br. J. Cancer*. 2006;95(3):272-281.

125. Liu K-J, Huang T-S, Lee C-C. Tumor-Associated Macrophage : Its Role in Tumor Angiogenesis. *Lung Cancer*. 2(4):135-140.

126. Toge H, Inagaki T, Kojimoto Y, Shinka T, Hara I. Angiogenesis in renal cell carcinoma: the role of tumor-associated macrophages. *Int. J. Urol*. 2009;16(10):801-807.

127. Banciu M, Schiffelers RM, Storm G. Investigation into the Role of Tumor-Associated Macrophages in the Antitumor Activity of Doxil. *Pharm Res*. 2008;25(8):1948-1955.

128. Folkman J. Tumor angiogenesis: therapeutic implications. *N. Engl. J. Med*. 1971;285(21):1182-1186.

129. Wojtukiewicz MZ, Zacharski LR, Memoli VA, et al. Fibrinogen-fibrin transformation in situ in renal cell carcinoma. *Anticancer Res*. 1990;10(3):579-582.

130. Woude GFV, Klein G. *Advances in Cancer Research*. Academic Press; 2005.

131. Gong Y, Hart E, Shchurin A, Hoover-Plow J. Inflammatory macrophage migration requires MMP-9 activation by plasminogen in mice. *J. Clin. Invest*. 2008;118(9):3012-3024.

132. Recenti R, Leone G, Simi L, et al. Clodronate acts on human osteoclastic cell proliferation, differentiation and function in a bioreversible manner. *Clin Cases Miner Bone Metab*. 2007;4(2):146-155.

133. Qian B, Deng Y, Im JH, et al. A Distinct Macrophage Population Mediates Metastatic Breast Cancer Cell Extravasation, Establishment and Growth. *PLoS ONE*. 2009;4(8):e6562.

134. Zhang J, Guo B, Zhang Y, Cao J, Chen T. Silencing of the annexin II gene down-regulates the levels of S100A10, c-Myc, and plasmin and inhibits breast cancer cell proliferation and invasion. *Saudi Med J*. 2010;31(4):374-381.

135. Rodriguez-Viciana P, Collins CH, Moule MG, Fried M. Chromosomal instability at a mutational hotspot in polyoma middle T-antigen affects its ability to activate the ARF-p53 tumor suppressor pathway. *Oncogene*. 2005;25(10):1454-1462.

136. Wyckoff J, Wang W, Lin EY, et al. A Paracrine Loop between Tumor Cells and Macrophages Is Required for Tumor Cell Migration in Mammary Tumors. *Cancer Research*. 2004;64(19):7022 -7029.

137. Drakaki E, Makropoulou M, Serafetinides AA. In vitro fluorescence measurements and Monte Carlo simulation of laser irradiation propagation in porcine skin tissue. *Lasers Med Sci*. 2008;23(3):267-276.

138. Shcherbo D, Merzlyak EM, Chepurnykh TV, et al. Bright far-red fluorescent protein for whole-body imaging. *Nat. Methods*. 2007;4(9):741-746.

139. Shimomura O. Discovery of green fluorescent protein (GFP) (Nobel Lecture). *Angew. Chem. Int. Ed. Engl*. 2009;48(31):5590-5602.

140. Shimomura O., Johnson F. H., Saiga Y. Extraction, purification and properties of aequorin, a bioluminescent protein from the luminous hydromedusan, Aequorea. *J Cell Comp Physiol*. 1962;59:223-239.

141. Matz MV, Fradkov AF, Labas YA, et al. Fluorescent proteins from nonbioluminescent Anthozoa species. *Nat. Biotechnol*. 1999;17(10):969-973.

142. Garcia-Parajo MF, Koopman M, van Dijk EMHP, Subramaniam V, van Hulst NF. The nature of fluorescence emission in the red fluorescent protein DsRed, revealed by single-molecule detection. *Proceedings of the National Academy of Sciences*. 2001;98(25):14392 -14397.

143. Shaner NC, Campbell RE, Steinbach PA, et al. Improved monomeric red, orange and yellow fluorescent proteins derived from Discosoma sp. red fluorescent protein. *Nat. Biotechnol*. 2004;22(12):1567-1572.

144. Hoffman RM. A better fluorescent protein for whole-body imaging. *Trends in Biotechnology*. 2008;26(1):1-4.

145. Beagles KE, Peterson L, Zhang X, Morris J, Kiem H-P. Cyclosporine inhibits the development of green fluorescent protein (GFP)-specific immune responses after transplantation of GFP-expressing hematopoietic repopulating cells in dogs. *Hum. Gene Ther*. 2005;16(6):725-733.

146. Stripecke R, Carmen Villacres M, Skelton D, et al. Immune response to green fluorescent protein: implications for gene therapy. *Gene Ther*. 1999;6(7):1305-1312.

147. Hojman P, Eriksen J, Gehl J. In Vivo Imaging of Far-red Fluorescent Proteins after DNA Electrotransfer to Muscle Tissue. *Biol Proced Online*. 2009;11(1):253-262.

148. Cadili A, Kneteman N. The Role of Macrophages in Xenograft Rejection. *Transplantation Proceedings*. 2008;40(10):3289-3293.

149. Nunez-Cruz S, Connolly DC, Scholler N. An orthotopic model of serous ovarian cancer in immunocompetent mice for in vivo tumor imaging and monitoring of tumor immune responses. *J Vis Exp*. 2010;(45).

150. Cao X, Jia G, Zhang T, et al. Non-invasive MRI tumor imaging and synergistic anticancer effect of HSP90 inhibitor and glycolysis inhibitor in RIP1-Tag2 transgenic pancreatic tumor model. *Cancer Chemother. Pharmacol*. 2008;62(6):985-994.

151. Pautler RG. Mouse MRI: concepts and applications in physiology. *Physiology (Bethesda)*. 2004;19:168-175.